

DISCLAIMER FOR FRONT PAGE OF MATERIALS TO BE MADE AVAILABLE VIA ETI INTERNET SITE

1. "Save to the extent set out in paragraph 2 below, this document and its contents are made available to you via the ETI's Internet Site "as is" without any representations, conditions, warranties or other assurance of any kind. The ETI and the authors, together with their employees, directors, servants or agents exclude to the maximum extent permissible by law all representations, warranties, conditions or other assurance whatsoever (whether express or implied) regarding the use of this document or its content including any warranties of title, merchantability, accuracy, completeness, non-infringement or that the document or its contents are of satisfactory or any particular quality or fit for any particular purpose. Any person accessing this document and using it or any of its contents accepts all risk in doing so.
2. Notwithstanding any statement to the contrary contained on the face of this document, the ETI confirms that the authors of the document have consented to its publication by the ETI."

REDAPT MD3.8 FINAL REPORT

**TIDAL ENERGY SITE CHARACTERISATION
AT THE FALL OF WARNESS, EMEC, UK**

ENERGY TECHNOLOGIES INSTITUTE REDAPT MA1001 (MD3.8)

June 19, 2015

INTERNAL DRAFT v1.0

v1.0

Brian Sellar and Duncan Sutherland
Institute for Energy Systems
School of Engineering
University of Edinburgh

Abstract

Complete at End

DISCLAIMER COPYRIGHT NOTICE

Nomenclature

ϵ	Turbulent Dissipation Rate [m^2s^{-3}]
η	Surface elevation [m]
λ	Integral Length scale [m]
Φ	Roll [$^\circ$]
Ψ	Yaw [$^\circ$]
Θ	Pitch [$^\circ$]
$D(z, r)$	Spatial structure function [m^2s^{-2}]
f	Frequency [Hz]
f_s	Sample Frequency [Hz]
H_{m0}	Significant wave height. Spectral wave parameter. [m]
H_m	Mean wave height. Time series zero crossing method. [m]
I	Turbulence Intensity [%]
R_D	Rotor Diameter [m] (500kW=16m tbc 1MW=16m tbc)
$S(f)$	Wave spectral density [$m^2.s$]
$S(f, \theta)$	Directional wave spectral density [$m^2s.rad^{-1}$]
$S_t(f)$	Spectral Density (turbulence) [$m^2s^{-2}Hz^{-1}$]
T_p	Peak wave period. [s]. Spectral wave parameter and approximate to T_m (mean wave period) from time series analysis.
TKE	Turbulent Kinetic Energy [m^2s^{-2}]
u	Streamwise velocity [m/s]
u'	Streamwise velocity fluctuations [m/s]
U, V, W	Mean velocity in x,y,z directions [m/s]
v	Transverse velocity [m/s]
v'	Transverse velocity fluctuations [m/s]
w	Vertical velocity [m/s]
w'	Vertical velocity fluctuation [m/s]
x	Streamwise distance from origin [m]
y	Transverse distance from origin [m]

z Vertical distance from origin (positive from seabed to surface) [m]

Contents

Nomenclature	3
1 Executive Summary	7
1.1 ReDAPT within the ETI Marine Programme	7
1.2 The ReDAPT Project	7
1.3 Modelling Work Package (MD)	8
1.4 Field Measurement Work Package (MD3)	9
1.4.1 Objectives of ReDAPT Work Package MD3	9
1.4.2 Outline of Activities of MD3	9
1.4.3 Acceptance Criteria of MD3	9
1.4.4 Acceptance Criteria of MD3.8	9
1.5 MD3.8 Summary of Findings	10
1.5.1 Tidal Site Characterisation	10
1.5.2 Site Characterisation within EMEC’s Fall of Warness	10
1.5.3 Case Study: ReDAPT Instrumentation	10
1.5.4 Recommendations and Guidance	10
2 Tidal Site Characterisation	11
2.1 Introduction and Overview	11
2.2 Background and Advantages of Tidal Energy	11
2.2.1 Tidal Industry Background	11
2.2.2 Challenges to the Tidal Energy Sector	12
2.2.3 Gaps in knowledge	12
2.3 Tidal Energy Site Characterisation	13
2.3.1 The Physics of Tidal Flow	13
2.3.2 Site Characterisation as an Input to Numerical Models	16
2.3.3 The Presence of Waves	18
2.4 Tidal Energy Site Characterisation: Candidate Metrics	18
2.4.1 Mean Flows: Depth Profiles	19
2.4.2 Quantifying turbulence magnitude and structure	19
2.5 Site Characterisation: Flow Measurement Technology	23
2.5.1 Tide Gauge	23
2.5.2 Rotational anemometer/impeller	23
2.5.3 Hot wire/film	23
2.5.4 Electromagnetic induction sensors	24
2.5.5 Differential pressure sensors	24
2.5.6 Piezo-electric Probes	24
2.5.7 Sensor Mounting Solutions	24
2.6 Sub-sea Acoustic Velocity Sensors (Doppler Sensors)	25
2.6.1 Doppler Theory	26
2.6.2 Range Gating	27
2.6.3 Design Variations	28

2.6.4	Relative Advantages and Limitations of Doppler Sensors	29
2.7	Site Characterisation: Wave Measurement Technology	30
2.7.1	Wave buoys	30
2.7.2	X-Band radar	31
2.7.3	Acoustic Doppler Profilers	32
2.7.4	HF Radar	33
2.7.5	LIDAR	33
2.7.6	Pressure gauges	34
3	Site Characterisation at FoW	36
3.1	Overview of the Measurement Campaign	36
3.1.1	TRNs	36
3.2	QC and Analysis Methodology	38
3.2.1	Coordinate Transformation	38
3.2.2	Out of Range Velocity Rejection	38
3.2.3	Low Amplitude Rejection	38
3.2.4	Median Absolute Deviation Rejection	38
3.2.5	Hardware Reported Error Code Rejection	38
3.2.6	Stationarity Period Selection	39
3.2.7	Detrending Method Selection	40
3.2.8	Instrument Noise and Noise Correction Factors	42
3.3	Measuring Waves at the Fall of Warness	44
3.3.1	Acoustic Surface Tracking with Vertical ADP	44
3.3.2	Combined Mode - Acoustic Surface Tracking with Vertical ADP and Wave Velocities	46
3.3.3	Pressure Gauge	47
3.4	Velocimetry: Wave Orbital Velocity to Wave Spectra	47
3.5	Combined Wave Measurements	48
3.6	Site Characterisation	54
3.6.1	Database Searching	54
3.6.2	Returned Metrics	54
3.6.3	Reference Velocities	57
3.7	Analysis: (Flood) Turbine-Mounted Instrumentation	60
3.7.1	Lengthscales	60
3.7.2	Turbulence Intensity	61
3.8	Analysis: (Ebb) Turbine-Mounted Instrumentation	67
3.8.1	TI EBB	67
3.9	Analysis: Seabed Mounted Instrumentation	88
3.10	Advanced Measurement Techniques (2D Array vs SB)	88
3.11	Advanced Measurement Techniques (C-ADP vs D-ADP)	88
3.12	Sensitivity Analysis	88
3.13	Conclusions on Convergence/Sensitivity/Uncertainty	88
4	Lessons Learned and Industry Guidance	97
4.1	Introduction and Overview	97
4.1.1	The Alstom DEEPGEN Turbines	97
4.2	Case Study: ReDAPT Instrumentation Systems	98
4.2.1	Introduction and Overview	98
4.2.2	Seabed Mounted Instrumentation	101
4.2.3	Turbine System Integration	105

4.2.4	Convergent Beam Doppler Velocimetry	112
4.2.5	Power Curve Production: IEC Inspired Test	112
4.2.6	Case Study Recommendations	112
4.3MORE WORK ON THE FOLLOWING SECTION TO FOLLOW.....	115
4.4	Data Acquisition, Data Analysis and Data Processing	115
4.4.1	Introduction and Overview	115
4.4.2	Data Acquisition	115
4.4.3	Data Analysis	115
4.4.4	Data Processing	115
4.4.5	Winter Campaigns	115
4.4.6	115
4.4.7	Instrument Configuration - non-SBD	116
4.4.8	Instrument Configuration - SBD	116
4.5	The ReDAPT Database	116

Chapter 1

Executive Summary

This six page summary seeks to provide a short introduction to the ReDAPT project, to set the individual work-packages in context - thus highlighting the level of inter-dependency between project partners' activities - and to provide a summary of the main findings of the University of Edinburgh's field measurement campaign and subsequent data analysis. Section 2 provides an introduction to the field of site characterisation for tidal energy sites. Section 3 reports on the analysis conducted from site measurements for the EMEC Fall of Warness test site specifically. Section 4 discusses the integration and operation of sensor systems and outlines various lessons-learned.

1.1 ReDAPT within the ETI Marine Programme

The Reliable Data Acquisition Platform for Tidal energy (ReDAPT) project was commissioned and co-funded by the Energy Technologies Institute (ETI) under their Marine Programme whose central objective is to accelerate the development and deployment of commercially viable marine energy technologies that will:

- Make a material contribution to the future UK energy system
- Deliver significant greenhouse gas emissions reductions
- Contribute to the delivery of long-term energy security in the UK

Specifically, their Marine Programme seeks to contribute to the delivery of marine energy cost reduction and performance improvements in line with the ETI Marine Energy Roadmap

1.2 The ReDAPT Project

ReDAPT is led by Alstom and includes the University of Edinburgh (UoE), DNV-GL Renewable Advisory, EDF Energy, E.ON, Tidal Generation Ltd., Plymouth Marine Laboratory and the European Marine Energy Centre (EMEC). The project centres around a commercial scale (1MW) tidal turbine developed by Alstom deployed at EMECs Tidal Test Site with the aim of producing a comprehensive suite of data on turbine operation, the flow field and the interaction between the two. ReDAPT is a three year programme intended to provide information to the Tidal Industry to facilitate rapid growth. Specific goals include:

- Accelerate development of tidal energy industry
- Successful deployment and operational testing of a 1MW system at EMEC, delivering substantial learning to the acceleration of commercial product roll-out.

- Data, insights and lessons learned are recognised as key reference materials and are used by the industry, e.g. Device performance.
- Environmental monitoring and resource assessment.
- Industry certification standards and protocols informed by ReDAPT outcomes.
- Increase confidence in tidal turbine technologies
- Validation and industry acceptance of tidal flow/machine models

A complete list of released project outputs can be found in Annex I.

1.3 Modelling Work Package (MD)

Specific to the “Modelling” (MD) work package, validation of engineering tools forms a core project outcome through comparison of predicted to experienced loads *under measured environmental conditions*. This document reports upon these field measurements of tidal currents and waves; data that enables the validation of engineering tools whilst also forming the basis of an in-depth site characterisation study.

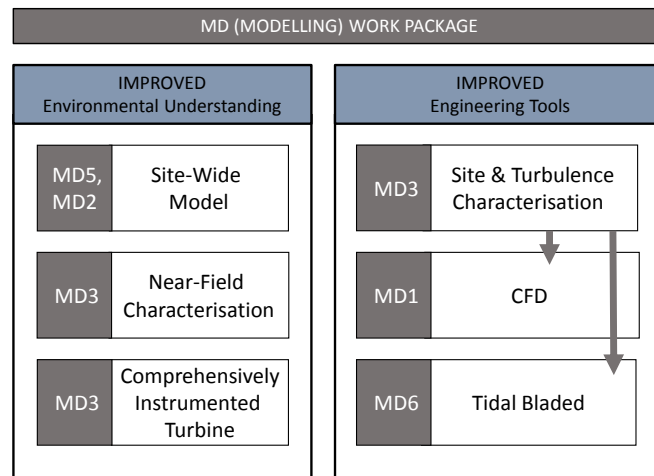


Figure 1.1: MD (Modelling) Work Package Activities with sub-package labels MD1-MD6.

Within the modelling work package, led by EDF, numerical modelling work was undertaken by E.ON, DNV-GL and the University of Manchester. MD1 involved cutting-edge numerical simulation of the Alstom 1MW tidal turbine in turbulent flows [1, 2]. MD5 involved the construction and validation of a model of the wider Fall of Warness, Orkney site [3, 4] and incorporated both an existing EMEC dataset and new UoE field measurements as part of MD2. These current profiles were used in the model build and model validation phase of MD5. MD6 involves the validation - through comparison to field and machine data - of the GLGH Tidal Bladed software which seeks to capture environmental and turbine characteristics in a desktop application [5-7].

1.4 Field Measurement Work Package (MD3)

1.4.1 Objectives of ReDAPT Work Package MD3

The objective of the University of Edinburgh's MD3 sub-project work package is to design and conduct a data acquisition campaign to increase understanding of the flow conditions in the nearfield of a tidal stream turbine and to increase confidence in flow measurement and analysis methods.

1.4.2 Outline of Activities of MD3

Activities centre on near-field flow characterisation where near-field is defined herein as up to 10 rotor diameters range from the turbine. Three primary activities were originally identified with a fourth added during project review:

1. Site and Turbulence characterisation
2. Acquisition, processing and dissemination of data for the validation of the ReDAPT numerical models
3. Recommendations for monitoring parameters and equipment type
4. Additional: Provision of data in a format suitable for archival and access by the Industry

1.4.3 Acceptance Criteria of MD3

The contracted description of work can be found below.

1. Procure, test and calibrate the Acoustic Doppler Profiler (ADP) instrument system, including power, foundations, data logging and retrieval system. (MD3.2)
2. Design and construct appropriate flexible support structures.
3. Interim turbulence characterisation activity outlined (MD3.4)
4. Perform multiple measurement campaigns with the instruments, analysing the data and improving the the turbulence characterisation. (MD3.15)
5. Provide a final report including characterisation of the near field flow, a sensitivity analysis, assumptions and estimate of confidence. (MD3.8)

1.4.4 Acceptance Criteria of MD3.8

The contracted acceptance criteria for MD3.8 is listed below.

1. Report describing a method by which robust descriptions of flow parameters incident to a tidal device can be generated using multiple high-resolution current profilers.
2. These flow parameters will inform the inflow conditions to both the MD CFD modelling and MD Engineering Tools activities

1.5 MD3.8 Summary of Findings

1.5.1 Tidal Site Characterisation

Complete at End

1.5.2 Site Characterisation within EMEC's Fall of Warness

Complete at End

1.5.3 Case Study: ReDAPT Instrumentation

Complete at End

1.5.4 Recommendations and Guidance

Complete at End

Chapter 2

Tidal Site Characterisation

2.1 Introduction and Overview

Flow characterisation of a tidal energy site centres on gaining information on water velocity over a range of spatial and temporal length scales suitably chosen to capture the key underlying fluid motions. These potentially include information varying across annual and seasonal time scales to fluctuations in velocity at timescales of seconds and below. Likewise, knowledge of spatial variation of flow parameters is required across a wide range, from orders of tens of blade diameters (for wake studies and array interaction for example) to variations of metres and below for investigations into blade fatigue. Ideally, 3D velocity information would be captured with high spatial densities of sub-metre resolution across the entire fluid domain of the turbine, at sample rates capable of measuring high frequency velocity fluctuations and for durations long enough to capture the characteristics of tidal cycles throughout the year. No instrument yet exists to provide these measurements. Identifying key velocity measurements and metrics that are obtainable, reliable and representative becomes the goal of any flow characterisation.

2.2 Background and Advantages of Tidal Energy

2.2.1 Tidal Industry Background

Amongst the first grid connected tidal turbines was the 300kW HS300 prototype built by Hammerfest (now Andritz Hydro) and was first installed in 2003 in Kvalsund in Finnmark, Norway. It has since been superseded by the HS1000 1MW commercial scale device, which had produced over 1.5GWh of electricity by the end of 2014 [8]. It is a single three-bladed rotor axial flow device based on a tripod support structure. Another early commercial ($\geq 1\text{MW}$) scale grid connected tidal turbine was Seagen which was installed in Strangford Narrows (Northern Ireland) in June 2008. This 1.2 MW device employs two two-bladed rotors either-side of a surface piercing central pile. It had by the end of 2014 achieved over 8GWh of production [9]. Since then other tested or currently operational 1MW or greater rated-power devices include the Alstom DeepGen IV, the Open Hydro ‘Open-Centre’, the Atlantis ‘AR1000’ and the Voith turbines.

At the time of writing, consent had been granted to begin development of the first tidal array projects. These were: MeyGen in the Pentland Firth, Scottish Power Renewables’ Sound of Islay project and France’s Agency for Environment and Energy Management project in Raz Blanchard, Normandy, France. It is hoped that these projects will significantly drive forward the sector and reveal information regarding device-flow interactions that will help improve longer term economic viability.

2.2.2 Challenges to the Tidal Energy Sector

2.2.3 Gaps in knowledge

It is often asserted that the tidal industry can build on the knowledge of the more established wind industry, since they are founded on the same principles of fluid dynamics (and the generator systems appear scaled versions of one-another in the case of three bladed horizontal access machines). However, a more dense fluid, more confined fluid depth compared with the device scale and the effects of waves at the upper boundary, in addition to the challenges of operating in the marine environment, mean the tidal energy sector has unique challenges.

Significant engineering challenges and areas of ongoing research include:

- Characterising the resource across multiple spatial and temporal scales.
- Determining maximum and fatigue-inducing design loads.
- Understanding device-device interactions within tidal device arrays.

Although the main drivers of the flow which make them a predictable resource are understood at site scale there remains uncertainty about local flow velocities and flow turbulence. The flow at site-scale is driven by local bathymetric features and coastline which can cause significant variation in flow over small ($< 100\text{m}$) scales [10].

Add latest tidal-loadings related references and tighten The loading on devices at tidal stream sites are a complex combination of: mean flow, turbulence and directionally-dependent wave orbital effects. In operational tidal arrays spatially and temporally varying wake-induced velocity variations will be added to this mix. These fluctuations in flow velocity magnitude, direction and duration effect the device loadings [11]. One of the key differences between wind turbines and tidal turbines is that for atmospheric wind flow, the most energetic turbulent structures are not restricted by an upper boundary layer and thus the highest energy containing structures can be very large, tending towards 280m as separation from the boundary increases [12]. In a tidal channel the turbulent structures are limited by the channel depth. Since turbine blade diameters are often close in scale to half the channel depth, the effect of turbulent structures of similar dimensions to the device on the loadings are an important factor and one that is not well understood. In addition, the dissipation scale of the turbulence can effect pressure differences across the blade increasing drag forces [13].

Tidal Flow-Specific Considerations

Although much work has been done on the theory and measurement of turbulence particularly in the area of atmospheric flows there has been less focus specific to turbulence in tidal flows. Tidal channel regimes have several key differences compared with atmospheric regimes:

- Increased number of boundary layers. Much of the flow field of interest may be exposed to boundary layer effects e.g., seabed, seasurface, coastline.
- Turbulence and flow statistics may be sensitive to parameters other than the mean flow speed e.g., tide direction and bathymetry.
- Characterisation of the flow-field will require the consideration of the effects of a local wave-field.
- Securing good data on which to build models is more challenging.

2.3 Tidal Energy Site Characterisation

2.3.1 The Physics of Tidal Flow

The Moon and the Sun

The first recorded knowledge of the drivers for the tides dates back to Pytheas of Massalia, a 4th Century BC Greek explorer and geographer [14]. He recognised the connection with the waxing and waning Moon with the rise and fall of the sea. Today the drivers of the tides are well understood. They are the result of the bodies which exert the strongest gravitational forces on the Earth, the Moon and the Sun, pulling the earth and thus the fluids on the surface towards them. The earth rotates relative to the moon once every 12.42 hours [15]. As the Moon is the the strongest of the forces on the earth this causes the largest of what are known as Harmonic Constituents, the M2. The harmonic constituents are the mathematical description of all the time varying forces on the tides, each with a magnitude and phase.

Types of Tidal Site

Tidal sites applicable for energy extraction are generally defined as anywhere where flow velocities are sufficiently fast ($> 1\text{ms}^{-1}$) for extended periods of time. In order for these velocities to occur, the tides must be constrained by landmasses which cause the flow to accelerate. There are several conditions that can facilitate these speeds and the first stage in site characterisation is to qualitatively define the types of site. There are 3 basic types of site: tidal basins, symmetrical (also referred to as rectilinear) bi-directional channels and asymmetrical bi-directional channels.

A tidal basin occurs where the tide flows into and out of a reservoir through a single narrow channel. Examples of this include Strangford Loch where Seagen is deployed and Digby Gut (along with other basins off the Bay of Fundy) in Nova Scotia. These sites are ideal as the narrow channels restrict the variability of flow angle thus they have very symmetrical tidal ellipses.

Examples of rectilinear flow include Admiralty Inlet in Puget Sound as per the example in figure ?? and the Fall of Warness Site in Orkney (see figure ??) on which the core of this work reports. Rectilinear sites are desirable as turbines can be designed to be mounted in a fixed position, pitching the blades to capture the tides from both directions. The final detail of this high level characterisation is the equality of the magnitudes of the Ebb and Flood tides at a site. Some sites have one tide which is significantly faster than the other such as certain areas of Ramsey Sound off the coast of Wales [10]. This is generally undesirable as it usually means one tide is only at a extractable flow speed for a smaller proportion of the time if at all, reducing the availability of the turbine to generate and hence reducing the extractable resource.

Generating power

The complete systems through which tidal energy extraction devices convert the kinetic energy of a fluid to grid-specification electrical energy are complex and vary widely. It is important to underline the most basic principles which flow characteristics will affect. In the majority of devices a hydrofoil is employed, a surface which is designed to maximise the pressure difference across it creating a force. The useful component of this force is termed lift and the one normal to it drag. A basic example of this principle is illustrated in figure 2.1. This force transfers the kinetic energy of the flow to the

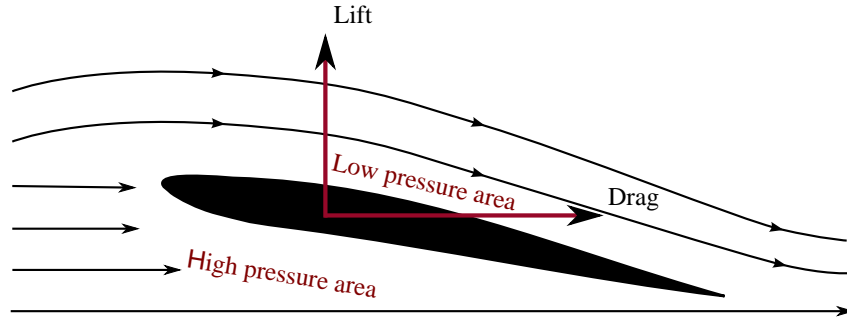


Figure 2.1: Basic principles of lift and drag

drive train of the device. In the case of a turbine, this rotational force is used to power a generator (often via a gearbox for speed regulation) to create electricity.

The force required to overcome the initial inertia of the device is related to a minimum flow speed, known as a cut-in velocity. In order to optimise the generator design a rated power is selected which is related to a maximum rotational speed of the generator for the common flow speeds at the site. A rated velocity is the minimum flow velocity needed to achieve this. As with most wind turbine designs, techniques such as adjusting the blade angle, are then employed to keep the rotational speed constant at higher flow velocities. The relationship of power extracted to inflow velocity is referred to as a "Power curve". The optimum power curve is site specific, hence the need for accurate long term resource predictions to enable designers to tailor a device for a specific site.

The theoretical extractable power (P) from the flow is defined as:

$$P = \frac{1}{2} \rho A c_v u^3 \quad (2.1)$$

$$(2.2)$$



Where ρ is the fluid density, A the swept area of the device and c_v is the efficiency coefficient for the specific device, which is limited to below the Betz limit of 0.593 [12]. For site characterisation the device dependant terms can be removed to define the kinetic power density K [16], given as:

$$K = \frac{\rho u^3}{2} \quad (2.3)$$

Estimates of minimum kinetic power density K to enable site viability have been suggested at 1 kW/m² [16].

In reality the flow over devices are in a constant state of flux and thus so are the pressures and resulting lift forces. The response of lifting surfaces to velocity fluctuations is complex and responds to fluctuations of different sizes and magnitudes in different ways [11, 13]. Hence the need to characterise the turbulent flow at tidal sites.

Turbulent Flow

Turbulent flows can be described, [17], as one which "varies significantly and irregularly in both position and time". Generally this is found in flows whose Reynolds number is above 4000 [18]. The equation of the Reynolds number, which is a ratio of the inertial to the viscous forces in a flow, is given as:

$$Re = \frac{\rho \bar{u} D_h}{\mu} \quad (2.4)$$

$$(2.5)$$

Where μ is the dynamic viscosity of the fluid and D_h is the hydraulic diameter which, for an open top rectangular cross section channel, is given as:

$$D_h = \frac{\text{area}}{\text{perimeter}} = \frac{2yz}{2z + y} \quad (2.6)$$

Here y is the channel width and z the depth [18]. Most tidal channel are well above this number, for example; a representative cut in speed for a commercial turbine of 1 ms^{-1} , a hydraulic radius of 91m (representative of a rectangular cross-section tidal channel 1km wide and 50m deep) the Reynolds number would be 91×10^6 .

The most basic explanation of the physical process which causes a flow to become turbulent is due to the water flowing over a rough surface in the seabed. The roughness of this boundary layer causes a gradient in the flow velocity, with the water slowest near the boundary, this gradient causes the faster higher flow to 'spill over' the lower flow causing large turbulent eddies to form. These large eddies then transfer energy by frictional momentum transfer to smaller eddies down to the scale where viscous forces dissipate the kinetic energy to heat.

The rate at which large eddies transfer energy to smaller scales is captured in the dimensional analysis work of [19] and the minus five-thirds law according to:

$$E(k) = \alpha \epsilon^{2/3} k^{-5/3} \quad (2.7)$$

Where $E(k)$ is the kinetic energy per unit mass per wavenumber, alpha is a constant, ϵ is the dissipation rate of kinetic energy and k is the wavenumber defined as:

$$k = \frac{2\pi f}{\bar{u}} \quad (2.8)$$

Where f is frequency and \bar{u} is the mean velocity over a period of stationarity (T_{stat}) [19].

This region is part of what is known as the turbulent cascade and the $-5/3$ slope region is known as the inertial sub-range. The turbulent cascade covers all regions of turbulent motion and a diagram illustrating the various scales is presented in figure 2.2. In tidal site analysis, there is uncertainty regarding the effect of the largest structures in the flow; how much kinetic energy they contain and what their impact on devices will be. It has been estimated that the scales of turbulence in tidal sites would be approximately one third the channel depth [20]. Studies by [21] of lengthscales have found an average streamwise integral lengthscale of approximately 17m for a 55m deep channel for a site (Admiralty Inlet) with flow speeds of $(1.5) \text{ ms}^{-1}$ which supports this estimate. In addition, the smaller scales of turbulence can also affect devices. The dissipation scale of turbulence, at which

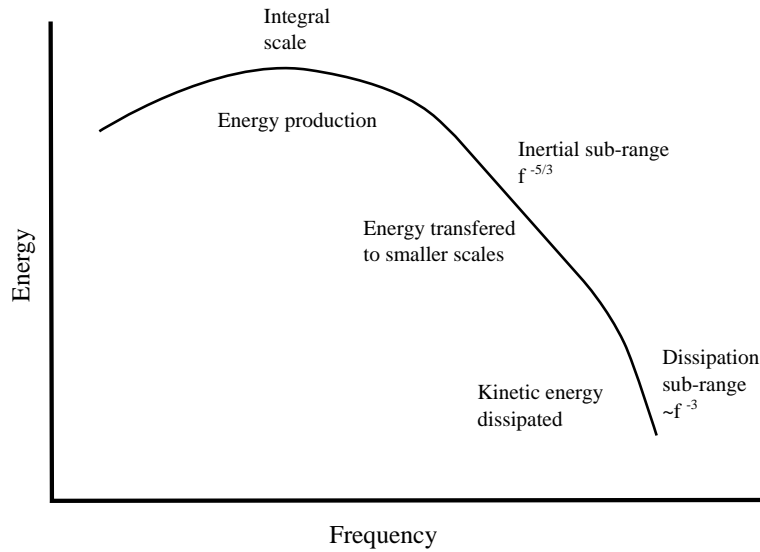


Figure 2.2: Illustration of the energy cascade highlighting the most important regions in tidal site characterisation. Adapted from [17].

the kinetic energy is transferred to heat via friction, has been shown to increase the drag forces on objects in a turbulent flow [13].

A final important theory in turbulence measurements is that of the ‘frozen field hypothesis’ developed by Taylor [22]. It is an assumption that the largest turbulent structures evolve far slower than they are advected and thus the flow past a given point can be considered as a snapshot of the structure moving with velocity \bar{u} .

2.3.2 Site Characterisation as an Input to Numerical Models

One technique of predicting the dynamics of turbulent flow (and in the presence of a wave field) is via computational modelling. Computational models exist for all scales of fluid motion from global oceanography models to Computational Fluid Dynamics (CFD) which resolve flows at tiny scales. The advantage of these models is that they don’t require expensive site surveys and can be modified for any site and used for the prediction of resource, with the inclusion of energy extracting devices in the form of tidal turbines. However these models all require high quality field data for validation. Furthermore, data ideally would be available from a range of sites so that the driving factors for inter-site variation can be better understood. One of the fundamental goals of field velocity measurements (and the ReDAPT project of which this work is a part) is to gather data suitable to improve the confidence in these models.

Numerical Modelling of Tidal Flows

Tidal flows are turbulent, exhibiting random motions across all dimensions. Whilst the equations to describe turbulent flows are known (the Navier-Stokes equations) the computational power required to model these flows across the entire scale of motion severely restricts a direct numerical approach (at present). Traditionally, extensive, expensive and careful experimentation has produced empirical formulae for simplified systems. As system complexity increases empirical methods become less realisable and/or reliable. In this regime, statistical methods can be applied to the Navier-Stokes equations to ‘smooth’ the fluctuations (turbulence) whilst maintaining a correct description of the averaged properties such as velocity. **The averaging of the turbulence terms cannot be fully neglected however.** In order to maintain conservation of energy in the system, information on the characteristics of turbulent motion needs to be injected in to the numerical simulations. The descriptions of these motions and the methods of inputting the information into the simulations are called “turbulence models”. These models simulate the effect of turbulence on the behaviour of the mean properties of the flow.



“Turbulence models can only give an approximate description, and, with a particular set of empirical constants, they are valid only for a certain flow or at most a range of flows.”

[23]

For reliable results consideration should be given to the following aspects of turbulence models:

- They need to be tailored for specific problems
- Their validity will likely be limited to specific types of flow or ranges of flows
- Extensive testing is required to have confidence in any extrapolations made
- Their associated computational expense increases with complexity

In order to build confidence in a selected turbulence model and numerical simulation, verification with measurements in both the field and the laboratory may be required.

MD1 - Detailed Numerical Simulations

In order to increase confidence in the outputs of CFD techniques, confidence in the inputs to these numerical models must be established. CFD conducted as part of the MD sub-project within ReDAPT was based upon EDF’s Code_Saturne [24]. This is an Open Source CFD code designed for efficient parallel computation of turbulent flow around and within complex geometries. The code includes a range of Reynolds Averaged Navier-Stokes (RANS) turbulence models and is widely used for Large Eddy Simulation (LES). The primary objective of the ReDAPT MD1 work was to compare numerical predictions of the characteristics of time varying load to measurements of time-varying loads on the TGL 1 MW turbine.

It is important that the inflow conditions are defined such that the spatial and temporal variation of the incident flow are representative of the conditions experienced by the DeepGen IV turbine.

Turbulent length scales are of particular significance to this work involving Large Eddy Simulation (LES). The software component that handles the generation of inflow data to these simulations, in this case the Synthetic Eddy Method (SEM), can use turbulence length scales to create velocity fluctuations that are more representative of the modelled environment [25]. Since the outputs of

an LES model are known to be sensitive to inflow conditions, it is important that the ambient flow-field is accurately modelled so that physical and modelled effects can be isolated. The University of Edinburgh is working with EDF and their partners to ensure that values of important inflow parameters can be measured or inferred to an acceptable level of confidence.

MD6 - Industry Design Tools

Sub-project MD6 aimed to improve confidence in GLGH's Tidal Bladed tidal turbine design tool. Tidal Bladed, in order to give information on loads and performance of a particular tidal turbine, requires a description of the turbine (blades, rotor, drive train etc.) and a description of the environment (currents, waves, turbulence etc.). At present Tidal Bladed describes the environment in terms of vertical profiles of velocity and the turbulence intensity (from a prescribed location or 'point') and incorporates the effects of waves through measurements of traditional wave spectral parameters such as H_{m0} .

Very few measurements of the turbulence intensity of tidal currents and their spectral distribution are known. Especially for the spectral distribution, no standard models as used in the wind industry or for sea state description [waves] exist. [26].

Unsteadiness in the flow, which imparts loads on to the tidal turbine, will be the result of both wave kinematics and turbulent fluctuations in the tidal stream. Unlike the wave-field, the tidal-flow-field does not have standardised parametric models which can be used to characterise it.

The objective of MD3.4 is to characterise turbulent flow where the measurable parameters are by definition random variables. As random variables are inherently unpredictable focusing on probabilistic characterisation is appropriate. [17].

Statistical tools for measuring probability include:

- Probability density functions including joint probability techniques
- Probability distributions
- Correlations
- Variances
- Spectra

[17, 27].

The range of complexity of models or descriptions that can be built upon these tools is large and confidence in their use is generally reliant on large quantity of high quality experimental measurements.

2.3.3 The Presence of Waves

To Follow

2.4 Tidal Energy Site Characterisation: Candidate Metrics

rework required

Early work on tidal site characterisation using D-ADP and C-ADP velocimetry include [28–30]. More recent works include [31, 33, 34].

2.4.1 Mean Flows: Depth Profiles

To estimate long term resource mean velocities should be collected and a harmonic analysis performed [35]. The flow measurement should either be at predicted hub height of a device or averaged over the probable rotor diameter. For early feasibility studies the two largest constituents are sufficient, but for an ‘advanced’ tidal project site assessment, a minimum of 3 months of continuous field data are required, in order to resolve 20 of the Harmonic Constituents. The longer period constituents are of up to 2191 hours and as they combine can cause variation in yield predictions over a period of years. Unfortunately most resource work is project specific and is therefore unpublished. This report does not include long term (project lifespan) characterisation or subsequent energy yield as the focus is on turbulence and parameter uncertainties arising from typical deployment methodologies.

Channel flows vary vertically as previously discussed thus flow measurements throughout the water column are required. The tidal industry uses a variety of curves to describe how the flow varies with depth, known as velocity depth profiles. Equation 2.9 gives the form of the relationship of velocity with depth ($u(z)$):

$$u(z) = \left(\frac{z}{H}\right)^{1/n} u_{z=0} \quad (2.9)$$

Where n is an approximate empirically calculated power normally in the range of 7 to 10 and H is the total depth.

It should be noted that equation 2.9 assumes no wind and wave driven surface effects or large scale bathymetric features which would be expected (and are shown herein) to significantly affect velocity depth profile.

2.4.2 Quantifying turbulence magnitude and structure

In order to derive subsequent turbulence measures from velocity time-series a period of stationarity (T_{stat}) of the flow must be defined. All turbulence metrics require the assumption that the flow is statistically stationarity over the period over which the metric is being calculated. As real flows evolve throughout their cycles this period assignation can only be done in a statistical sense. [36] looked at a series of periods from 1 to 20 minutes before concluding that 5 minutes was the longest period that could be considered stable in terms of mean and variance. Although it should be noted that this result is based on measurements at only two locations and may be site specific. **Validity** of stationarity analysis has been conducted for the FoW under this work and is presented in section **((x))**.

Velocity Perturbations

Turbulence analysis involves analysis of a defined mean value and derived fluctuating component. A velocity perturbation u'_n for a single velocity sample (n), is defined as [17]:

$$u'_n = \bar{u} - u_n \quad (2.10)$$

Where \bar{u} is the mean velocity over a period of stationarity. The same equation is used to define v'_n and w'_n .

Signal Detrending

Analyses can be sensitive to the method used to estimate the representative mean of a signal particularly for dynamic systems and for those comprised of varied physical drivers (chaotic multi-scale eddies, pseudo-deterministic wave oscillations, periodic constituents etc.) Common methods of defining a mean value include constant-value detrending, linear and higher order polynomial detrending, pre-filtering data to remove known oscillations and moving average detrending. This is discussed further in section ((x)).

Turbulence Intensity

One of the metrics commonly used to quantify the magnitude of turbulence is the Turbulence Intensity (I). This term is adopted from the wind industry as a measure of the magnitude of fluctuation as a percentage of the mean flow velocity. It is defined as the root-mean-square (rms) of the velocity perturbations divided by the mean velocity over a period of stationarity as given by:

$$I = \frac{\sqrt{\frac{1}{3}\langle u'^2 + v'^2 + w'^2 \rangle}}{\bar{u}} \times 100 \quad (2.11)$$

Where u' , v and w' are the velocity perturbations along the three Cartesian vectors. If the turbulence is assumed to be isotropic (i.e. equal in all directions) only a single velocity perturbation measurement is required [12]:

$$I_i = \frac{\sqrt{\langle u_i'^2 \rangle}}{\bar{u}_x} \times 100 \quad (2.12)$$

Where u'_i for the i^{th} Cartesian vector (i.e. $u'_y = v'$). Note that I is always normalised by the mean streamwise velocity component \bar{u}_x .

An alternate expression for the magnitude of turbulence is the Turbulent Kinetic Energy (E_{TKE}) which is based on the standard kinetic energy equation. In the case of (E_{TKE}) no normalisation by \bar{u} is carried out. The definition is given as [31]:

$$E_{TKE} = \frac{1}{2} \langle u_i'^2 \rangle \quad (2.13)$$

This relation also assumes isotropic turbulence.

Reynolds Stresses

To quantify the driving forces that generate turbulence the standard metric set are the Reynolds stresses. First introduced by [37], they are a measure of the shear forces which generate the turbulent

flow conditions, again calculated from velocity perturbations. They are defined by the Reynolds stress tensors, given as:

$$\tau''_{uw} = -\langle \rho u' w' \rangle \quad (2.14)$$

$$\tau''_{vw} = -\langle \rho v' w' \rangle \quad (2.15)$$

Where τ'' is the Reynolds stress tensor and ρ is the density of the fluid. The density term can be omitted (and often is in tidal site characterisation work) for a fluid where the variation in density is negligible.

In theory these stresses are the driver that cause the velocity to vary with depth as discussed in Section 2.4.1. This relationship is:

$$u(z) = \frac{\tau''_{uw}}{c_{vk}} (\ln(z) - \ln(z_0)) \quad (2.16)$$

This is often referred to as "the law of the wall". Here $u(z)$ is the streamwise velocity as a function of depth (z), z_0 is a roughness length and c_{vk} is Von Kármán's constant which is approximately 0.41 [45].

Several of the site characterisation reports referred to in this section include a measure of the Reynolds stress [38], [30] and [39] who also measured integral lengthscales in the flow as well as [34]. [30] found values of the order of $10^{-4} \text{m}^2 \text{s}^{-2}$ at a depth of 15.6m for a channel with a peak flow of 1ms^{-1} . [34] using results from peak flows at EMEC (estimated at 3ms^{-1}) found longitudinal Reynolds stresses of up to $0.0124 \text{m}^2 \text{s}^{-2}$ with smaller ($5 \times 10^{-3} \text{m}^2 \text{s}^{-2}$) transverse values. Reynolds stress depth profiles for the FoW are presented in section ((x)).

Integral Lengthscale

The integral lengthscale (ℓ) is defined qualitatively as the average size of the largest eddies in a turbulent flow [17]. There are several methods of estimating this value. The most robust method is the Spatial Correlation method, where velocities at multiple points are measured at the same instant in time. The correlation coefficient is then calculated for a range of spatial separations or 'lags'

$$R(\Delta x) = \frac{\langle (u_x - \bar{u})(u_{x+\Delta x} - \bar{u}) \rangle}{\sigma_u^2} \quad (2.17)$$

$$(2.18)$$

Where $R(\Delta x)$ is the correlation coefficient, x is a location along the streamwise axis, Δx is a spatial separation and σ_u^2 is the variance of the velocity [17].

$$\ell_x = \sum_{\Delta x=0}^{R(\Delta x)=0} R(\Delta x) d\Delta x \quad (2.19)$$

The integration is only performed on R values up to the first zero axis crossing as recommended by [40].

The drawback of this method is that the maximum spatial range must be ~ 7 times that of the desired lengthscale or the value calculated will be biased low [40]. [39] used this method and found lengthscales of $\sim 2m$ for a $9m$ deep channel.

A variation on this method utilises the timescale \mathfrak{S} of turbulence which is calculated from the time based autocorrelation function given by:

$$R(\tau) = \frac{\langle (u_t - \bar{u})(u_{t+\tau} - \bar{u}) \rangle}{\sigma_u^2} \quad (2.20)$$

$$\ell_x = \bar{u} \cdot \mathfrak{S} = \bar{u} \cdot \sum_{\tau=0}^{R(\tau)=0} R(\tau) d\tau \quad (2.21)$$

Assuming the largest turbulent structures are frozen as proposed by [22] the timescale multiplied by the mean velocity advecting the structures will yield the lengthscale as given in equation 2.21.

This method has been used by [21] where an ADV suspended in the channel on a bouyant line was used to measure the velocities. The lengthscales for the fastest flow speeds were approximately 17m for a 55m deep channel 10.5m above the seabed at $\sim 1.5\text{ms}^{-1}$.

Alternatively the integral lengthscale can be estimated by the maximum turning point of the power spectral density. The Power Spectral Density (PSD) uses a Fast Fourier Transform (FFT) of a de-trended statistically stationary velocity sample defined as:

$$Y(f) = \int_{-\infty}^{\infty} y(t)e^{-i2\pi ft} dt \quad (2.22)$$

Where $y(t)$ is a time series, f is the frequency, t is time and $Y(f)$ spectral periodogram. This is then modified to give the PSD ($S(f)$) via :

$$S(f) = \frac{2}{(N + K)\Delta t} |Y(f)|^2 \quad (2.23)$$

Where N is the number of points in $Y(f)$, Δt is the period and K is the number of lags [?]. The maximum turning point of $S(f)$ represents the frequency at which there is most energy in the velocity, which is by definition the frequency of the integral lengthscale. Assuming the frozen field hypothesis, This can be stated as:

$$\ell = \frac{\bar{u}}{f_{S-max}} \quad (2.24)$$

Where the frequency f_{S-max} is the frequency corresponding to the maximum value of $S(f)$, to calculate the integral lengthscale ℓ .

Turbulent Kinetic Energy Dissipation rate and the Structure Function

[41] introduced the Structure function, $D(z, r)$ as a method to estimate the turbulent kinetic energy dissipation rate (ϵ). ϵ describes the rate at which the viscous forces in the flow transfer the kinetic energy to heat at the smallest scales of the turbulent cascade. The structure function which is a

version of the two point spatial autocorrelation function with a point separation or lag (r), is given as:

$$D(z, r) = \overline{(u'(x) - u'(x + \Delta x))^2} \quad (2.25)$$

$$(2.26)$$

Calculating $D(z, r)$ from [Equation 2.25](#) for a range of r values allows the use of the calculation of ϵ :

$$D(z, r) = C_v^2 \epsilon^{2/3} r^{2/3} \quad (2.27)$$

where C_v is a constant. [\[31\]](#) showed that for a site in Puget Sound, ϵ could vary in order of magnitude from 10^{-6} Wm^{-3} at slack water to 10^1 Wm^{-3} at peak flow velocities.

2.5 Site Characterisation: Flow Measurement Technology

There are a wide variety of established techniques for measuring fluid velocities. This section introduces these techniques, the theory behind them and their main advantages and relative drawbacks. Acoustic sensors which are used throughout this work are discussed in more detail in [Section 2.6](#).

2.5.1 Tide Gauge

A ‘Tide Gauge’ or water level meter, is a sensor which records surface elevation while averaging out variation due to waves. Sensors use a variety of technologies including pressure which are mounted on the seabed and radar which are mounted on the shore. If the cross section of the channel is known this elevation can be used to inform the average volume flowrate. It cannot give information about variation of flow with depth or any smaller scale motions.

2.5.2 Rotational anemometer/impeller

For the wind industry one of the most common velocity measurement devices is a rotational cup anemometer, a positive displacement meter which responds to the fluid causing multiple cups to rotate around a fixed axis. This is a cheap and effective system that calibrates a rotational speed to a given wind speed. It captures wind from all directions so is often paired with a vane to give directional information. A common adaptation for the tidal industry is to replace the rotating cups with an impeller mounted on a directional vane. For tidal applications it is a significant challenge to mount such a device in the appropriate part of the water column.

2.5.3 Hot wire/film

Hot wire anemometers use a heated wire which is cooled by convection as fluid flows over it. The resistance of the wire changes with temperature and the wire is installed in a Wheatstone bridge and

calibrated such that the voltage output changes commensurately with flow velocity. Hot wire probes have been used in tidal turbulence analysis such as in work by [38]. However the sensor calibration can drift and it is only capable of measuring an single point. Multiple wires can be used to calculate flow velocities in multiple directions be the individual filaments can not be completely isolated from convection due to off angle flow.

2.5.4 Electromagnetic induction sensors

As water (and in particular brackish water) has electrically conductive properties, it is able to influence magnetic fields [42]. Electromagnetic induction sensors use this effect by creating a magnetic field which, as the water flows through it, induces a potential difference by an amount directly proportional to the flow velocity perpendicular to the flux lines. Multiple electromagnetic fields can resolve fluid flows across multiple axes. The direction of the electro-magnetic fields generated by these devices is often alternated, inducing a voltage that also changes in polarity which counteracts interfering voltage effects. This technique has also been adapted for tidal velocity measurements, but are limited to a single point measurement at the location of the sensor. As an example, the Valeport 803 ROV Current Meter can measure at 16Hz with an accuracy of 0.01ms^{-1} [43].

2.5.5 Differential pressure sensors

Pressure driven flow meters cover a whole range of sensor technologies that would exceed the scope of this technology review. Included are a subset of those most applicable to the tidal industry. Most flow sensors work on Bernoulli's principle whereby a moving fluid will create a pressure that increases proportionally with the square-root of the velocity, assuming no changes to the ambient pressure. This is often measured by the difference between the pressure due to the fluid flow (the dynamic pressure) and the pressure of the stagnate flow (the static pressure). These devices are generally referred to as differential pressure gauges such as the Pitot tube, commonly used in the aerospace industry.

2.5.6 Piezo-electric Probes

A piezo-electric sensor is composed of a solid surface (often a ceramic) that generates an electrical charge when subjected to mechanical strain. As the pressure increases due to the dynamic pressure the strain on the probe surface will increase creating a voltage. Multiple probes orientated at different angles can be used to measure the velocity fluctuations in multiple axes. One advantage of these devices is that the probe face can be very small allowing measurements of the smaller scales of turbulent flow, particularly as they can operate at sample rates of up to 200Hz [44]. A drawback is that they do not measure the mean velocity thus a secondary sensor is required to give a reference flow velocity for these fluctuations. Similar devices can use a piezo-resitive strain gauge where a deformable diaphragm is strained by dynamic pressure. When attached to a Wheatstone bridge they can be calibrated to calculate the change in output voltage.

2.5.7 Sensor Mounting Solutions

Tidal channel flows vary with separation from solid boundaries, where the frictional processes cause stresses which cause a velocity gradient [45]. With tidal channels being of the order of 50m deep flow

sensors must be mounted $\sim 25\text{m}$ from either the sea surface or the seabed. In the absence of an existing superstructure in the channel to mount to, there are various solutions for taking measurements at the required depths. A selection of the most common solutions are presented : Seabed gravity frames, buoy suspended lines, boat mounted and sub-sea gliders.

Seabed gravity frames and boat mounted systems require instruments that can measure remotely to the $\sim 25\text{m}$ range. A gravity frame is a heavy non-buoyant structure designed such that the frictional force of the frame exceeds the drag force caused by the flow. Instruments are sometimes mounted in a two axis of rotation gimbals-set to allow them to sit horizontal on an uneven seabed. However, the trade off is that forces induced by the fluid (which is often very turbulent in the boundary layer) on the sensor can cause extreme pitching and tilting, thus the stiffness of gimbals (which can be affected by bio-fouling over long deployments) is important. The effect of small dynamic pitching and tilting on velocity measurements can be corrected for in post processing if they are accurately measured. Boat mounted sensors require correction for the boat's pitch, roll and yaw in a similar fashion but with the additional requirement of measuring and subtracting the boat velocity. Small boat designs can also be tethered to a mooring system and used as a stationary surface measurement platform.

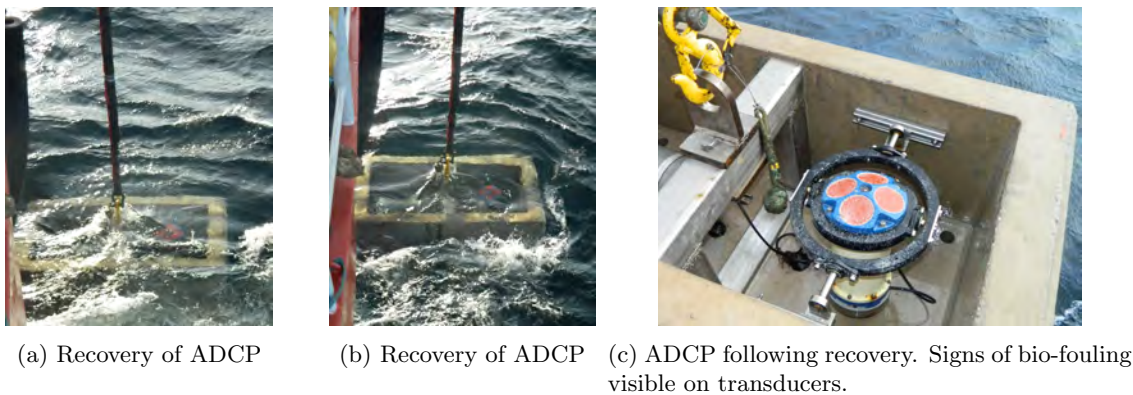


Figure 2.3: Images from ADCP July 2013 Recovery and Re-Deployment

A glider is a remotely operated underwater vehicle tailored to operate smoothly in high flow conditions. A buoy suspended line requires a gravity base as previously described as a tether point for a buoy which provides the up-force and resulting tension in a line to which measurement sensors can be mounted. An acoustic release can be employed to release the equipment without needing to retrieve the gravity base.

All these solutions (with the exception of a non-gimbaled gravity base) have multiple degrees of freedom for the sensor to move which is undesirable and will affect the velocity measurements. This is frequently achieved with a combination of tilt sensors, to measure the instrument's angle in the three rotational degrees of freedom and/or accelerometers to measure the speed of the sensor's movements in up to 6 degrees of freedom. This allows correction of the magnitude of the initial measurement and the direction of resolved velocity vectors where required.

2.6 Sub-sea Acoustic Velocity Sensors (Doppler Sensors)

The final sensor technology for measuring flow velocities, is acoustic Doppler velocimetry.

Acoustic Doppler velocimetry techniques, particularly geometrically diverging configurations, are widely used in the field measurement of offshore flow velocities due to the relative ease of configuration and installation, unobtrusive flow measurements, as well as the ability to sample throughout the water column. Acoustic Doppler profilers have been successfully used to characterise the mean flow conditions and energy flux in several sites for MF installations [29, 46–49]. Conventional ADPs emit acoustic signals from a number of transducers on a single device. While a variety of beam configurations exist, in order to deduce a three-dimensional velocity measurement, these acoustic beams must be transmitted in at least three directions [50]. The beam directions are therefore necessarily diverging, typically at an angle of $20^\circ - 30^\circ$ from vertical. A conventional D-ADP is shown in Figures 2.4a and 2.3c. Because the velocity measurement of each beam is calculated from the Doppler shift (resulting from the scattering of sound by suspended particles in the water) the velocity component is measured in the direction of the beam itself.

These sensors are the most commonly used in tidal channels as, unlike all the other technologies discussed, they can measure the flow remotely at a significant range from the device. This means they can be mounted on the seabed, which is the simplest mounting option, and still give hub-height flow measurements. This section gives an overview of the technology and the variety of available device configurations which utilise it.

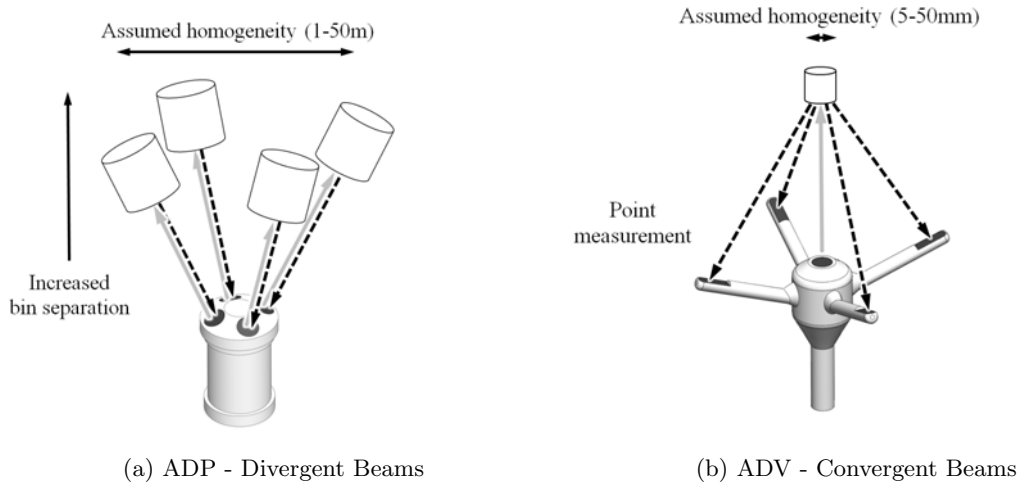


Figure 2.4: Comparison of beam directions for representative a) D-ADP and b) ADV instruments. The gray arrow in the direction of the sample volume represents the transmitted acoustic signal, and the dashed black arrow in the direction of the receiver represents the reflected signal.

2.6.1 Doppler Theory

A Doppler sensor has a transducer that transmits an ultrasonic pulse or ‘chirp’ into the water. The path of this pulse through the water is referred to as the ‘beam’. As this chirp passes through the water it is reflected by particulate matter (of the order of 1-30mm in size) suspended in the water. These particulates are known as backscatters. As the reflected pulse is not reflected by the water itself, it is a key assumption that the particulates move with the same velocity as the water. At the end of transmitting the pulse, the transducer acts as a receiver and listens for the response from the

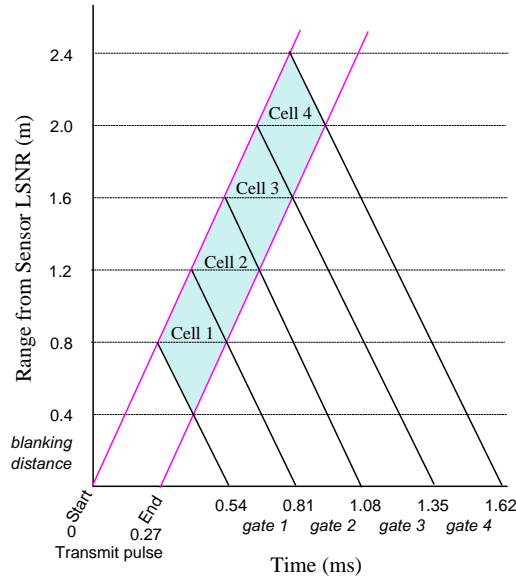


Figure 2.5: Example of range gating for a sensor with a bin size and blanking distance of 0.4m. Image adapted from [51].

reflections back along the beam axis. The reflected beam will be affected by an effect known as the Doppler shift.

The Doppler shift is a phenomenon discovered by Austrian physicist Christian Doppler. It states that if the source of a wave is moving relative to an observer, the observed wave is compressed or expanded as a function of the velocity component along the observer's line of sight [51]. A commonly given example of this is a siren on an ambulance which is raised in pitch (frequency) as it comes towards an observer (as the waves are compressed) and falls in pitch as it moves away as the waves are stretched.

The change in frequency ratio is proportional to that of the flow speed relative to the speed of sound in that medium. The relation is given as:

$$f_d = f_{pulse}(u_{beam}/C) \quad (2.28)$$

Where f_d is the shifted frequency, f_{pulse} is the transmitted pulse frequency, u_{beam} is the fluid velocity along the beam axis and C is the speed of sound in the appropriate medium, in this case sea water. It is this frequency shift in the reflected signal that allows Doppler velocimeters to estimate the velocity along each beam.

2.6.2 Range Gating

The acoustic pulse will theoretically travel on indefinitely through whatever medium, losing power as an inverse square of distance. Thus reflections from backscatters are also constant. This means the received signal has to be processed in sections. The receiving phase of the transmit-receive cycle is divided into even sections based on a fixed time period. This time period corresponds to the reflections from even measurement volumes. Each of these volumes is referred to as a range bin.

This process is illustrated in figure 2.5. The gap between the end of the transmitting of the pulse and the start of the first listening period is known as the ‘blanking distance’. 2.5 shows that the cells are weighted towards the centreline of the measurement volume for a cell. In reality the beam will spread out with separation from the sensor and thus measurement volumes increase slightly with range.

2.6.3 Design Variations

Some sensors have only a single range bin. Others can have up to one hundred depending on the design. The general design trade off is range versus resolution at the expense of increased random error. A lower frequency pulse will travel further through the water but requires larger cell sizes to process the received pulse without increasing noise. A higher frequency instrument can resolve very small spatial scales and has a lower random error associated with it, but the range can be limited to a few centimetres.

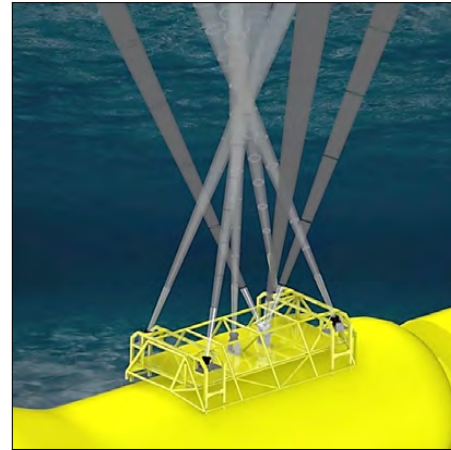
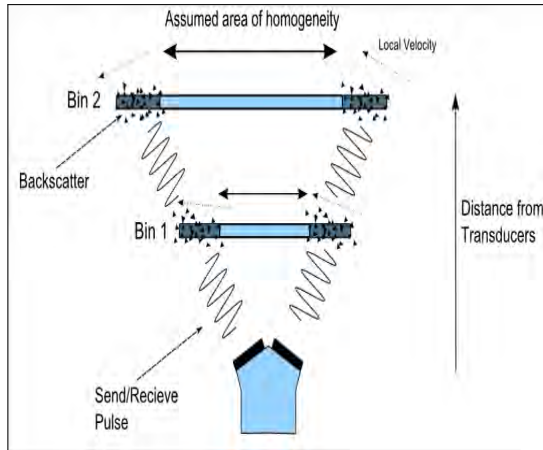
In addition to range, the main design variation is the number of transducers used. A single beam can only resolve one velocity component along the angle of the beam. With three beams three velocity vectors can be resolved, although many designs employ a fourth beam in order to generate an additional vertical velocity estimate. Having two measurement of the same velocity vector allows an error velocity to be calculated which is a good indicator of measurement quality. Finally, where wave measurements are of interest an additional vertical beam can be used to track the surface elevation.

Subsea Doppler sensors can be split into two basic types: Diverging Beam Doppler Profilers (DBDP) and Acoustic Doppler Velocimeters (ADV). DBDPs are short to long range field sensors that employ three to five transducers, each of which act both as a transmitter and a receiver (see figure 2.4a). They are able to resolve three velocity vectors and are available in configurations optimised for different range and accuracy trade offs: from 8Hz sample rate, 2 MHz pulse frequency over 1m range [52], to 1Hz sample rate, 190kHz pulse frequency over 300m [53]. The ADV has one transmitting and three to four receiving transducers around it, all angled to focus on a single measurement volume, generally resolved into a single cell as shown in 2.4b. They can operate at high sample rates (up to 200Hz output with internal sampling above this rate) but are limited in range to $\sim 3 - 10\text{cm}$ [54].

In addition, single beam variants of these profilers have recently been released. These are designed for situations where they can be easily mounted in the centre of the water column such as on a tidal turbine. These sensors were widely used in this work.

Since 1991 Doppler sensors have greatly improved with the use of ‘broadband’ technology in many instruments, as supposed to the precursor ‘narrowband’. A broadband pulse is composed of a repeated pattern of changing frequencies allowing a more accurate assessment of the Doppler shift compared with the single frequency narrowband pulse. This advancement allows the velocities to be resolved with far greater accuracy. Device developer (RDI), claims that it reduces the variance in measurements by a factor of ~ 100 [51]. There is a third type of pulse processing which is called ‘coherent’ where two or more very short pulses are sent with silence between them to allow any ‘ringing’ of the transducer to dissipate before sending the next pulse or listening for the reflected pulse. Sensor manufacturer Nortek have suggested that this technique reduces sensor noise by up to 4 orders of magnitude compared with narrowband technology, but it is limited to short ranges of $\leq 1\text{m}$.

For a comprehensive guide to the workings of DBDP it is recommended that the reader refer to “Acoustic Doppler Current Profiler Principles of Operation A Practical Primer” [51].



(a) Sketch showing assumed area of flow homogeneity on Divergent Acoustic Doppler Profiler (D-ADP) system. (b) ReDAPT Convergent Acoustic Doppler Profiler (C-ADP) concept render.

Figure 2.6: Divergent and Convergent Acoustic Doppler Profiler (C-ADP)

2.6.4 Relative Advantages and Limitations of Doppler Sensors

A key advantage of acoustic technology, in particular of DBDPs, is the ability to take readings remotely and throughout the water column. Devices can be mounted on the seabed in a relatively fixed position and take three vector water measurements up to the surface. The uncertainty involved with constantly moving floated sensors is high and only gives a single point in the water column. Having a fixed body is often impractical and (if large enough) will impede the flow. This has made DBDP a standard technology for characterising potential tidal sites.

In order to deploy a DBDP a solution for power and data storage must be devised. Most devices use batteries and memory cards, which limit deployment goals. Data readings must often be taken less frequently to maximise the deployment length, which is often desirable as the cost of deploying devices is high. Alternatively a higher data sample-rate can be used at the expense of longevity. The data capture set up along with the range and spatial resolution are decisions site surveyors face to get the most appropriate data for their requirements.

Co-ordinate Transformation

The transformation of the velocity components from the beam direction to the instrument coordinate system requires the assumption of flow homogeneity [55]. That is, the velocity vector transformation assumes that the velocities in sample bins at the same distance from the transducer are identical. This is often a reasonable assumption for mean flow velocities, which typically do not vary considerably within the spread of the acoustic beams.

In energetic tidal flows, the instantaneous flow velocity is seen to vary over a wide range of time and length scales. Coherent turbulent structures smaller than the distance separating the diverging beams of D-ADPs at a given elevation are unable to be resolved. Large scale eddies, although greater in scale than these beam separations, are misinterpreted through conventional D-ADP processing algorithms [56]. Furthermore, Doppler noise is an inherent feature of the measurements arising

from this technique. While able to be removed in post-processing of bulk statistics [57, 58], the contamination of the signal by this white noise limits the use of the instantaneous velocity time series acquired using existing D-ADP configurations.

Acoustic Doppler velocimeters (ADV), like D-ADPs, also use the Doppler shift of an acoustic signal to determine the beam-wise velocity components of the flow but operate in a converging beam configuration. A single point is measured, as shown in Figure ??, as opposed to a pseudo-central point located centrally between diverging beams in the case of a D-ADP. The ADV operates in a bi-static mode, where the receivers are not collocated with the transmitter. Through the converging beam arrangement, the sample volume of all three beams is coincident and velocity perturbations with significantly reduced length scales can be resolved. Additionally, an ADV takes advantage of its smaller instrument dimensions and distance to the focal point to allow both higher emitted acoustic and sampling frequencies.

ADVs (both commercial and bespoke) have been used successfully in a range of laboratory and field applications including localised velocity measurements [59–63] and sediment transport studies [64, 65].

A significant limitation in ADV technology’s applicability in the field of offshore flow measurement is the relative difficulty in installing the instrument at distances from the seabed and other flow-affecting structures. Furthermore, simultaneous velocity measurements throughout the depth of the water column are not available using a single device. With the sample volume located within 100 mm from the instrument, measuring the flow at a significant distance from a conventional mounting structures is practically reduced. In recent studies, multiple ADVs were mounted on compliant moorings to achieve measurement locations at significant distance from the seabed [21, 66]. The velocity signal is corrected for instrument motion using the simultaneously measured instrument accelerations, with promising results. The measurement of high resolution velocity profiles has been achieved using a number of recent ADV designs [65, 67], however the range remains small for this application in the order of several tens of centimetres.

2.7 Site Characterisation: Wave Measurement Technology

2.7.1 Wave buoys

Update re influence of current on moorings, performance and survivability

Since the pioneering work of Longuet-Higgins et al. [68] buoys have been deployed for monitoring the wave field and meteorology over the ocean. Buoys provide good quality wave height, period and often direction measurements but suffer from poor spatial coverage. Whilst proven technology, wave buoys remain expensive to build, deploy and operate. In the case of large, offshore and long-term monitoring buoys deployment, maintenance and removal involves the use of expensive vessels. Being located on the surface, buoys are exposed to shipping, fishing and storm damage/loss.

Wave buoys intended for long open ocean deployments are usually of diameter of several metres. The large diameter arises from having to carry a large payload (instruments and moreover power supply) whilst supporting heavy mooring lines. These buoys suffer from lower resolution compared with small buoys such as the Datawell, waverider, as their ability to track the moving surface is hindered by higher inertias and mooring influences [69]. Smaller buoys intended for shorter period deployments can be lightly moored on elastic, compliant moorings. Even so incidents involving buoys becoming

detached from their moorings are not uncommon. The availability of micro-electro-mechanical sensors (MEMS) offers the ability to reduce the volume and weight of a buoy sensor payload therefore reducing the diameter of floatation material needed. Previous buoys contained a large mechanised platform which adds undesired weight and load on the power supply. The Hippy 40 sensor package (a gravity-stabilized disc surrounded in a liquid inside an aluminum cylindrical can) is an example of this type of sensor package and forms the benchmark device against which new buoys are measured [70].

Buoys have been traditionally deployed for marine weather forecasting for the shipping/fishing industry and for storm warnings. The timeseries generated are processed on board the buoy and the summary statistics of a selected period (typically 20 minutes to meet the requirement of pseudo-stationarity for spectral processing) are transmitted. This level of data may not be sufficient for the marine renewable sector where access to the raw time series is needed, either in near real-time or after a deployment for post processing. As is to be expected in the dynamic marine environment, the quality of these time series can be variable and can require extensive post processing [71].

In summary, buoys are the standard method for providing spectral parameters (including directional information) at a *point* in the ocean and the recently completed Equimar project recommends their use in offshore renewable resource assessment [72]. Further advances in buoy technology may be required for the renewable sector leading to smaller and lighter buoys capable of supplying full raw data via high bandwidth telemetry. By residing on the surface and therefore having access to through-air telecommunication frequencies buoys have an advantage over their submerged competitors and can access cellular, radio or satellite communication networks.

2.7.2 X-Band radar

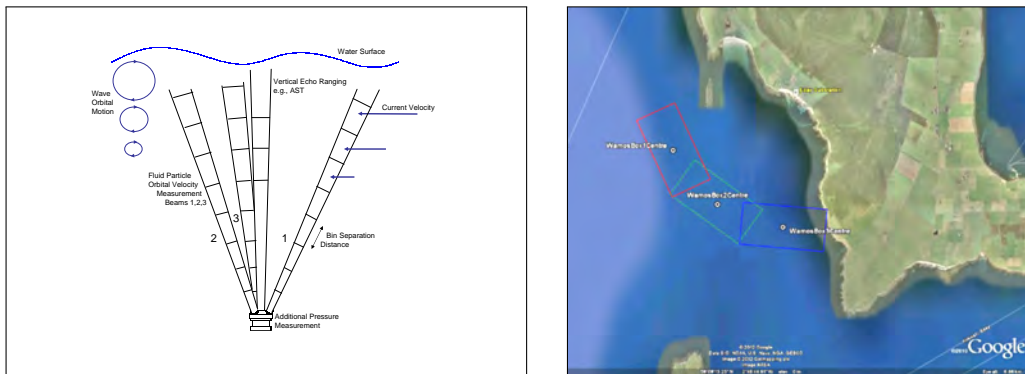
Commercially-available X-Band Radar can be installed on fixed (e.g. offshore oil installations, lighthouses) or moving (e.g. vessel-based) platforms. Operating on the principle of measuring the backscatter of radar energy from the ocean surface they offer massive spatial coverage improvements over Buoys with a typical system being able to cover a swept area of radius 2km at a spatial resolution down to 10m. Systems include Miros, WAVEX and OceanWaves WaMoS II. Shorter range, higher resolution set-ups exist, using a system covering an area of 20x20m with a resolution of 0.4m [73]. For spectral sea-state parameters H_{m0} , T_p , etc. X-Band Radar-based techniques have been shown to give good agreement (in trial conditions) with other measurement methods such as Buoys [74, 75]). However, these are averaged parameters and do not give information about individual waves. Recent software developments such as the DWFA algorithm in WaMoS II can identify individual waves from a radar image through linear wave theory as the basis of an inversion technique. Typical systems suffer from poor temporal resolution ($\Delta t=2.5s$) limited by the rate of rotation of the radar emitter and the number of images required for analysis and in addition may not be able to pick out wave heights below 0.5m [74]. Recently, an X-Band radar in conjunction with the inverting software was used to measure sea surface elevations. The results were compared to a co-located wave buoy with the sampling rate of this buoy reduced to allow comparison to the radar and software system. Although there is general agreement, large errors are present particularly in wave amplitude [76]. Since the heights are picked out by an algorithm this could possibly be tuned to reduce errors but importantly a benchmark data set would be required. Other manufacturers include Nortek's SeaDarQ which whilst primarily used for oil spill detection will be undergoing trials (2015/2016) in wave measurement applications [77].

A WaMoS II system is installed at EMEC with the antenna positioned on the island of Eday overlooking the Fall of Warness. The measurement campaigns were conducted in parallel - but outwith - the ReDAPT and University of Edinburgh's MD site characterisation work. A sample of post-processed

results supplied to UoE is included in section ((3)) for reference.

2.7.3 Acoustic Doppler Profilers

Whilst measuring the Doppler shift of suspended particles in a water column and inferring the surrounding fluid's velocity was originally intended for use as a tool in current flow measurement this **principal** is being increasingly used to measure waves. Being situated on the seabed reduces the risk of shipping damage to an ADP but large forces remain which can lead to data loss and sensor damage (an example of which can be seen in [78]). Design and implementation of the locating frame are critical to an ADP's deployment and operation. Experiences such as during the Strangford narrows programme suggest that frames have to be extremely robust to survive prolonged deployment leading to installation difficulties for diver teams [79]. Fig ?? shows the configuration of a Nortek AWAC on a tripod frame with auxillary battery and data storage cannister.



(a) Schematic showing **principal** of AWAC ADP in wave measurement mode. (b) Screenshot of map of Fall of Warness showing WaMoS regions of measurement. From EMEC (IPRTBC)).

Figure 2.7: .

Some ADPs (e.g., RDI Workhorse Sentinel with Waves Upgrade) give directional wave data using software to convert orbital velocity measurements into wave frequency and directionality. The software makes use of linear wave theory to derive elevation. The Nyquist theorem dictates a maximum bed depth for a required surface wavelength resolution. At 50m depth and dependent on beam alignment an ADP can resolve only waves above approximately 3.5 seconds and, in terms of the directional spectrum are further limited to periods of approximately 6 to 9 seconds [80], [81].

The Nortek AWAC with Acoustic Surface Tracking (AST) measures wave direction, surface elevation (wave height). The AST echo-ranges to the surface using a vertically orientated (if the instrument is deployed level) transducer. This allows the measurement of short period, locally-generated waves and can output either time series histories of surface elevation or the summary statistics as produced by wave buoys. Via a co-installed pressure sensor the user has the ability to select to process wave time series through either the PUV method or SUV method.

ADPs often store the data onboard with battery life of the order of six months to a year depending on configuration. This data is retrieved at the end of the deployment after instrument recovery. If data is required on-the-fly there are several methods to achieve this including a cable to shore (up to 5km using RS422 protocol) [82], acoustic modems to shore or acoustic modems or cables

to either a hard-wired asset (e.g., tidal turbine) or a surface platform which can then relay via radio/satellite/GSM.

2.7.4 HF Radar

High Frequency (HF) Radar emits radio waves from ground base stations with wavelengths in the range 10-100m and can sense from 10km out to 200km with resolutions decreasing with range to a maximum of a few hundred metres for short range set-up [83]. Whilst it operates under the same principal as X-Band systems the longer electromagnetic wavelength explains the greater range but reduced spatial resolution. Accuracy of the directional spectrum and derived wave parameters depends on radar power spectrum frequency resolution, temporal and spatial variability in the measurement cell, angle between two radar look directions, antenna sidelobe levels, and waveheight, noise, and interference levels [84]. Algorithms have been developed to process the radar images to extract sea-state parameters. HF Radar's use as a current measurement device is well established but there is some debate as to its ability to measure accurately these sea-state parameters. RF Licensing, interference and planning issues also affect the implementation of the technology [74, 76].

HF radar comprises two types: phased-array radar e.g., ocean current surface radar (OCSR) and Pisces, and direction-finding radars e.g., coastal ocean dynamics application radar (CODAR) and SeaSonde [84].

Experience from the 2003-2005 trial of dual Pisces deployment (intersecting beams from north Devon and South Wales) suggests that significant wave heights below 1m are unreliable. [84] Further, accuracy in period and mean wave direction increases with even larger sea states of 2m and above.

There may be scope for improved radar performance by altering the frequency based on the changing environmental parameters including interference and wind, precipitation, wave climate. Using the WERA radar system which is a hybrid of both phased-array and direction-finding radar, the EU-funded EuroROSE experiment in Fedje, Norway suggests that HF radar may have limitations in its ability to cope with sudden changes in wave climate. This limitation may be a result of minimum reliably measured wave frequency of 0.35Hz inherent to the system's scanning frequency. [83]

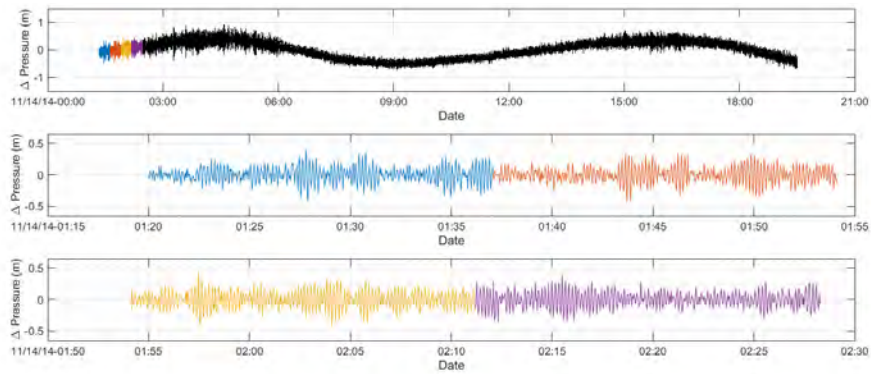
2.7.5 LIDAR

Light Detection and Ranging systems (LIDAR), whereby light of a choice of frequencies (from UV to near infra-red) is used to highlight a surface and report the range to that surface, have been used widely in atmospheric and terrain mapping fields. In the context of oceanography they were first developed for aerial surveying of coastal bathymetry and were later used in underwater obstacle detection tasks [85]. These lidars were operated at a near normal angle to the surface. A more practical installation for the use in measuring wave fields in the shipping, oil and gas and renewable sector would be vessel mounted lidar systems which would negate the inability of moving systems to continuously measure a fixed region. These would be able to monitor the vicinity around a vessel, rig or WEC but would be operating at much shallower angles (limited by the tower height). Difficulty arises in the signal processing of the very weakly returned and heavily scattered light. In one trial processing power is dynamically allocated depending on the distance from the optical radar and the condition of the signal [85]. This is typically used line scans where the wave field is sampled at various points in a line away from the radar. This technique can be expanded to planar scanning, where the emitter and receiver would sweep a field of view and build up a wave field from many line scans.

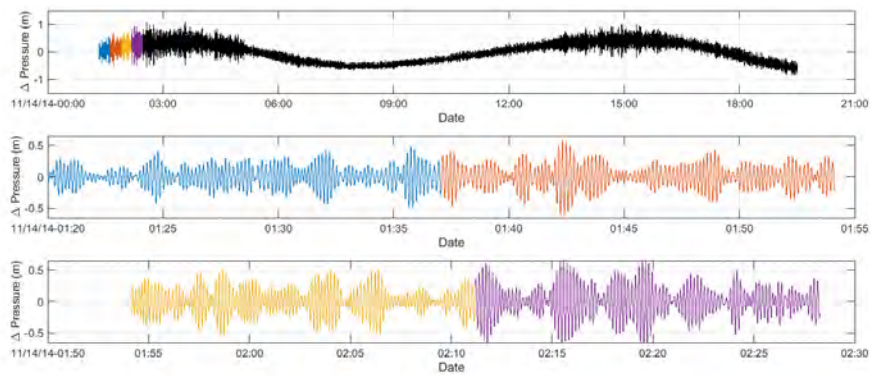
Evidence to support the utility of remote sensing technologies (both radar and laser systems) in the field and in the absence of absolute references comes from the WACSIS project [86] where good agreement was found between wave measurements taken via collocated laser and radar instruments - despite their varied measurement techniques [87].

2.7.6 Pressure gauges

Bottom mounted pressure transducers have been used for a long time (since around 1947) to measure surface elevation. A good example of their use is their configuration in bottom mounted directional-sensing arrays as part of the DUCK, USA instrumentation trials in the 1990s [88]. They benefit from being out of harm's way regarding surface traffic and comprise relatively cheap components. As information from the surface is attenuated through the water column accuracy falls off with depth. However, non-linearity of the surface profile is stronger in shallow water and careful handling of the pressure data to reveal surface elevation is needed in this regime to maintain accuracy [89]. Further consideration of the pressure to surface elevation transfer function is required in the presence of strong currents. The form of these frequency dependent transfer functions can lead to rapid increases in errors and can only be used reliably within defined wave frequency bands depending on installed depth. Pressure transducers are often used to provide complimentary data to other methods (such as acoustic surface tracking) where their disadvantages are offset by their reliability and insensitivity to sources of acoustic noise such as bubble formation from breaking waves. Figure 2.8 shows pressure data recorded during ReDAPT for a seabed mounted ADCP and a turbine-mounted high frequency pressure gauge during winter storms of 2014.



(a) Pressure time-series measured using seabed mounted ADCP.



(b) Pressure time-series measured using turbine mounted gauge.

Figure 2.8: Variations in pressure measured from seabed-mounted ADCP pressure gauge sampling at 1Hz and mid-depth-mounted pressure gauge sampling at 10Hz during ReDAPT project in large storm waves, November 2014

Chapter 3


Site Characterisation at FoW

3.1 Overview of the Measurement Campaign

Phase I Activities

Preliminary work within MD3 involved identification and discussion of the numerical modelling techniques proposed and to subsequently identify the fluid velocity measurement requirements of these numerical modelling activities. Thereafter the extent to which these measurement requirements could be met within ReDAPT was investigated and a prioritisation and scheduling of these measurements developed. Once complete, the instrumentation and measurement specification was used to design, procure and assemble instrumentation systems. This process was conducted in parallel with the design work of the Alstom 1MW DEEPGEN IV.

Phase II Activities

In order to de-risk later deployments and gain some experience of the returned data , deployments were sanctioned and conducted on the already available Alstom 500KW DEEPGEN III.

In 2012 UoE instrumentation systems were installed and commissioned on the now available 1MW machine.

Phase III Activities

3.1.1 TRNs

Summary of Test Request Notices including key tests and lessons learned from the project-integrated test method.

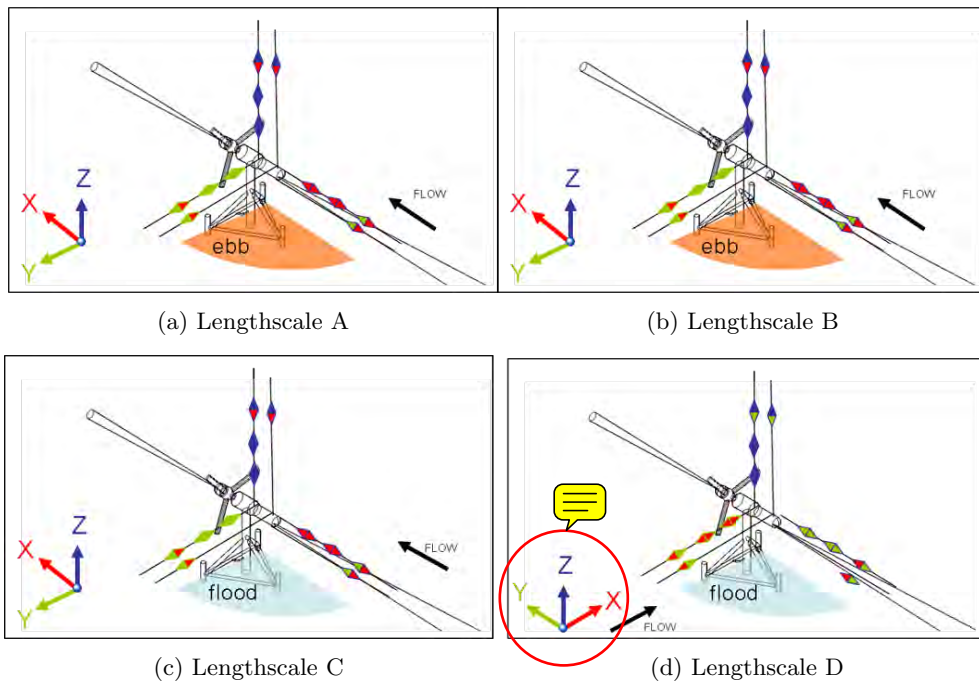


Figure 3.1: TRN Planning Schematics: Target Lengthscales

3.2 QC and Analysis Methodology

This section outlines the processes applied to data from instrument to database. It includes a list of required software both proprietary and open-source. Topics covered:

- Data Conversion
- Data Transfer, Storage and Logistics
- Data Quality Control and Data Rejection
- Data Averaging
- Metric Production

3.2.1 Coordinate Transformation

Outline of process in going from instrument beam coordinate system to instrument Cartesian (where applicable e.g., ADCP) to global Cartesian: Streamwise, Transverse and Vertical.

3.2.2 Out of Range Velocity Rejection

3.2.3 Low Amplitude Rejection

3.2.4 Median Absolute Deviation Rejection

3.2.5 Hardware Reported Error Code Rejection

3.2.6 Stationarity Period Selection

Stationarity period selection summary: Statistical scoring techniques applied to ADCP data set. Intra-variation and impact on turbulent metrics. Gives confidence in 5 minute period used throughout but raises questions going forward.

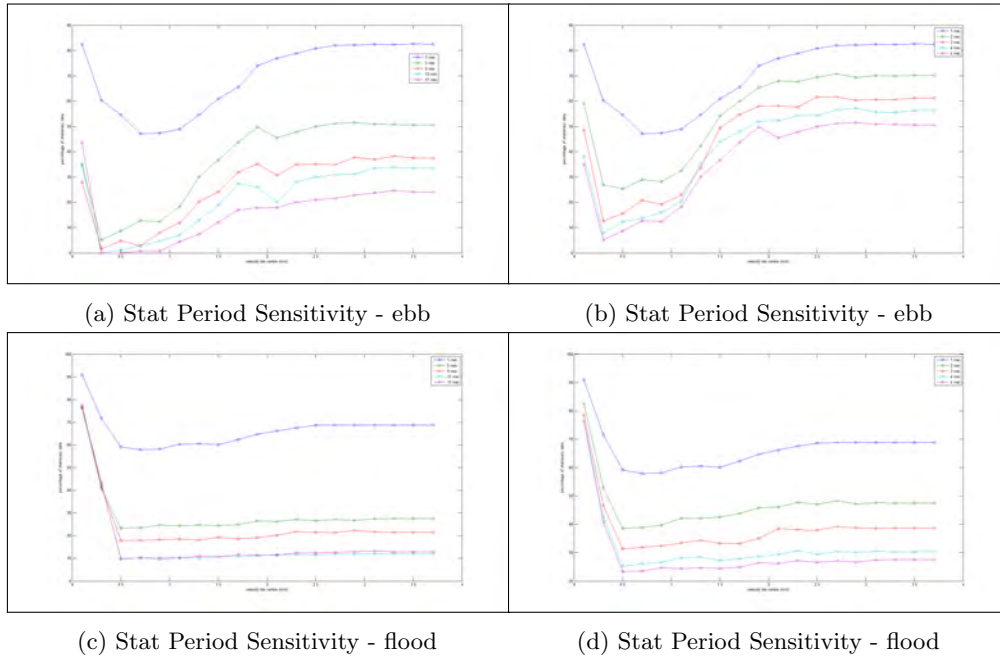
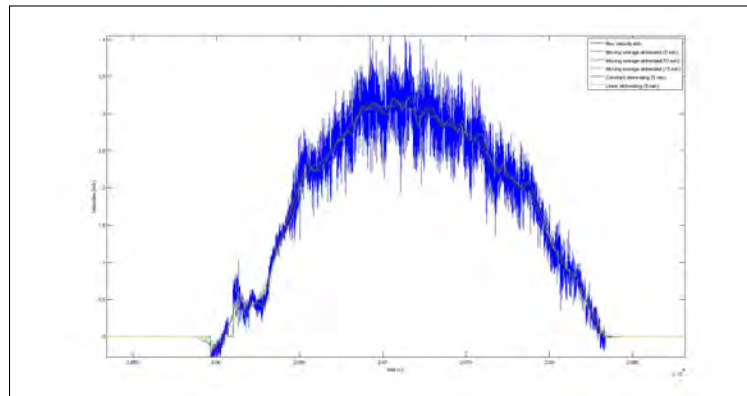


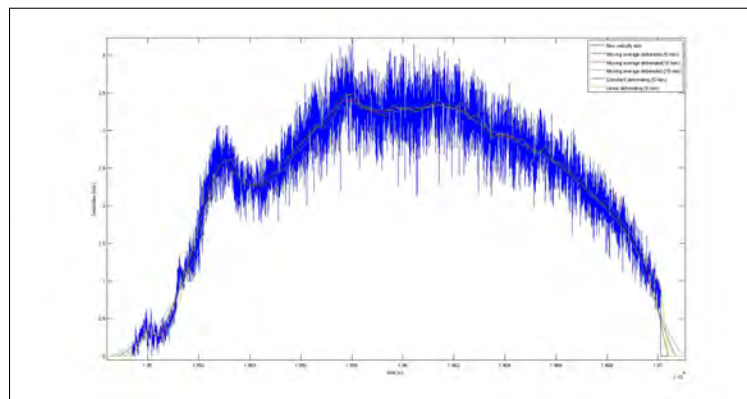
Figure 3.2: Stat Period Sensitivity: TBUpdated for clarity. Flood and Ebb

3.2.7 Detrending Method Selection

Detrending methods summary: mean, linear, moving average. Intra-variation and impact on turbulent metrics.



(a) Detrending methods - flood



(b) Detrending methods - ebb

Figure 3.3: Detrending methods: various. TBUpdated for clarity

[Impact on individual data segments under various system states](#)

[Summary Trend Graph](#)

[Summary Table](#)

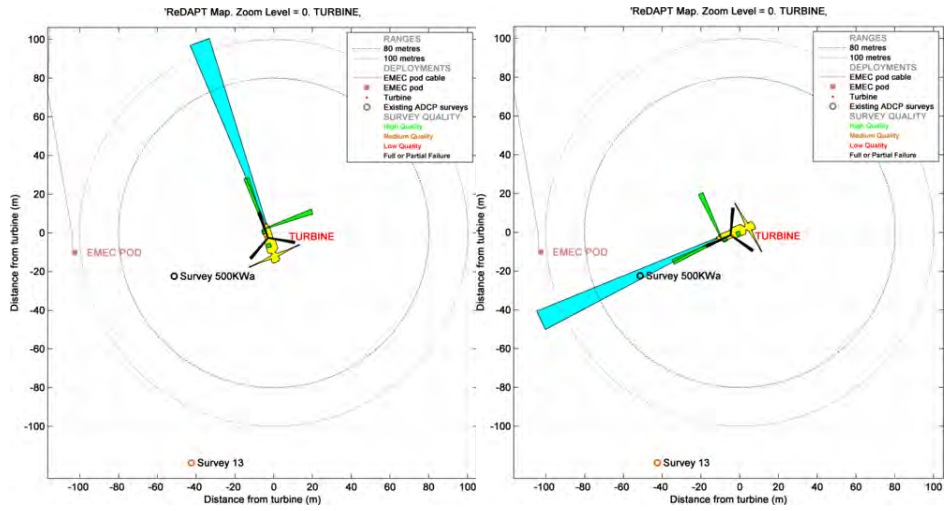
Detrending	Reference velocities	Turbulence intensities	Turbulence intensities	Velocity filter
			Comparison Constant, linear, moving average	
Constant ebb	Accounts for real flow quite well, but some non turbulent features of the flow are missed	Has expected values and behaviour as a function of the velocity.	- Lower boundary for the turbulence: moving average with lowest window	Mean error : - 0.84 % (in TI, not relative) without filter - 0.77 % with filter applied
Constant flood	Same as ebb	Same as ebb	- Average differences: C - MA: -0.32 % L - MA: -1.38 % for flood L - MA: -1.17 % for ebb	Mean error : - 0.91 % (in TI, not relative) without filter - 0.83 % with filter applied
Linear ebb	Strictly equivalent to constant detrending	- Good agreement with constant. - Mean difference with constant: 0.83 % - Linear < Constant (Always).	_ On average, best agreement between Constant and Moving average, for both flows.	Mean error : - 1.45 % (in TI, not relative) without filter - 1.43 % with filter applied
Linear flood	Almost equivalent to constant detrending (98% of data is the same)	Good agreement with constant. - Mean difference with constant: 0.98 % - Linear < Constant (Always).		Mean error : - 1.63 % (in TI, not relative) without filter - 1.63 % with filter applied
Moving average ebb	For averaging windows > 8 min, a lot of flow features are missed. For small windows (<1 min, but this is not well defined), the velocity is turbulent, and the effect of averaging is null	- Likewise, has expected values and behaviour - But differences occur between small and big windows - The biggest differences occur when the second derivative of the velocity reaches extreme negative values		Mean error : - 0.65 % (in TI, not relative) without filter - 0.68 % with filter applied (With a window of 5 min)
Moving average flood	Same as ebb	- Same as ebb, but biggest differences are more pronounced		Mean error : - 0.72 % (in TI, not relative) without filter - 0.80 % with filter applied (With a window of 5 min)

(a) This table to be translated to quantified summary table!

3.2.8 Instrument Noise and Noise Correction Factors

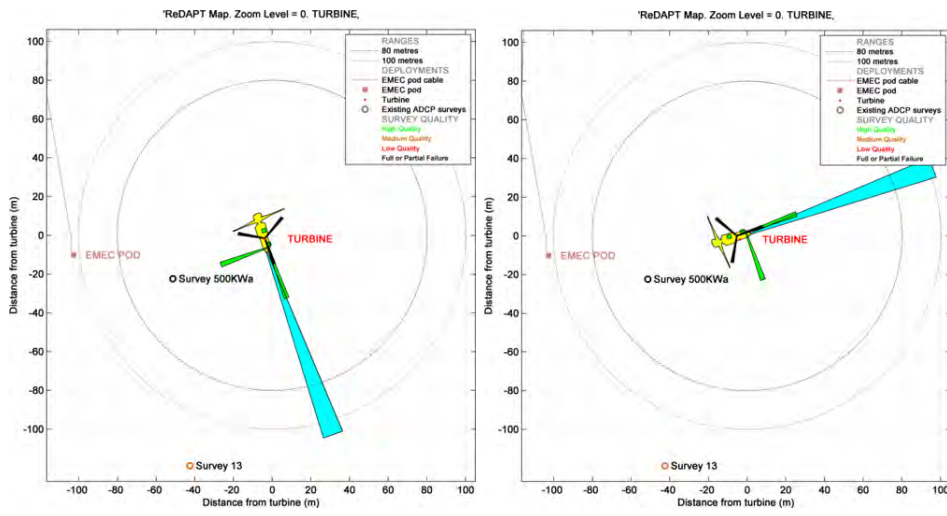
Duncan PhD Noise Correction Summary

Summary Table



(a) Reversed to Flood

(b) Broadside to Flood



(c) Reversed to Ebb

(d) Broadside to Ebb

Figure 3.5: Turbine Scheduled Orientations

3.3 Measuring Waves at the Fall of Warness

It was agreed at programme onset that wave measurement would form an auxiliary and non-core component of the ReDAPT measurement campaign. It transpired that a large proportion of early to mid-campaign data acquisition was carried out in the summer months due to programme schedule, logistics and technical issues. Following completion of core current data collection in October 2014, supplementary data was acquired in volume in the subsequent winter months through to January 2015. During these months several storms were observed for the first time and the impact of waves in these conditions on the data set became apparent.

Due to the non-continuous acquisition of wave data and low prioritisation of analysis previous to this deployment and the requirement to re-analyse the data set including wave data, significant resource has been expended assimilating an auxiliary and in places patchy data stream with the core tidal current data. The following section describes this process of assimilation.

For clarity, much of the following activity goes beyond the scope of the original report and will be continued by the authors in 2015.

3.3.1 Acoustic Surface Tracking with Vertical ADP

Multiple SBDs were installed on both the 500KW and 1MW via ESIP-1 in a vertical orientation wrt turbine on quayside stand. Initially these instruments were solely used for flow measurement in the vertical direction. Inspection of the data later revealed a strong correlation between large gradients in amplitude return and the air-water interface (sea surface). Thereafter, where possible within a specific test programme, vertically mounted SBDs were programmed to have an extended listening range to provide sufficient head-room of range in order to pick up the acoustic surface return from the surface. An example of SBD AST is shown in figure 3.6.

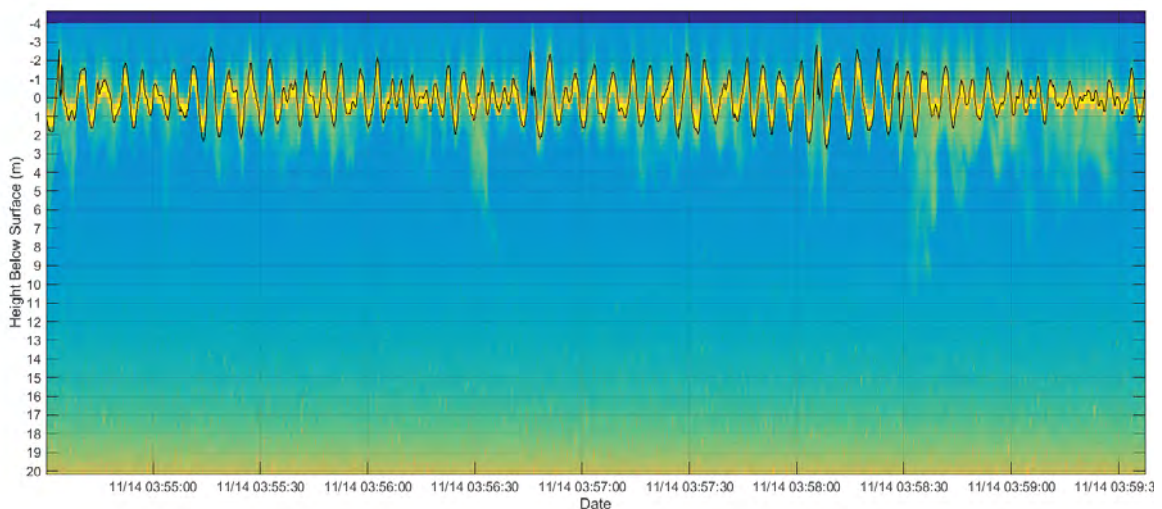
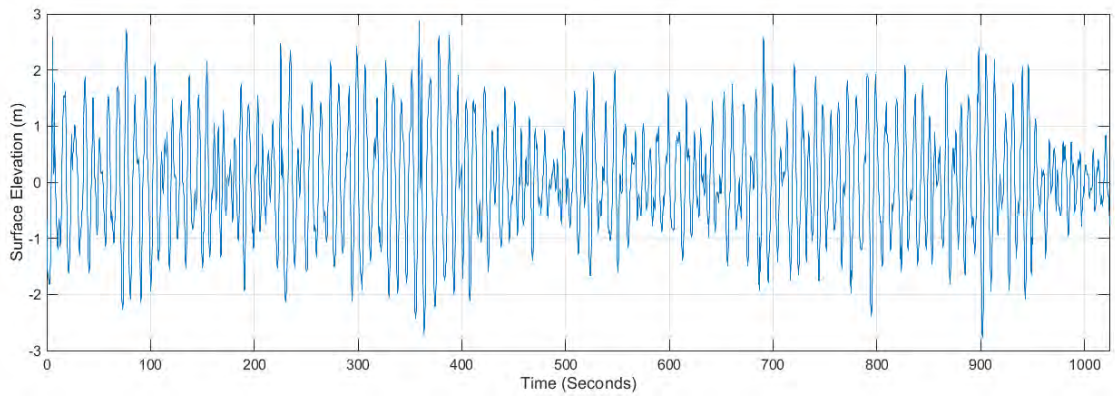
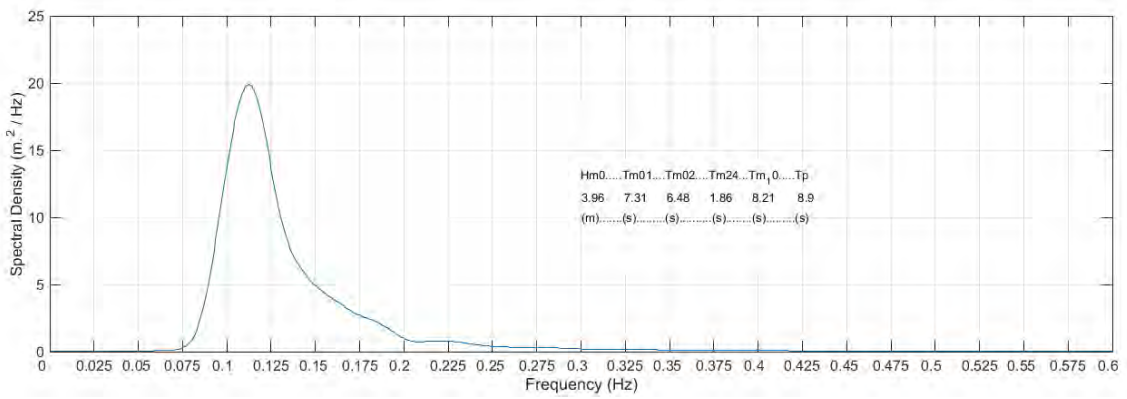


Figure 3.6: Signal Amplitude with post-processed surface elevation overlaid (red). 

Outline Processing Steps

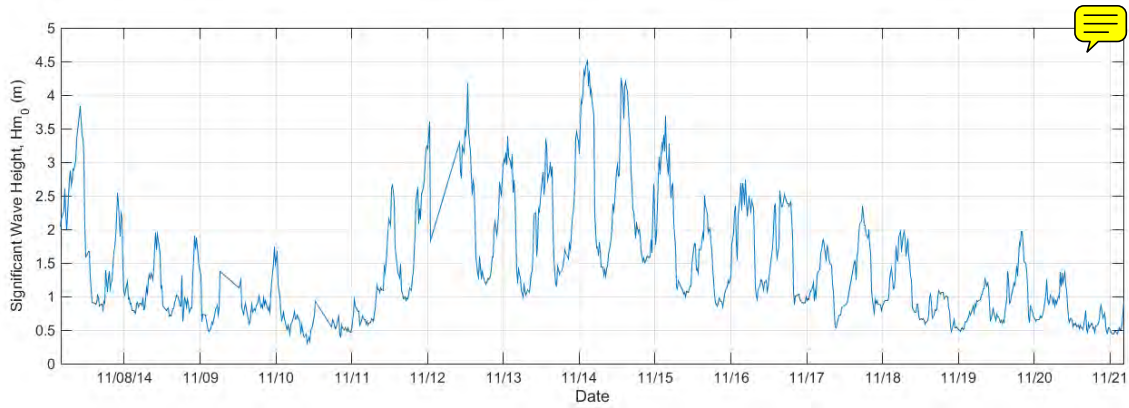


(a) Result of image processing: moving surface tracking, edge detection, filtering



(b) Spectral Analysis to provide wave spectral parameters.

Figure 3.7: A figure



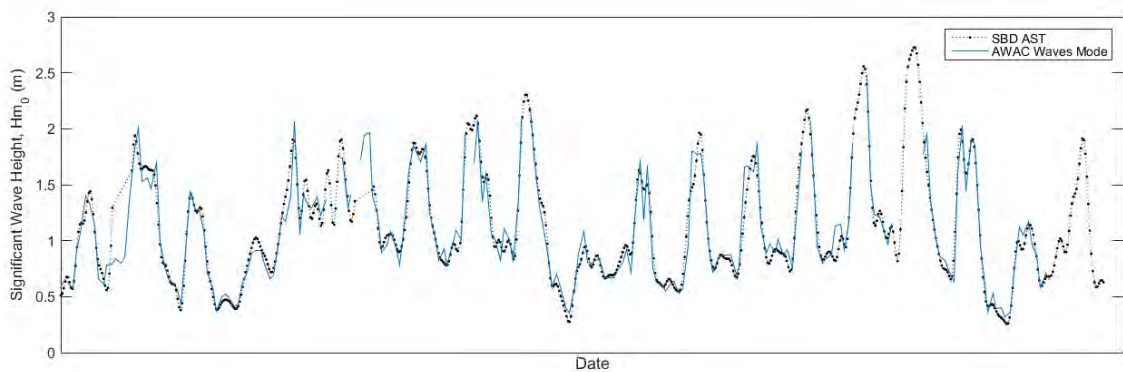
(a) Individual spectral analysis collated into database signal time-series of Hm_0 .

Figure 3.8: A figure

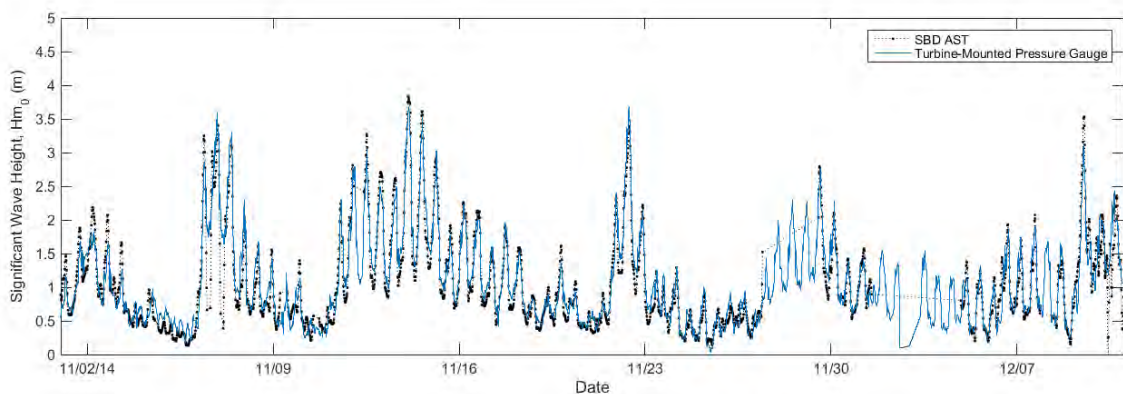
- Raw instrument data of one hour duration converted from proprietary format to MATLAB format.
- Data collated to 24 hour sections.
- 24 hour sections QC'd.
- Data re-categorised by instrument configuration (varying bin size, sample rate etc.).
- Image processing routines used to select best local fit to air-water interface.
- Time series extracted.
- Spectral analysis conducted.
- Data collated and interpolated onto standard database 5 minute grid.

3.3.2 Combined Mode - Acoustic Surface Tracking with Vertical ADP and Wave Velocities

A multi-beam D-ADP (Nortek AWAC 1MHz) was installed on to the 500KW turbine and the ESIP-1 on the 1MW turbine. This was remotely controlled over the internet via serial over ethernet extenders. Once high priority tidal current tests were complete this instrument became available to conduct wave studies.



(a) Time series of W-AWAC vs SBD-AST significant wave height, H_{m0}



(b) Time series of Pressure Gauge vs SBD-AST significant wave height, H_{m0}

Figure 3.9: Comparison of W-AWAC and SBD-AST measurements of significant wave height

Whilst wave data is updated and available visually on the instrument’s software GUI, post-processing of recording files is required to extract wave data for further analysis. The software is a separate purchase. Data shown in 3.12 is the direct output from the Nortek software using their proprietary routines [90,91]. Custom algorithms have been developed in MATLAB to post-process Nortek wave software outputs and indeed to produce wave parameters from the raw data itself, thus circumventing the proprietary method. This work is outside of the scope of this document and is not reported herein.

3.3.3 Pressure Gauge

Alstom installed a pressure gauge to the 1MW turbine at a depth of 21.5m and following the winter storms of 2014/2015 supplied this long-running and robust data set. Data was supplied at a sample rate of 10Hz.

Outline Processing Steps

- Alstom supplied time-stamp-corrected pressure gauge data at sampling rate of 10Hz.
- Transfer function applied to pressure data to correct for varying attenuation of pressure rates with depth and frequency.
- Additional transfer function applied to correct for local time-averaged site parameters i.e., wave direction and swell, tide direction and current velocity.
- Constant gain and offset applied across entire set calibrated against SBD-AST.

Equation 3.1 was used to transform pressure spectra to wave spectra.

$$T = \left(\frac{\cosh(kd)}{\cosh(kd_{pg})} \right)^2 \quad (3.1)$$

where d is the total water depth in metres, d_{pg} is the depth of the pressure gauge in metres and k is the wavenumber in rad/m calculated through an iterative approximation of the dispersion relation [92] shown in 3.2.

$$w^2 = gk \tanh(kd) \quad (3.2)$$

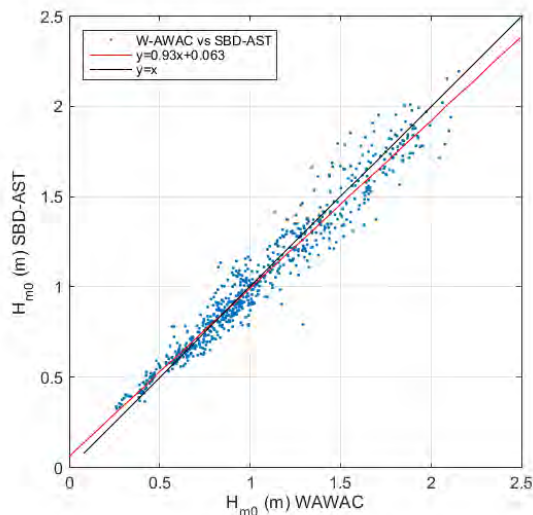
where w is the wave frequency in rads/s and g is acceleration due to gravity.

An experimental additional transfer function which takes into account local instantaneous and local averaged wave and current parameters is under development. The difference in agreement between un-corrected and corrected wave spectra obtained via pressure gauges is shown in figure 3.18.

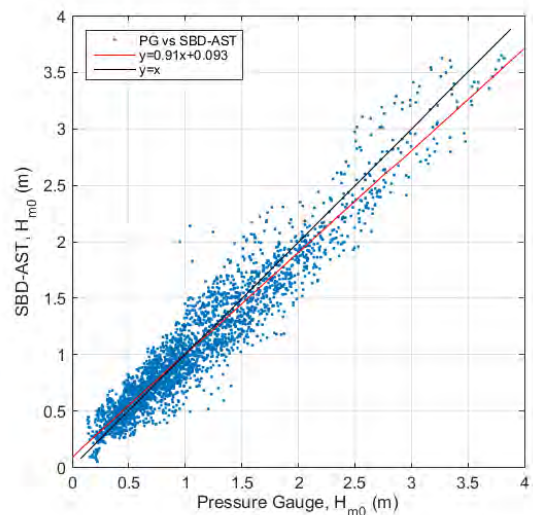
3.4 Velocimetry: Wave Orbital Velocity to Wave Spectra

Outline Processing Steps

- Hourly to 24 Hour
- QC
- Upsampling (Interpolation) and Filtering
- Low Frequency Surface Tracker Applied
- Velocity Bin Selection (moving in time)
- Velocity to Wave Spectra via DIWASP
- Transfer Function as per PG



(a) Comparison of W-AWAC vs SBD-AST significant wave height, H_{m0} and best-fit



(b) Comparison of Pressure Gauge vs SBD-AST significant wave height, H_{m0} and best-fit

Figure 3.10: Comparison of W-AWAC and SBD-AST measurements of significant wave height

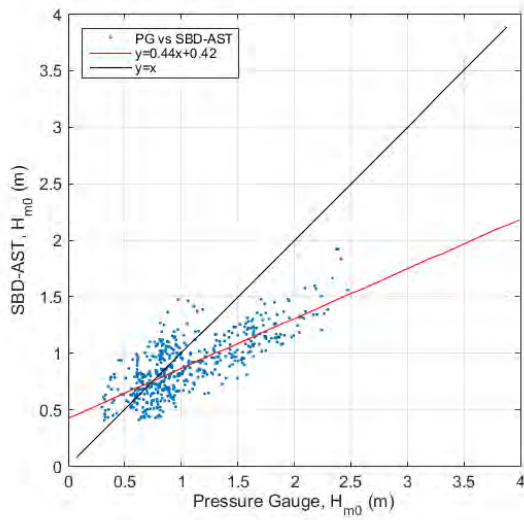
An ADCP sampling rate of 0.5Hz was the primary configuration for most of the turbine-proximal deployments. This resulted from a trade-off between deployment duration and the battery consumption and on-board storage capacity of the instrument. Given how difficult it proved to align turbine operating point, tide and wave system point and the CFD simulations this low sampling rate, whilst sub-optimal for turbulence and wave studies, proved necessary in other components of the ReDAPT test programme. It was unknown if this minimal sampling rate could provide wave information.

3.5 Combined Wave Measurements

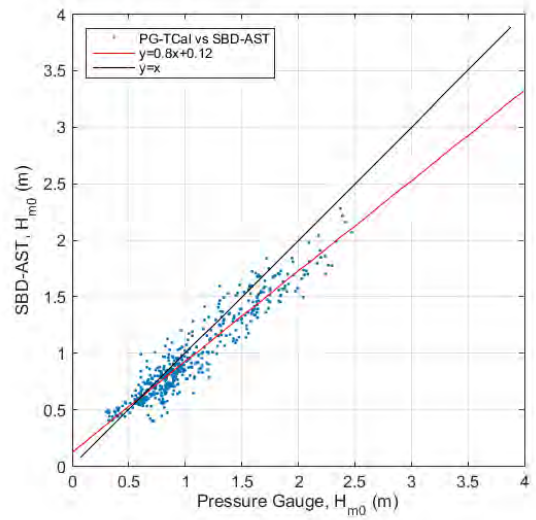


Wave measurements extracted from available instrumentation between 2013 and 2015 are assigned to 5-minute average values within the ReDAPT database with the following ranking:

- 1) AWAC in Waves Mode
- 2) Vertically Orientated SBD
- 3) Wave Orbital Velocity from turbine-upstream and turbine-downstream ADCP.
- 4) Calibrated Pressure Gauge
- Transfer Function as per PG

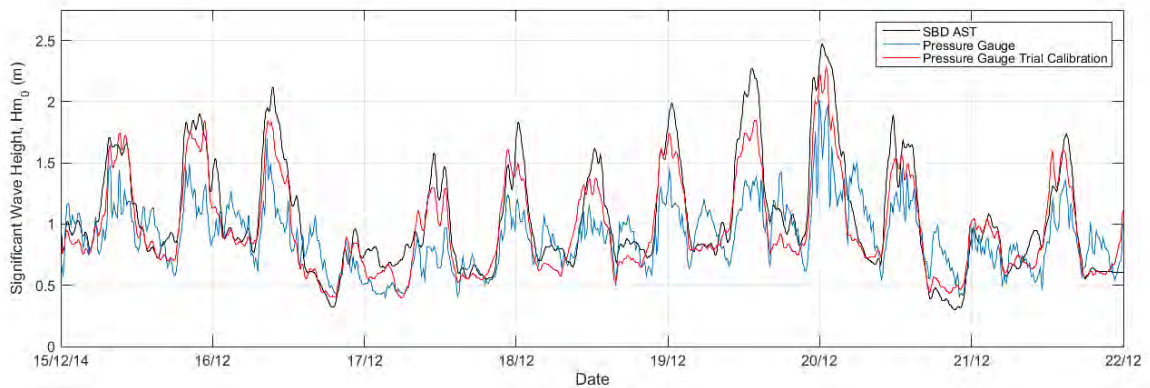


(a) Comparison of W-AWAC vs SBD-AST significant wave height, H_{m0} and best-fit



(b) Comparison of Pressure Gauge vs SBD-AST significant wave height, H_{m0} and best-fit


Figure 3.11: Comparison of Pressure Gauge and SBD-AST measurements of significant wave height under different pressure gauge calibration routines.

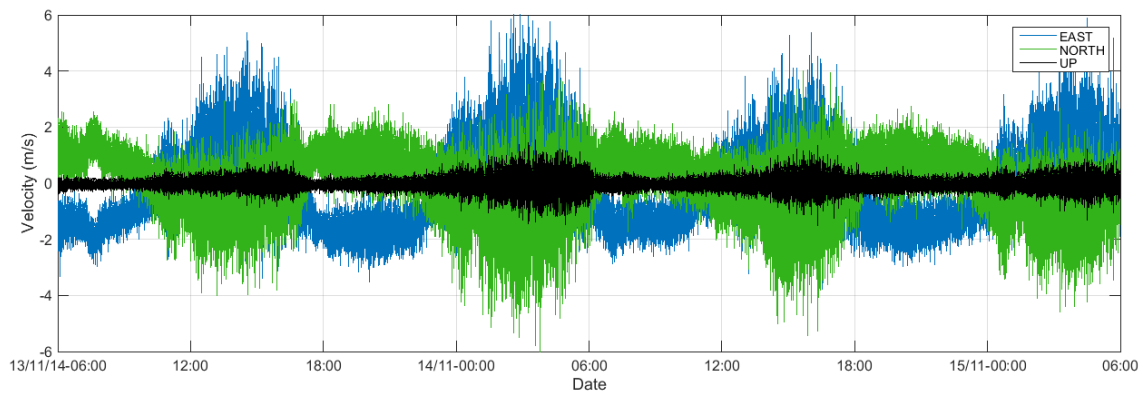


(a) Time series of Pressure Gauge vs SBD-AST significant wave height, H_{m0}

Figure 3.12: Comparison (time-series) of Pressure Gauge and SBD-AST measurements of significant wave height under different pressure gauge calibration routines.

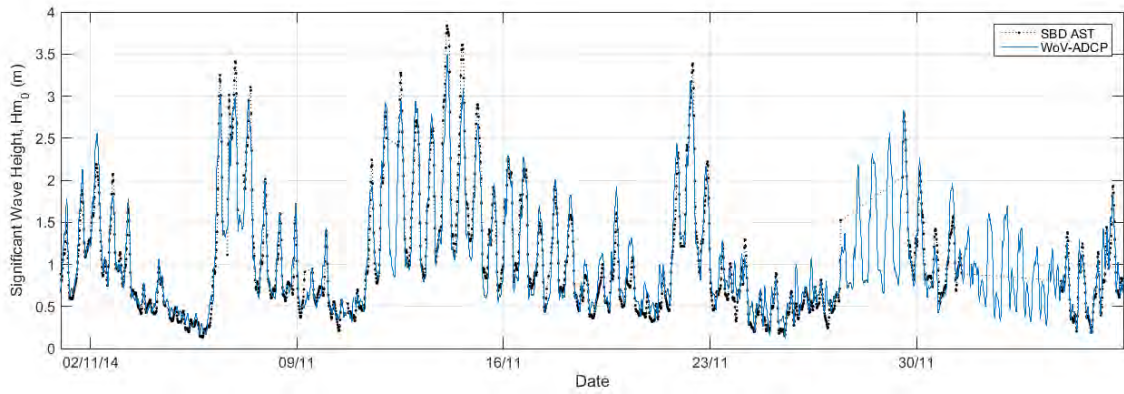
Table 3.1: Wave Measurement Methods

Instrument	Measurement Principle	Description
SB-ADP (SBD)	Surface detection via high amplitude return	Instrument vertically orientated on Turbine
DIRECT		Fast sample rates for waves (4Hz) Real-Time Data Low Spatial Resolution (0.4m) Point source (no directional data).
Div-ADP Vertical Beam (AWAC)	Surface detection via high amplitude return	Instrument vertically orientated on Turbine
DIRECT		Fast sample rates for waves (2Hz) Low-Delay Data Good Spatial Resolution (0.1m) Point source (no directional data).
Div-ADP Array (AWAC)	Surface detection via high amplitude return. + Array based processing to give full directional spectra	Instrument vertically orientated on Turbine
COMBINATION		Fast sample rates for waves (2Hz) Low-Delay Data Use of this mode affects ability to gather current data. Good Spatial Resolution (0.1m) Array gives directional data
Div-ADP Array (ADCP)	Array based processing to give full directional spectra	Instrument vertically orientated on Seabed.
INDIRECT		Fast sample rates for waves (2Hz) No Real-Time Data (unless hard wired) Use of this mode affects ability to gather current data.
WAMOS	Radar backscatter transformed to surface elevation maps	Radar located on land (Eday) overlooking deployment site. Preliminary use of instrument (not calibrated)
INDIRECT		Wide area coverage Long-term data set
SB-ADP mounted Pressure Gauge (SBD)	Surface detection via transform from pressure to surface elevation via linear wave theory.	Less complex measurement principal than velocimetry.
INDIRECT		Fast sample rates for waves (2Hz) Real-Time Data High resolution (cm) Point source (no directional data) Highly sensitive to depth via wave orbital velocity attenuation.
ADCP mounted Pressure Gauge (SBD)	Surface detection via transform from pressure to surface elevation via linear wave theory.	Less complex measurement principal than velocimetry.
INDIRECT		Fast sample rates for waves (2Hz) No Real-Time Data (unless hard wired) High resolution (cm) Point source (no directional data) Highly sensitive to depth via wave orbital velocity attenuation.
HF Turbine mounted Pressure Gauge	Surface detection via transform from pressure to surface elevation via linear wave theory.	Less complex measurement principal than velocimetry.
INDIRECT		Very fast sample rates for waves (10Hz) High resolution Real-Time Data Point source (no directional data) Highly sensitive to depth via wave orbital velocity attenuation.

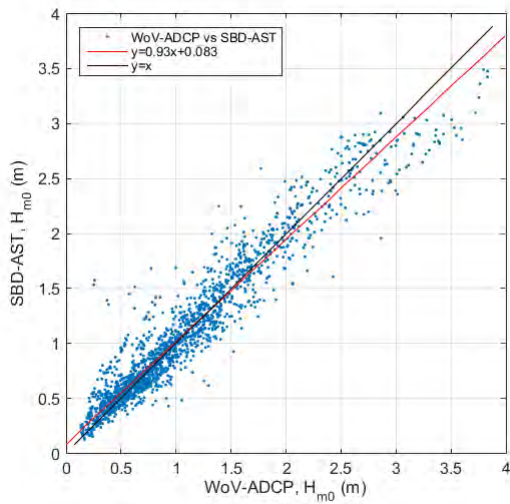


(a) Time series of Pressure Gauge vs SBD-AST significant wave height, H_{m0}

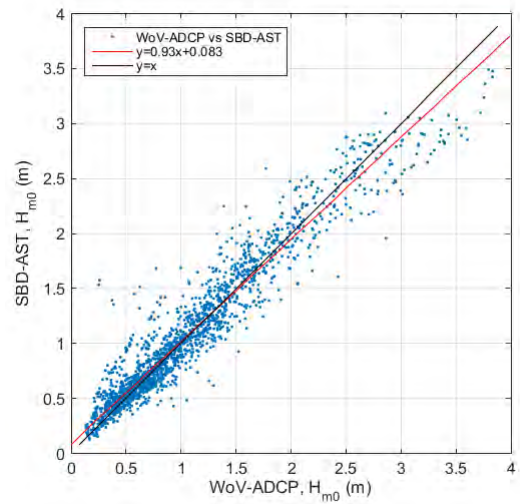




(a) Comparison of WoV-ADCP vs SBD-AST significant wave height, H_{m0} and best-fit

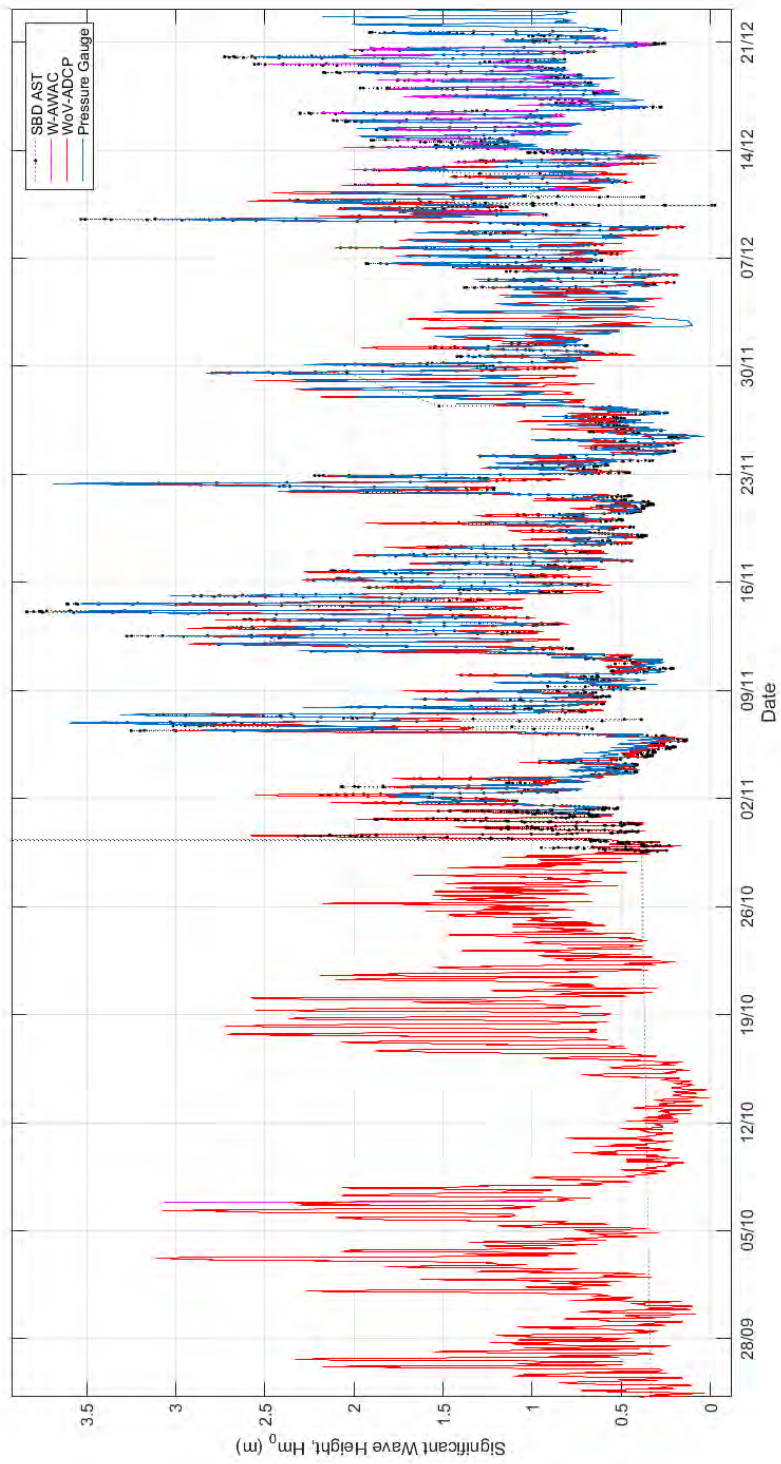


(b) Update Graph with Uncalibrated Data



(c) Comparison of WoV-ADCP vs SBD-AST significant wave height, H_{m0} and best-fit

Figure 3.14: Comparison of WoV-ADCP and SBD-AST measurements of significant wave height under different ADCP calibration routines.



(a) Comparison of all wave measurement signals' significant wave height H_{m0} and best-fit

3.6 Site Characterisation

The following section shows analysis for the FoW Flood and Ebb Tides using ReDAPT data acquired and post-processed between March 2013 and December 2014.

Contents:

- SBD U,V,W TI
- SBD U,V,W Lengthscale
- ADCP U,V,W TI
- ADCP U,V,W (resultant in this draft)
- SBD U,V,W TI in the presence of waves
- SBD U,V,W Lengthscale in the presence of waves
- ADCP U,V,W TI in the presences of waves
- ADCP U,V,W (resultant in this draft) in the presence of waves

3.6.1 Database Searching

The primary search filters are based upon tidal flow system state i.e., flood or ebb, flow velocity and wave height. Wave-length and wave-steepness will be added in the final report. Following sensitivity studies (see section X) flow acceleration filters are implemented. The output of a particular data query [flood tide, 0.4m/s velocity bins, all wave conditions] is shown in figure 3.17. The impact of additional acceleration filtering can be seen.

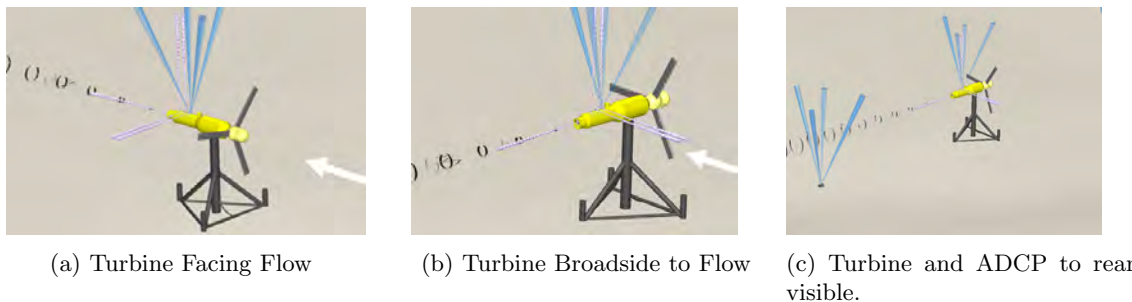


Figure 3.16: Visualisation of database querying: selecting turbine and instrumentation orientations wrt flood/ebb

3.6.2 Returned Metrics

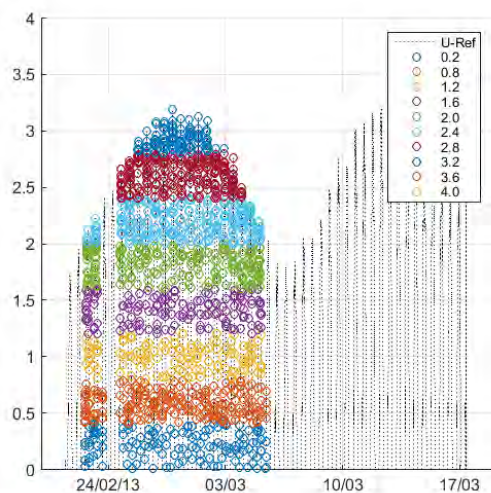
The analysed parameter set is shown in 3.2. This table to be updated with the now extended set of metrics

Integral Lengthscale

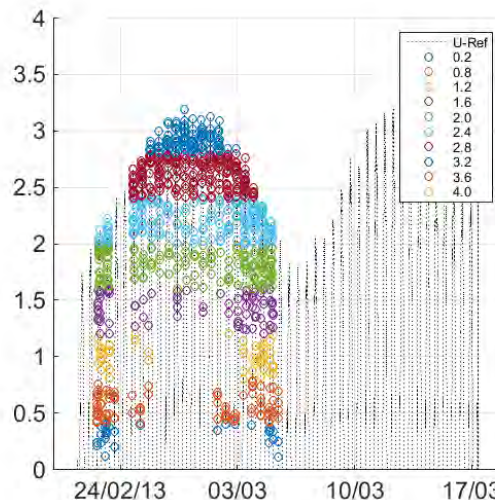
Integral lengthscales were calculated using multiple time auto-correlation techniques (see earlier Section XX for more information). As previously stated turbulent length scales are of particular significance to numerical modelling tools which display sensitivity to this parameter.

Parameter	Location(s)	Data Used
	Profile (z) or Point (zhub)	Obtain from...
1 Upstream axial velocity: & turbulence intensity: Longitudinal length scale:	U(x,zhub) Ix(x, zhub) Lx(zhub)	Multipoint correlated U(t,x)(z) Synchronised measurements of U(t) at multiple x-ordinates at hub height.
2 Depth profile of velocity:	U(z) profile V(zhub), W(zhub)	e.g. U(t) at each z-ordinate
& of Turbulence intensity:	Ix(z) profile Iy(zhub), Iz(zhub)	e.g. U(t) at each z-ordinate (to obtain anisotropy)
3 Lateral length scale:	Ly(zhub)	V(t,y)(z) Synchronised measurements of V(t) at multiple y-ordinates at hub height.
4 Vertical length scale:	Lz(zhub)	W(t,z)(z) Synchronised measurements of W(t) at multiple z-ordinates either side of hub height

Table 3.2: **Table to be updated.** Velocity field parameters



(a) Timestamps returned following a database query based on velocity bins of width 0.4 m/s. With acceleration filters applied.



(b) Timestamps returned following a database query based on velocity bins of width 0.4 m/s. With acceleration filters applied.

Figure 3.17: Example of velocity binning and the effect of acceleration threshold on the returned data sets prior to flow metric analysis

Spectra

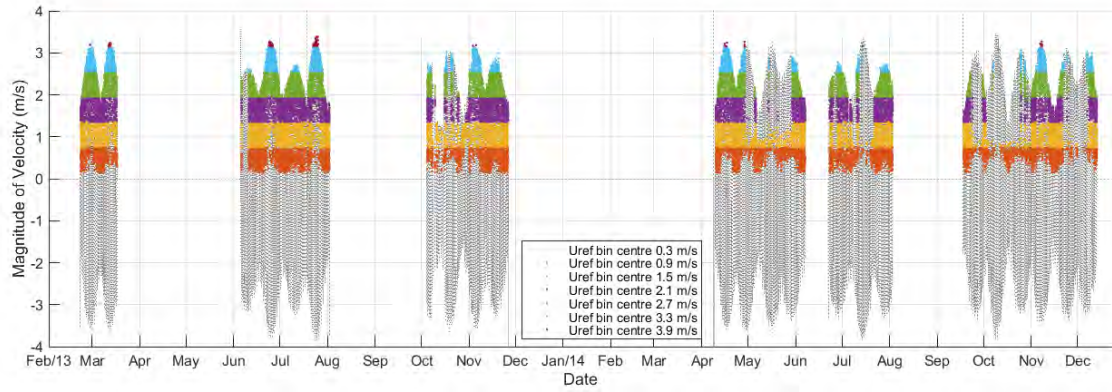
Energy Density Spectra, a form of statistical description and an examination of a signal via the energy distribution across signal frequency or wave-number, are one particularly useful tool in the characterisation of systems [27]. They allow the time domain properties in a statistically stationary process to be represented in the frequency domain, which is significant for processes which display frequency dependency. Also:

- They are relatively straightforward to obtain
- They provide information that cannot be obtained by analysis of the signal in the time domain.
- They can be calibrated and improved upon in parallel to data measurements.
- They can be reversed to provide statistically representative time series of parameters.

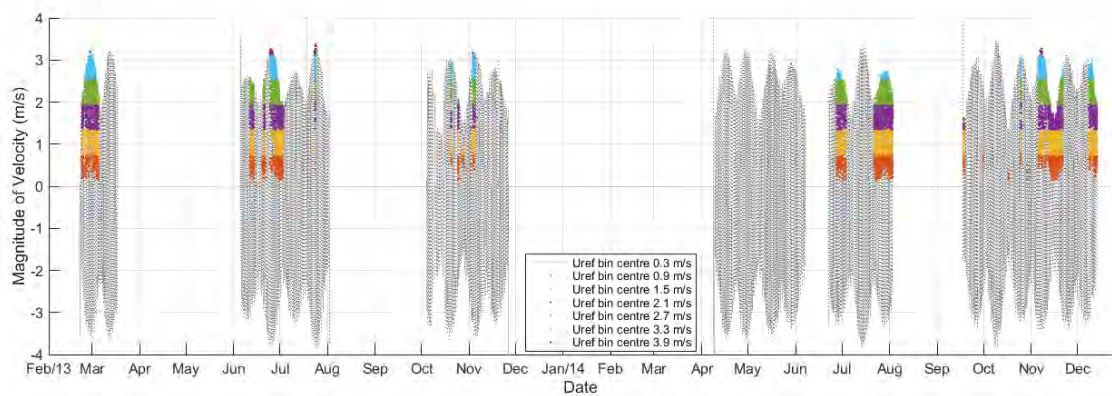
Once identified, spectra provide insight into features of the underlying system, such as the likelihood of the occurrence of extreme events. This proves highly useful in wave-field studies where, for example, 100 year waves which play a role in the design of marine structures can be described from the analysis of the shape of the tail of the utilised spectra.

Turbulence Intensity

Turbulence Intensities (TI) were calculated using equation X (see earlier Section XX for more information).



(a) Returned ADCP data for non-generating times



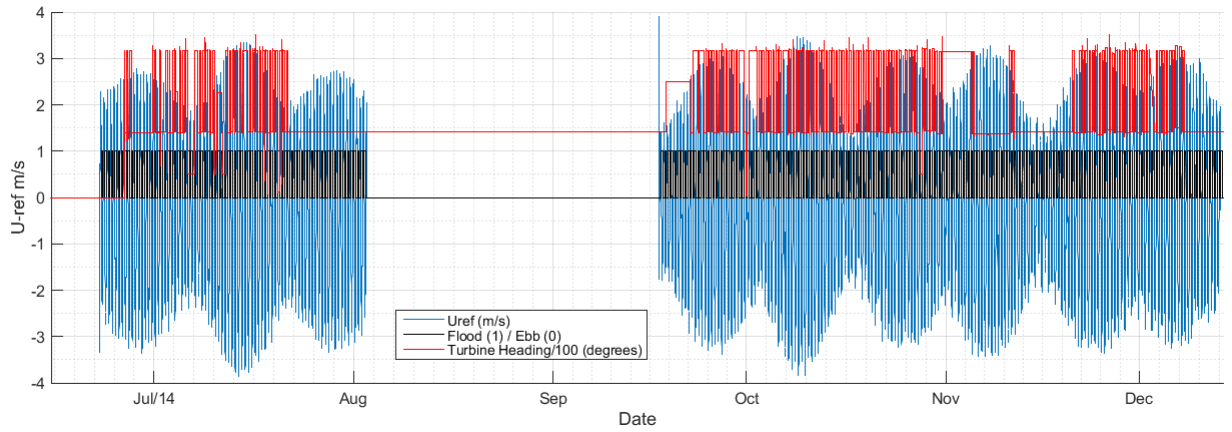
(b) Returned ADCP data for specific turbine conditions: reversed to Flood tide

Figure 3.18: Example of database querying

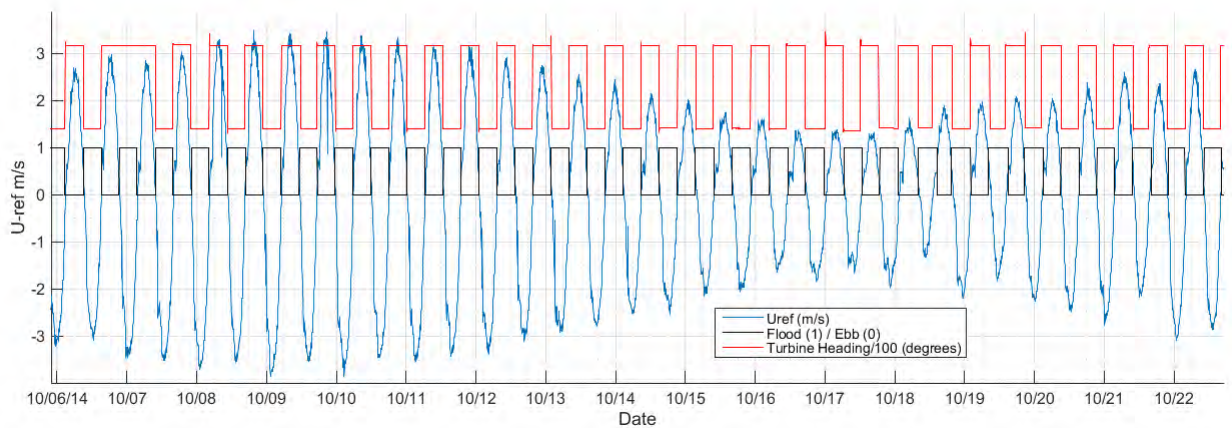
To Be Added (Specific To This Section)

3.6.3 Reference Velocities

Reference velocity (u_{ref}) is constructed by taking the (time-stamp corrected) non-power-weighted depth average of the section of upstream ADCP depth profile which coincides with the vertical extent of the turbine blades. An algorithm detects flood and ebb tidal cycles and through comparison to the position of the ADCPs relative to the turbine selects the appropriate ADCP which can provide undisturbed incident flow. Resultant (maximum) velocity is used throughout for u_{ref} .

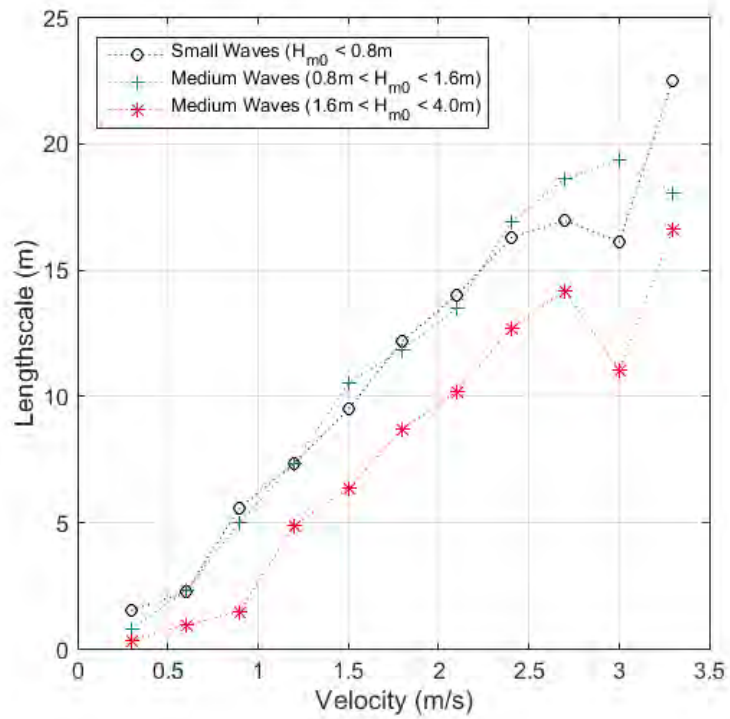


(a) Database reference signals showing date range June 2014 to December 2014

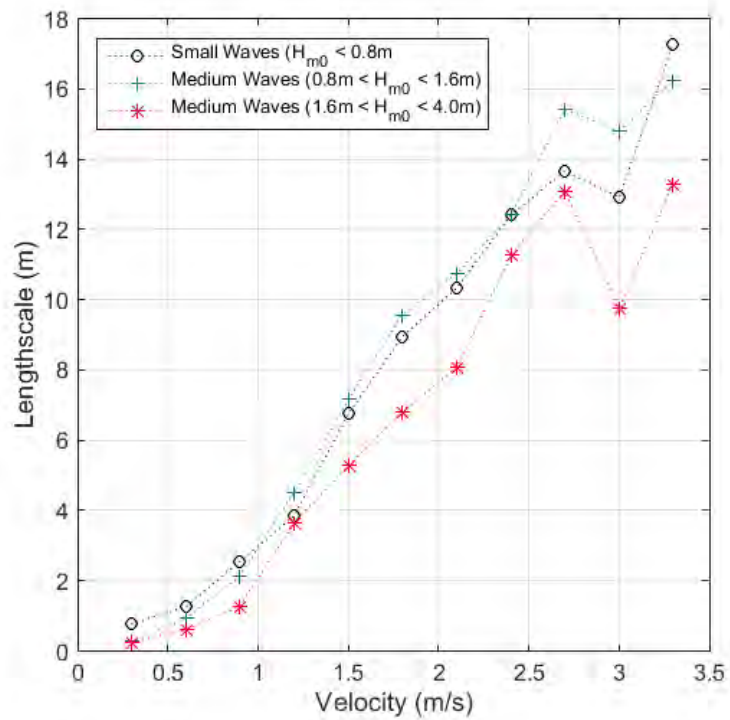


(b) Database reference signals showing more detail: date range October 2014

Figure 3.19: Database reference signals. Blue trace shows u_{ref} . Black shows tidal state: 1 = ebb, 0 = flood and red shows the turbine heading (/100). Further signals are added as required and form the building blocks of data queries (e.g., return all data corresponding to tide=flood, turbine heading <300 degrees and $u_{ref} >2.5$ m/s.)



(a) LS detrend method 1 - constant mean detrend



59

(b) LS detrend method 2 - linear fit detrend

Figure 3.20: Streamwise Lengthscale as a function of tidal reference velocity.)

3.7 Analysis: (Flood) Turbine-Mounted Instrumentation

The following section shows analysis for the FoW Flood Tide.

3.7.1 Lengthscales

Figure 3.21 and 3.22 shows stream-wise length-scales returned with the turbine orientated reversed to FLOOD flow for post processing involving constant-mean detrended and linear detrended velocity signals respectively under the influence of small, medium and large wave field conditions specified as:

- Small Waves: $0.0m < H_{m0} < 0.8m$
- Medium Waves: $0.8m < H_{m0} < 1.6m$
- Large Waves: $1.6m < H_{m0} < 4.0m$

Figure 3.20a and 3.20b shows stream-wise length-scales (constant-detrend and linear-detrend) as a function of velocity. *std/scatter to be added, line of best fit and confidence. Axis to be standardized.*

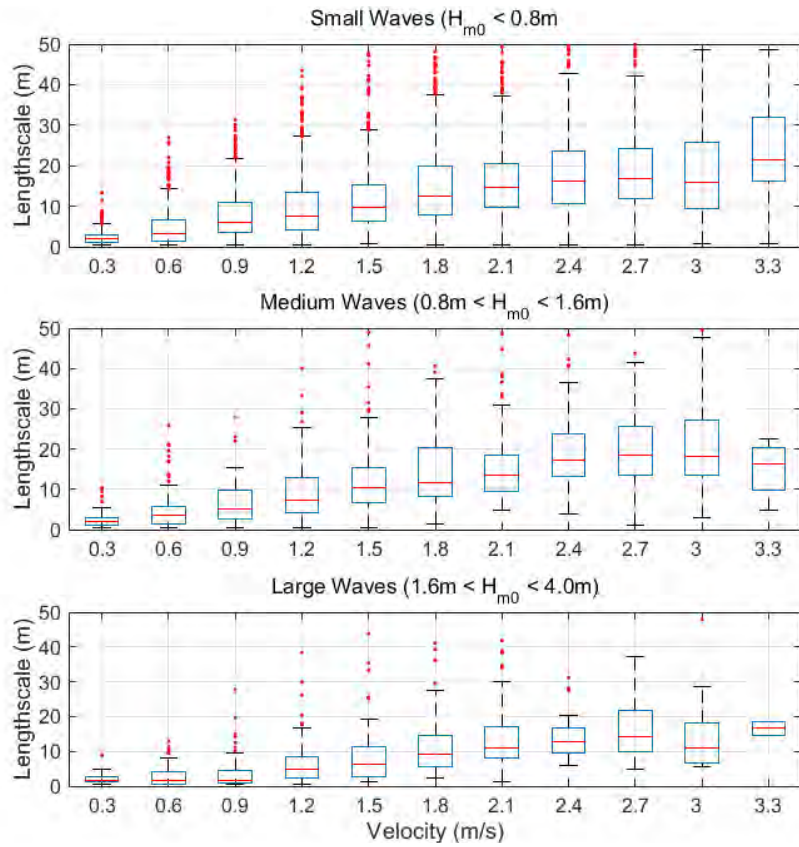


Figure 3.21: Streamwise lengthscale versus reference velocity - Constant De-trending.

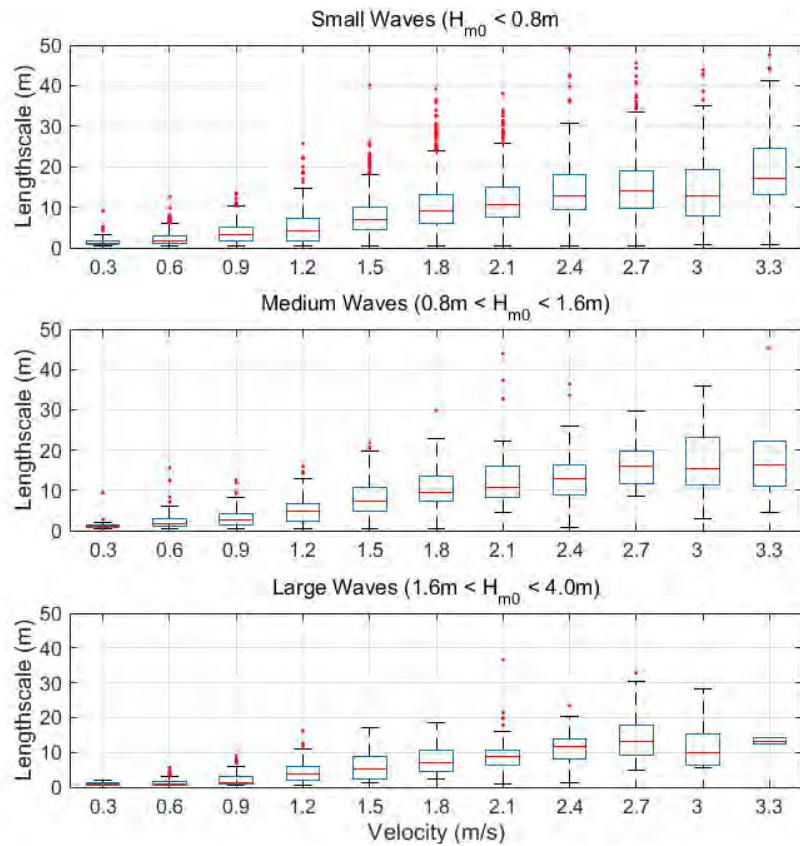


Figure 3.22: Streamwise lengthscale versus reference velocity - Linear Detrending.

Summary Trend Graph Summary Table

3.7.2 Turbulence Intensity

Figure 3.23 shows stream-wise Turbulence Intensities returned with the turbine orientated reversed to FLOOD for post processing involving default-detrended (linear) velocity signals under the influence of small, medium and large wave field conditions. TI in these plots are not corrected for Doppler noise. Figure 3.24 and 3.25 show respectively TI for the transverse and vertical directions. Figure 3.26 shows uncorrected stream-wise TI for the three wave conditions as a function of velocity. *std/scatter to be added, line of best fit and confidence.*

Section to be Added (Uncertainties Adding to TI)

- Detrending, Constant, Linear, MA, System Identification
- Stationarity Period
- Instrument Noise Correction

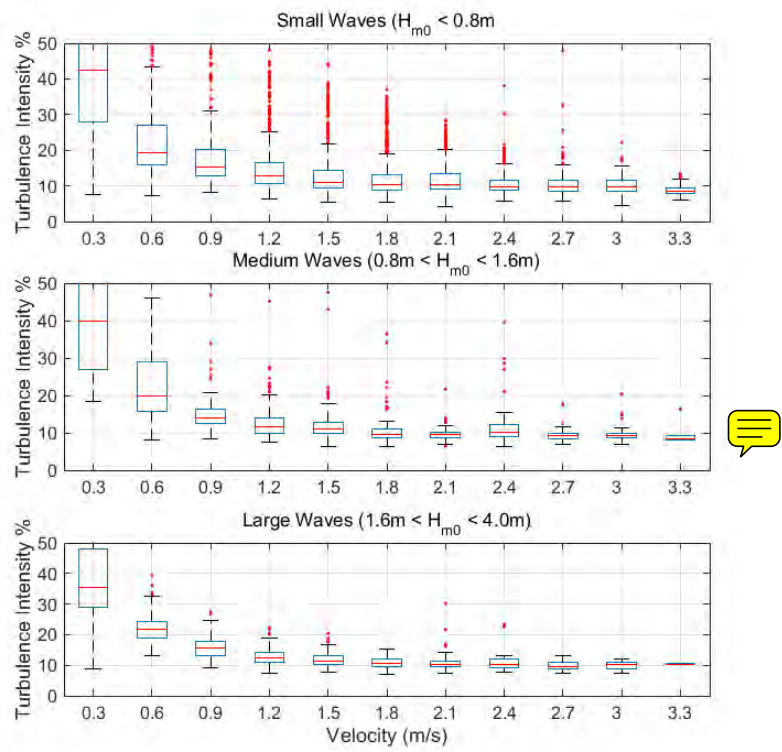


Figure 3.23: Streamwise TI - Turbine Reversed to Flood

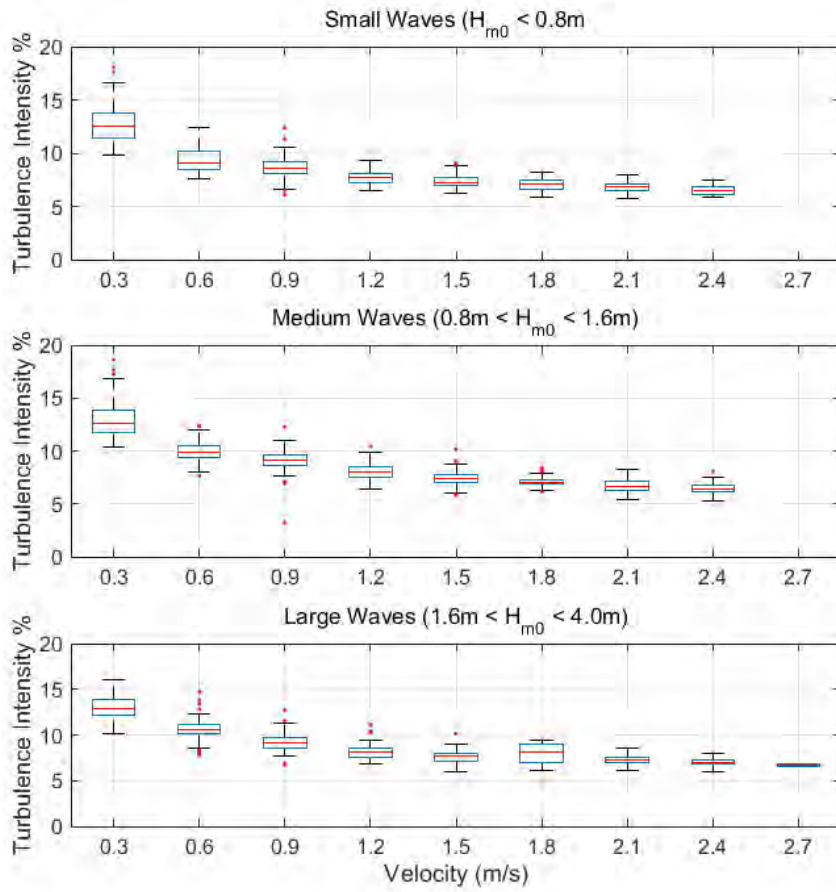


Figure 3.24: TI Transverse Direction

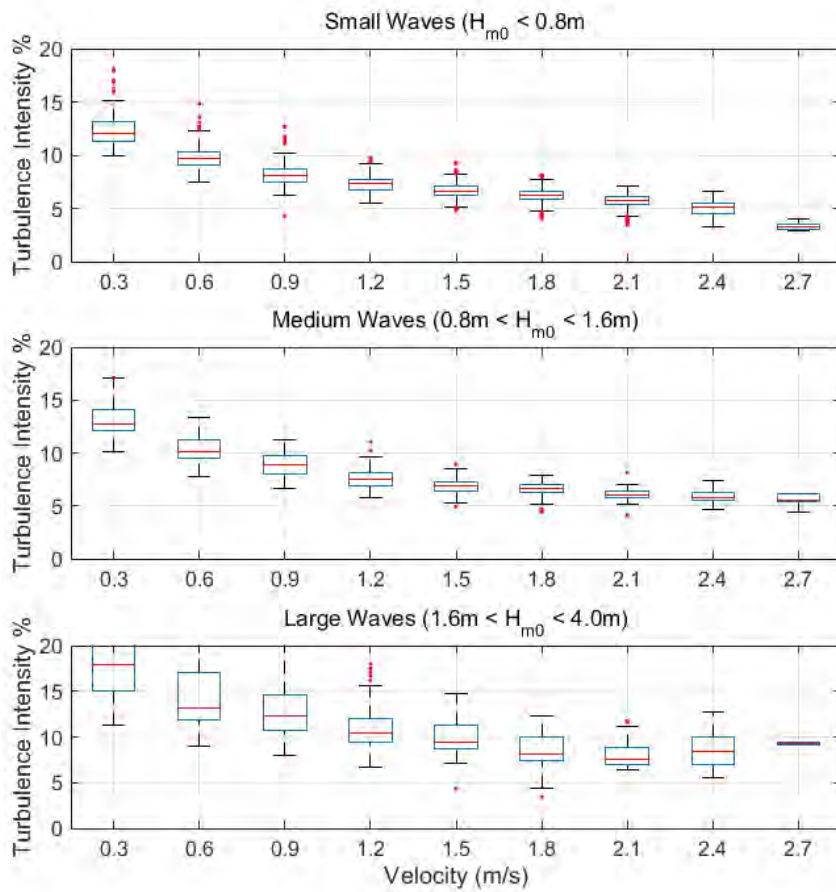


Figure 3.25: TI Vertical Direction

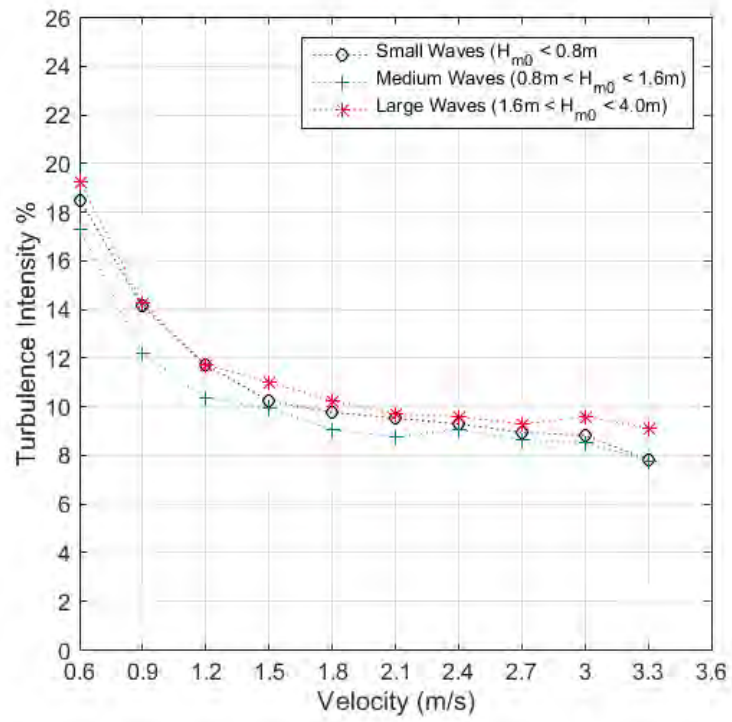
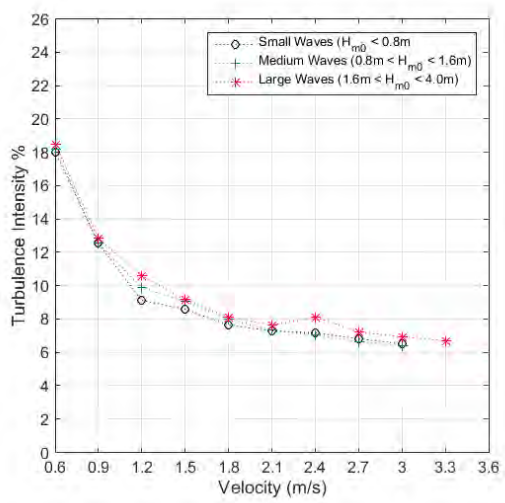
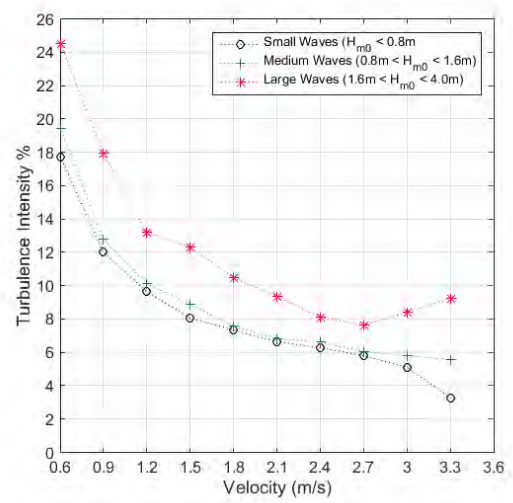


Figure 3.26: TI Streamwise Direction [Uncorrected - No Noise Floor Correction Method]



(a) TI Y Direction



(b) TI Z Direction

Figure 3.27: TI Y and Z Direction

3.8 Analysis: (Ebb) Turbine-Mounted Instrumentation

INSERT THE PRODUCED GRAPHS FOR EBB (AS PER ABOVE FLOOD SECTIONS)

Figure ?? and ?? shows stream-wise length-scales returned with the turbine orientated reversed to EBB flow for post processing involving constant-mean detrended and linear detrended velocity signals respectively under the influence of small, medium and large wave field conditions.

3.8.1 TI EBB

Figure 3.23 shows stream-wise Turbulence Intensities returned with the turbine orientated reversed to FLOOD for post processing involving default-detrended (linear) velocity signals under the influence of small, medium and large wave field conditions. TI in these plots are not corrected for Doppler noise. Figure 3.24 and 3.25 show respectively TI for the transverse and vertical directions. Figure 3.26 shows uncorrected stream-wise TI for the three wave conditions as a function of velocity. **std/scatter to be added, line of best fit and confidence.**

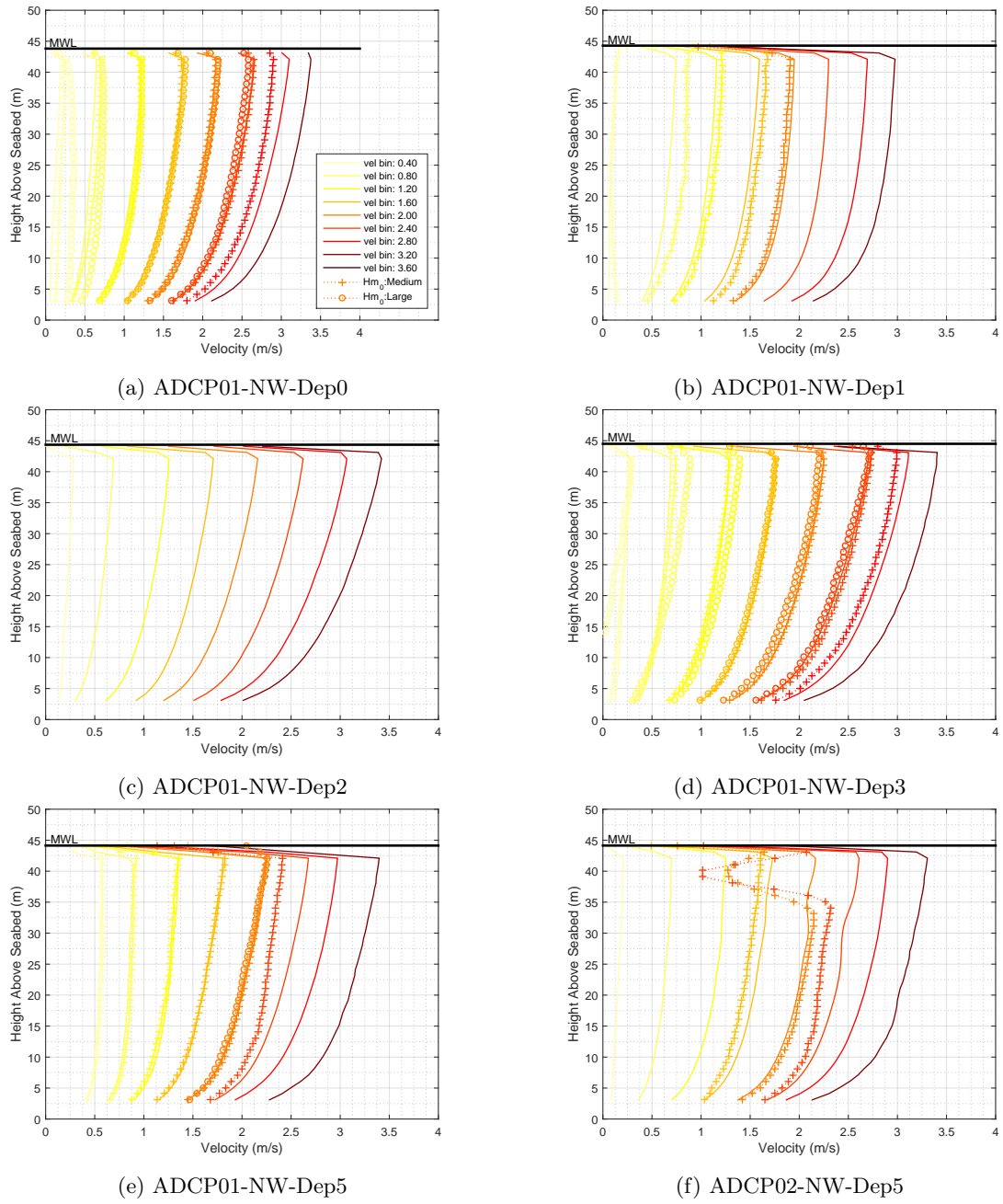
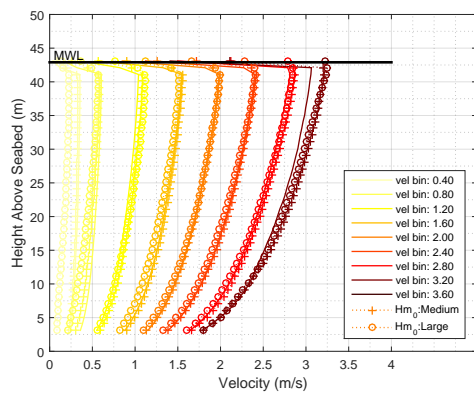
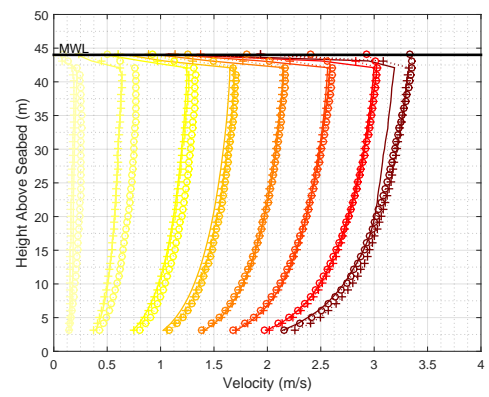


Figure 3.28: Depth profiles of velocity (m/s) for seabed ADCPs upstream of flood tidal flow

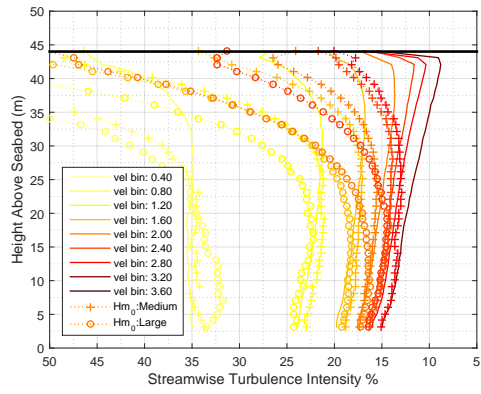


(a) ADCPTD7-01-Dep1

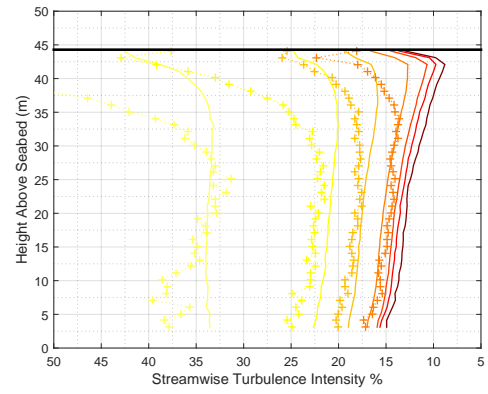


(b) ADCPTD7-02-Dep1

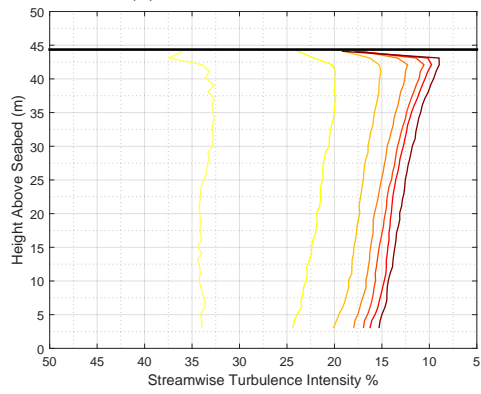
Figure 3.29: Depth profiles of velocity (m/s) for seabed ADCPs upstream of flood tidal flow



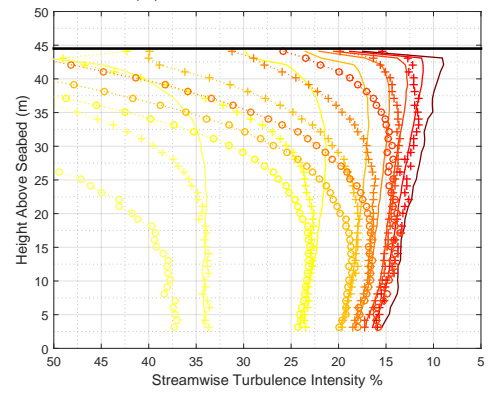
(a) ADCP01-NW-Dep0



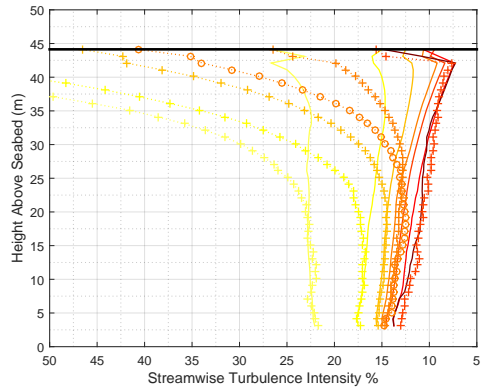
(b) ADCP01-NW-Dep1



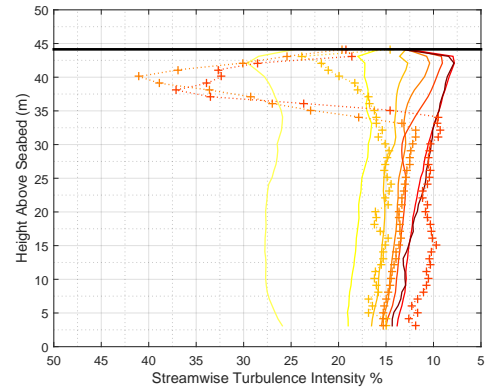
(c) ADCP01-NW-Dep2



(d) ADCP01-NW-Dep3

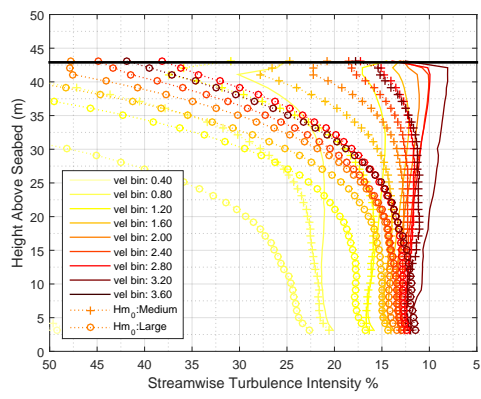


(e) ADCP01-NW-Dep5

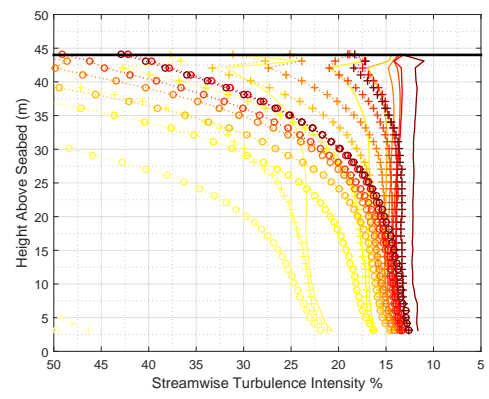


(f) ADCP02-NW-Dep5

Figure 3.30: Depth profiles of streamwise turbulence intensity for seabed ADCPs upstream of flood tidal flow



(a) ADCPTD7-01-Dep1



(b) ADCPTD7-02-Dep1

Figure 3.31: Depth profiles of streamwise turbulence intensity for seabed ADCPs upstream of flood tidal flow

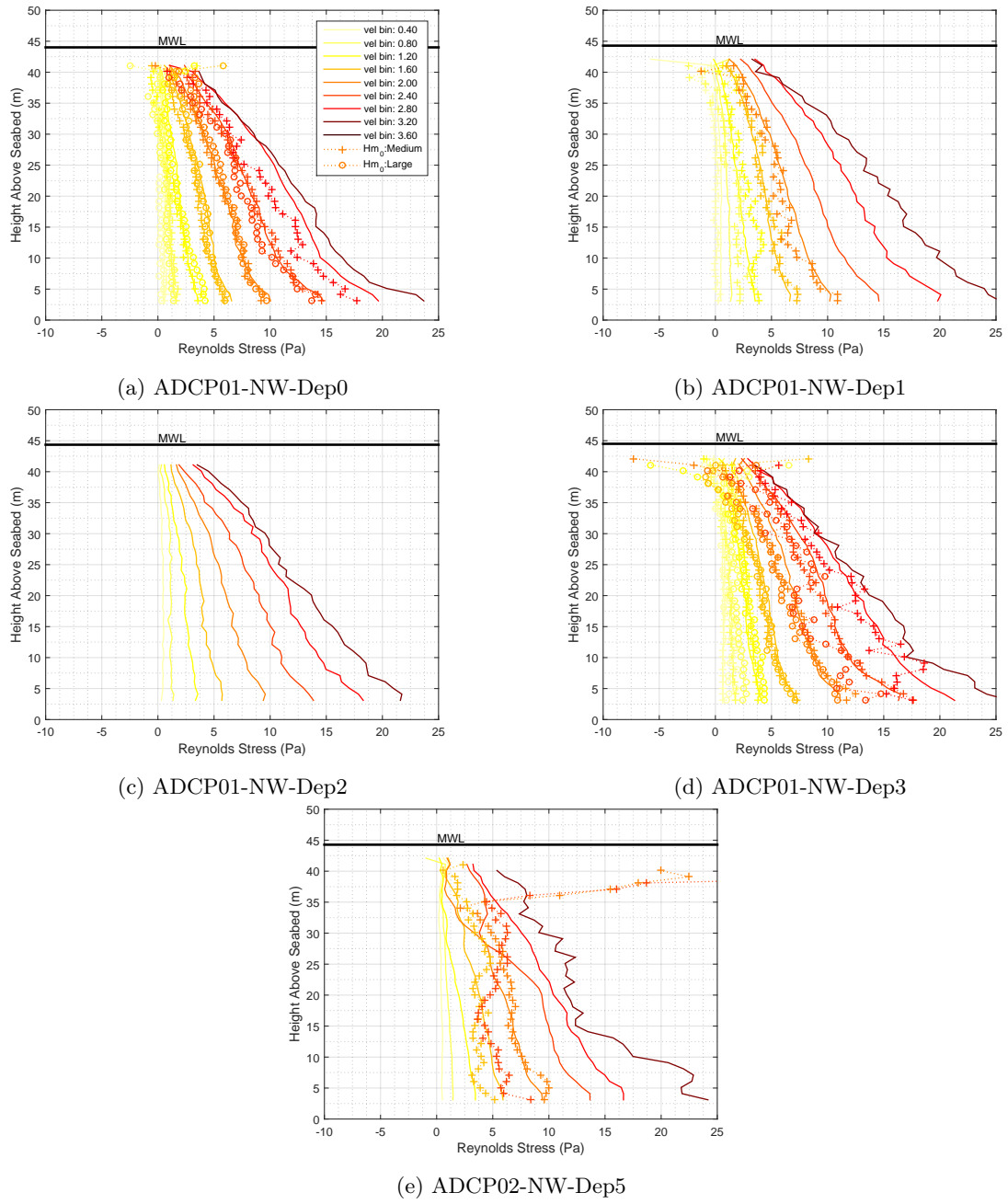
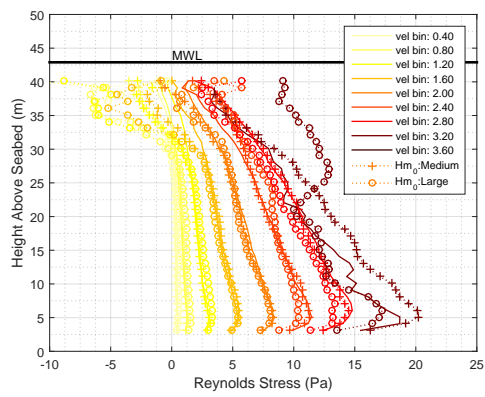
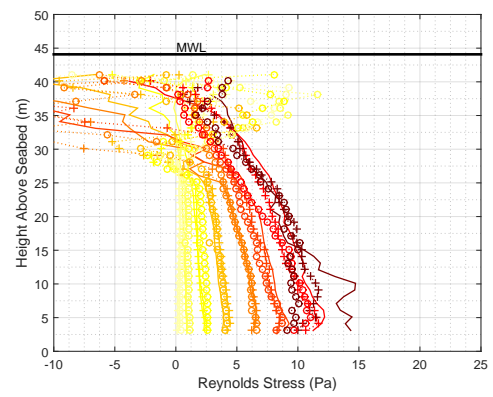


Figure 3.32: Depth profiles of Reynolds Stress (uw) for seabed ADCPs upstream of flood tidal flow

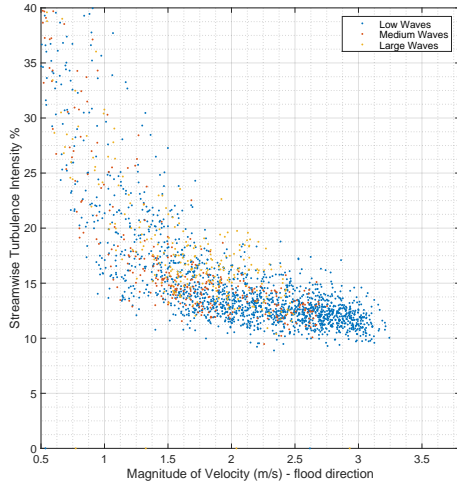


(a) ADCPTD7-01-Dep1

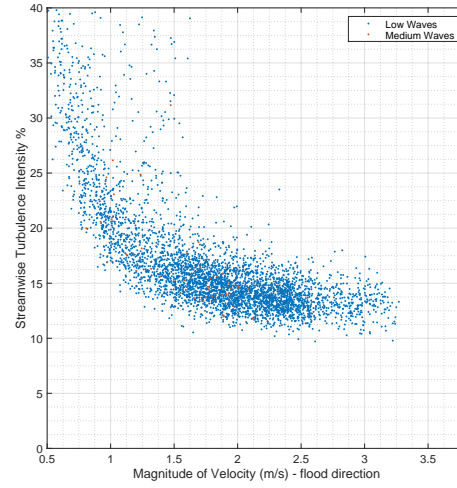


(b) ADCPTD7-02-Dep1

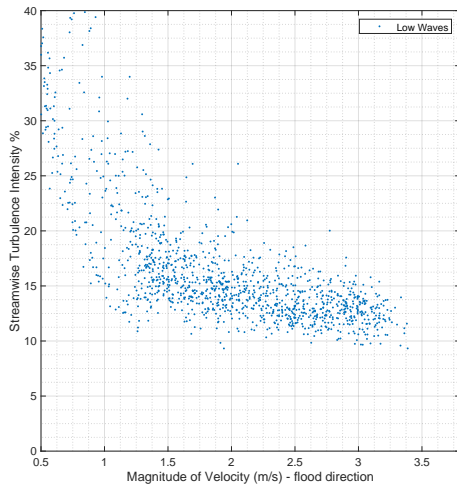
Figure 3.33: Depth profiles of Reynolds Stress (uw) for seabed ADCPs upstream of flood tidal flow



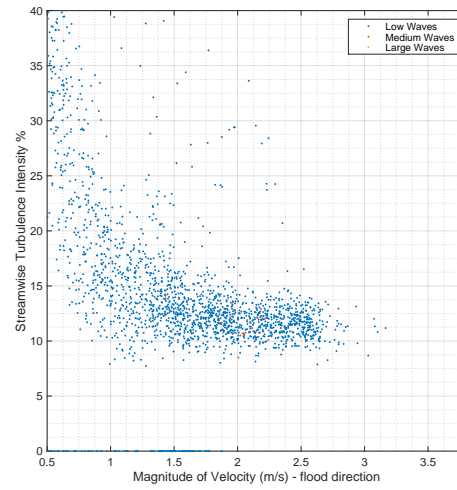
(a) ADCP01-NW-Dep0



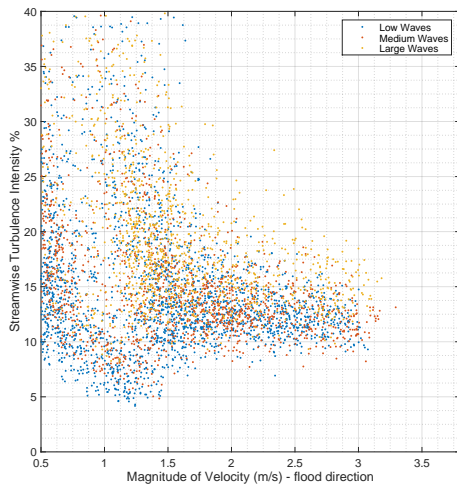
(b) ADCP01-NW-Dep1



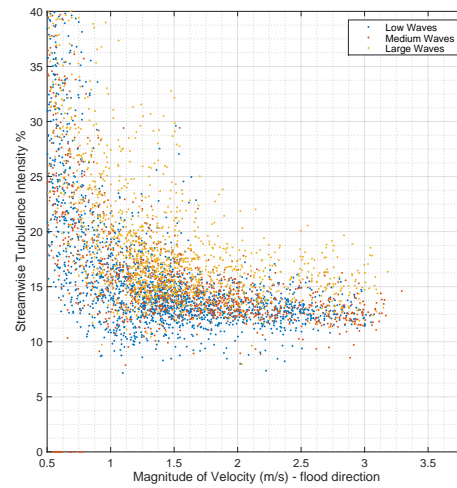
(c) ADCP01-NW-Dep2



(d) ADCP02-NW-Dep5

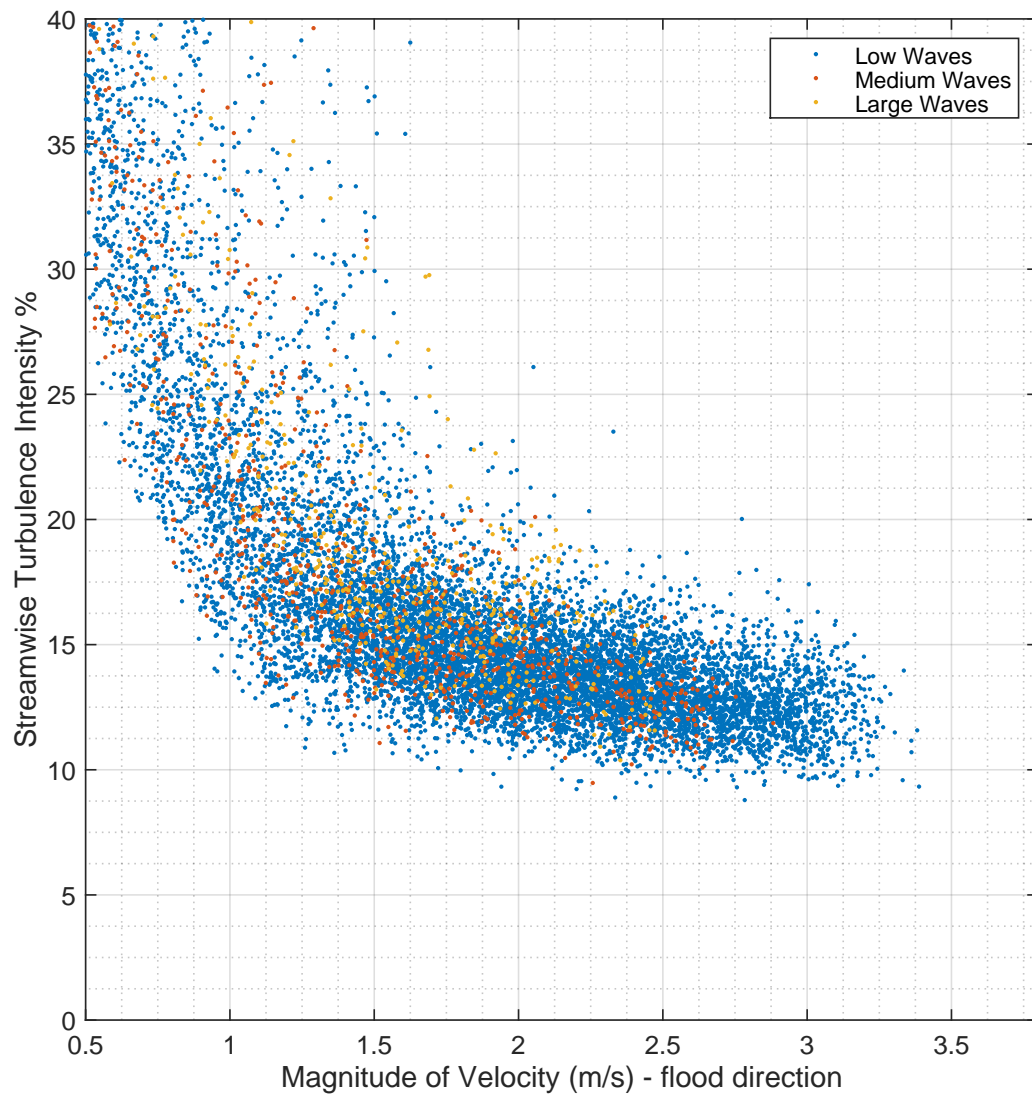


(e) ADCPTD7-01-Dep1



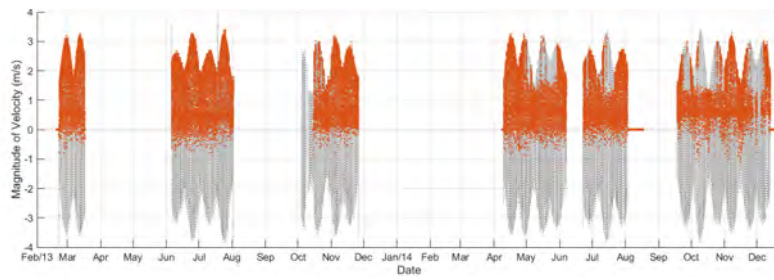
(f) ADCPTD7-02-Dep1

Figure 3.34: Streamwise Turbulence Intensity at turbine hub-height for seabed ADCPs upstream of turbine on flood tidal flow. Acceleration filter applied.

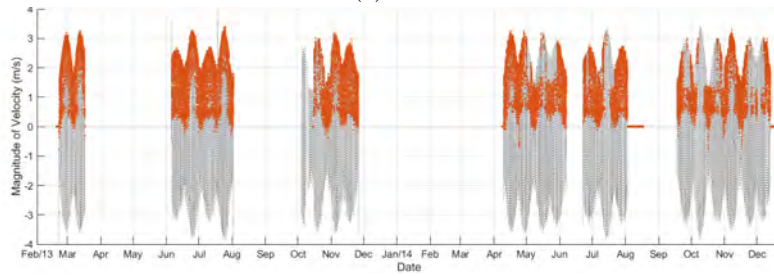


(a) Combination (inline ADCPs)

Figure 3.35: Streamwise Turbulence Intensity at turbine hub-height for seabed ADCPs upstream of turbine on flood tidal flow. Acceleration filter applied.

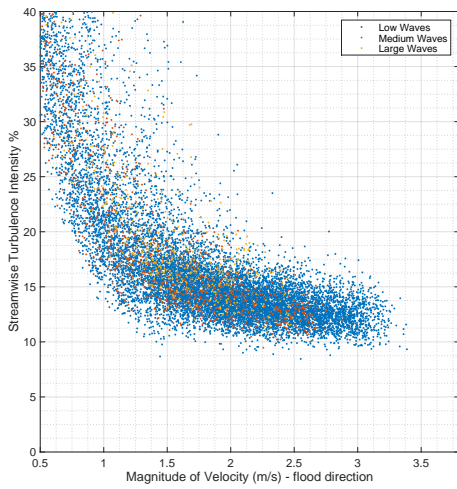


(a) No acceleration filter

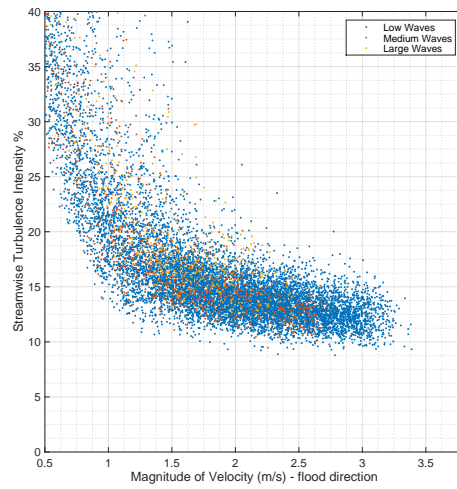


(b) Acceleration filter applied

Figure 3.36: Data Query:flood flow; turbine generating power below 0.2MW

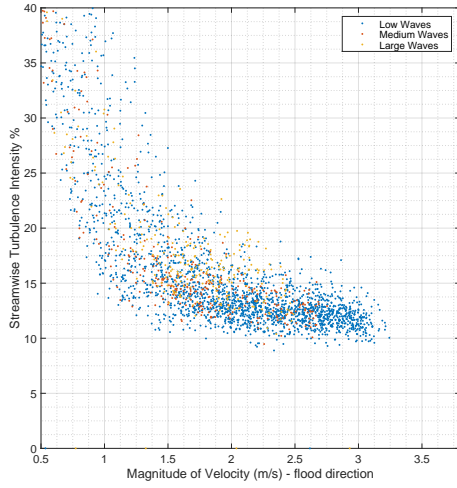


(a) Combination (inline ADCPs). No acceleration filter applied.

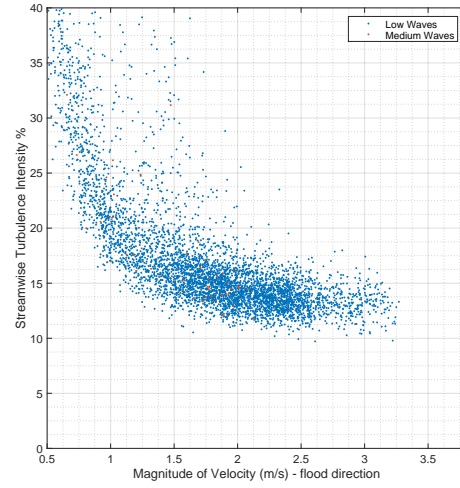


(b) Combination (inline ADCPs). Acceleration filter applied.

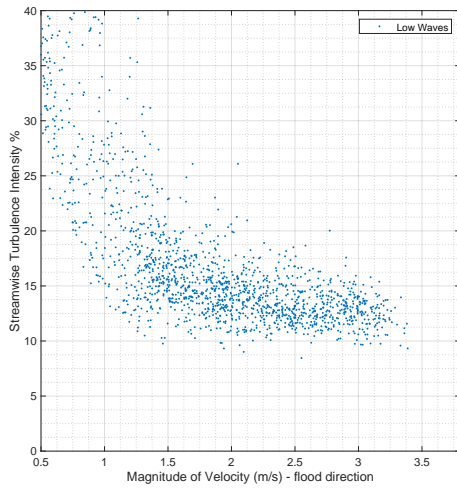
Figure 3.37: Aggregated Streamwise Turbulence Intensity at turbine hub-height for inline seabed ADCPs upstream of turbine on flood tidal flow



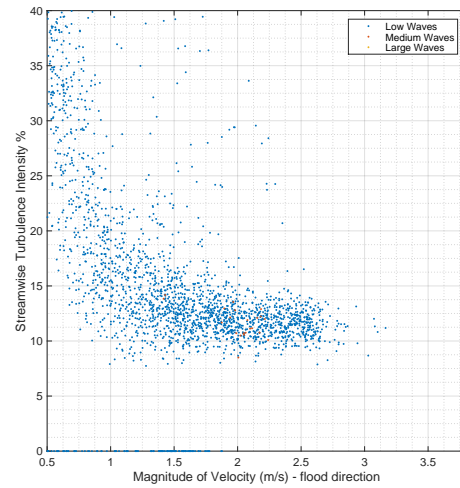
(a) ADCP01-NW-Dep0



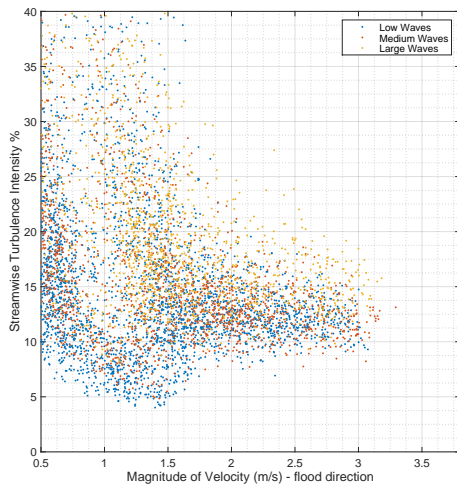
(b) ADCP01-NW-Dep1



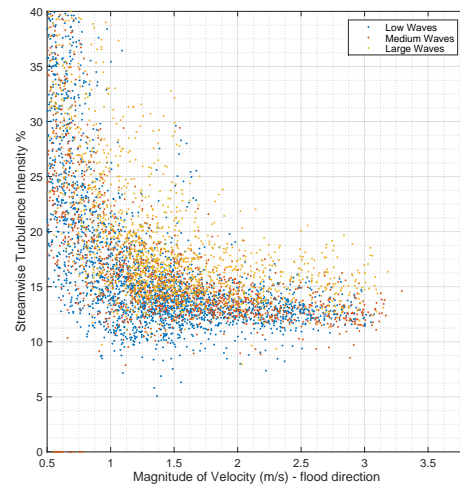
(c) ADCP01-NW-Dep2



(d) ADCP02-NW-Dep5

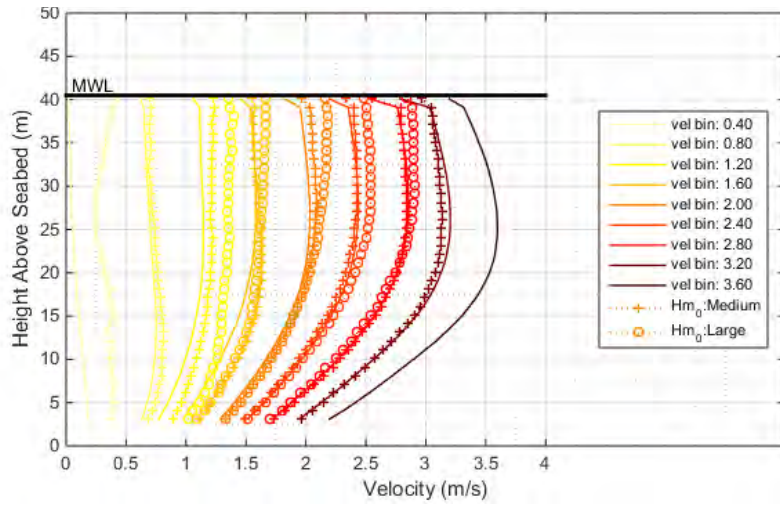


(e) ADCPTD7-01-Dep1

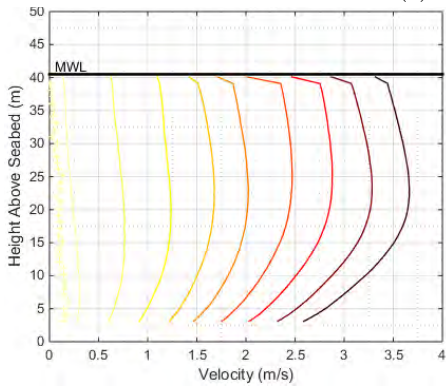


(f) ADCPTD7-02-Dep1

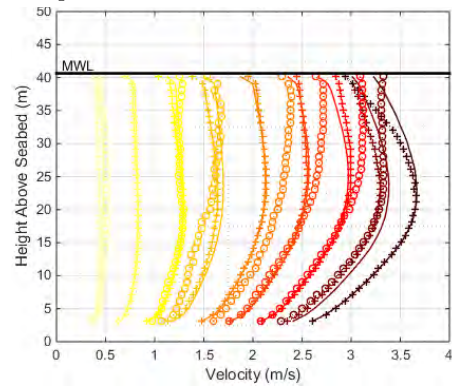
Figure 3.38: Streamwise Turbulence Intensity at turbine hub-height for seabed ADCPs upstream of turbine on flood tidal flow. No acceleration filter applied.



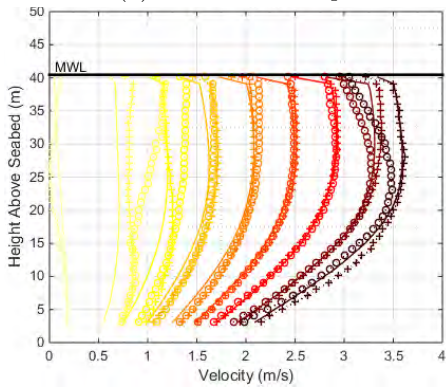
(a) ADCP02-SE-Dep1



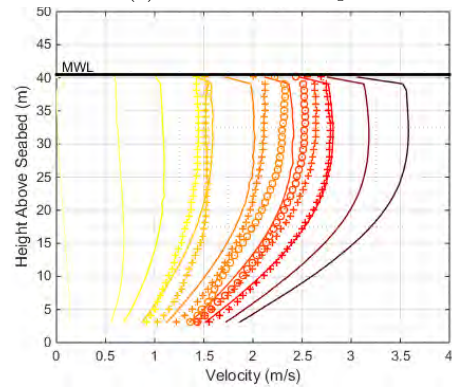
(b) ADCP02-SE-Dep2



(c) ADCP02-SE-Dep3

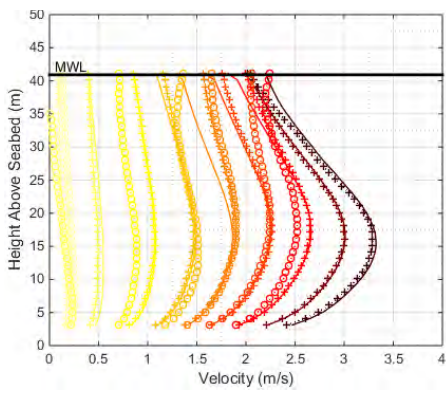


(d) ADCP02-SE-Dep4

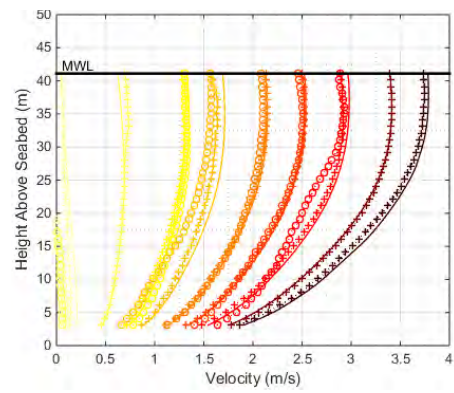


(e) ADCP03-SE-Dep1

Figure 3.39: Depth profiles of velocity (m/s) for seabed ADCPs upstream of ebb tidal flow

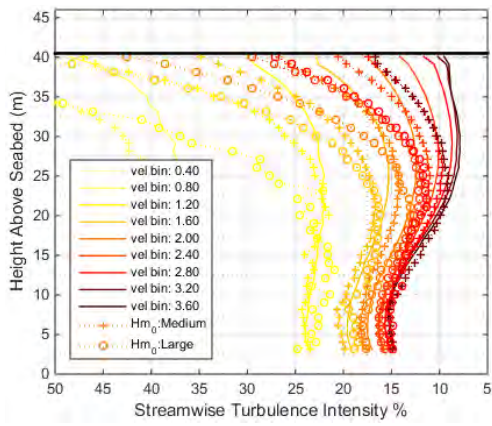


(a) ADCPTD7-01-Dep1

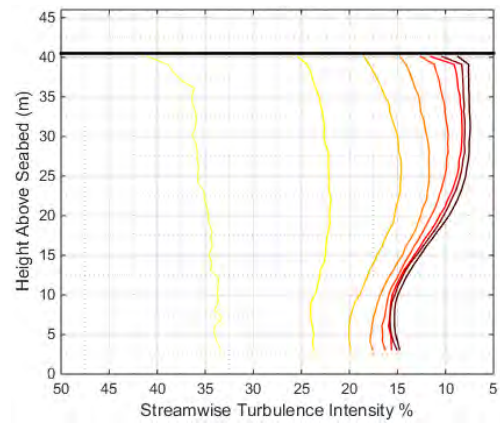


(b) ADCPTD7-02-Dep1

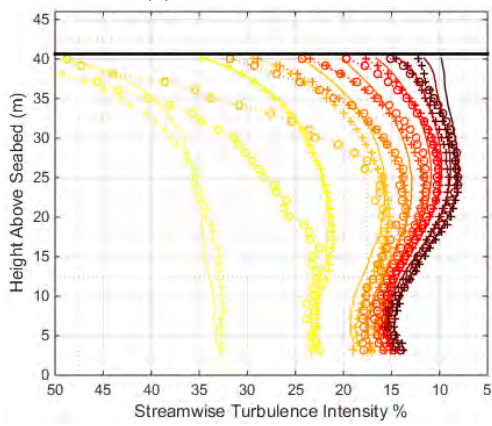
Figure 3.40: Depth profiles of velocity (m/s) for seabed ADCPs upstream of ebb tidal flow



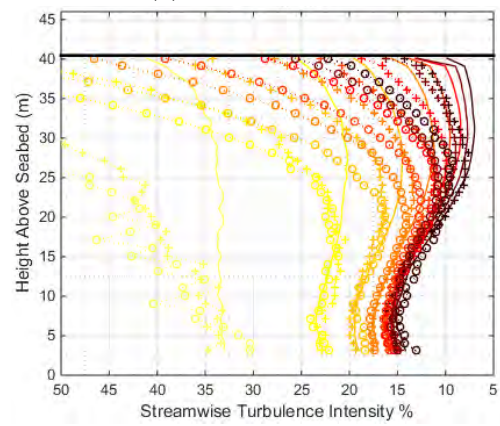
(a) ADCP02-SE-Dep1



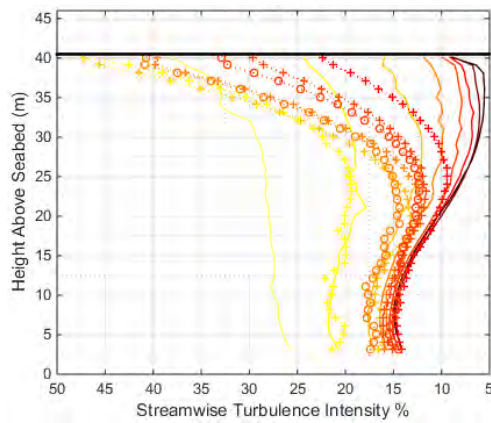
(b) ADCP02-SE-Dep2



(c) ADCP02-SE-Dep3

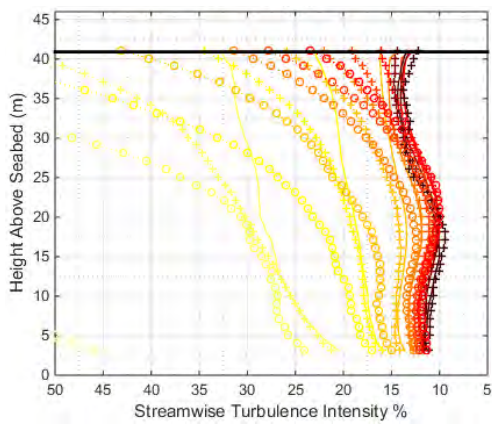


(d) ADCP02-SE-Dep4

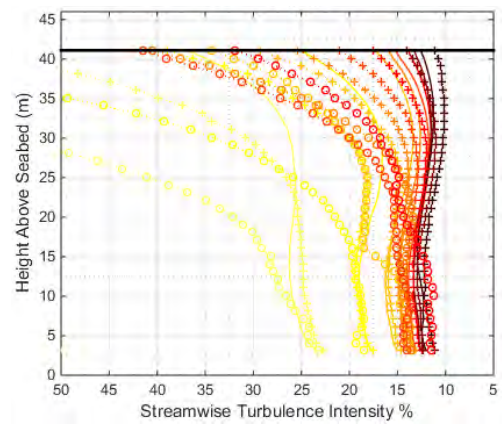


(e) ADCP03-SE-Dep1

Figure 3.41: Depth profiles of streamwise turbulence intensity for seabed ADCPs upstream of ebb tidal flow



(a) ADCPTD7-01-Dep1



(b) ADCPTD7-02-Dep1

Figure 3.42: Depth profiles of streamwise turbulence intensity for seabed ADCPs upstream of ebb tidal flow

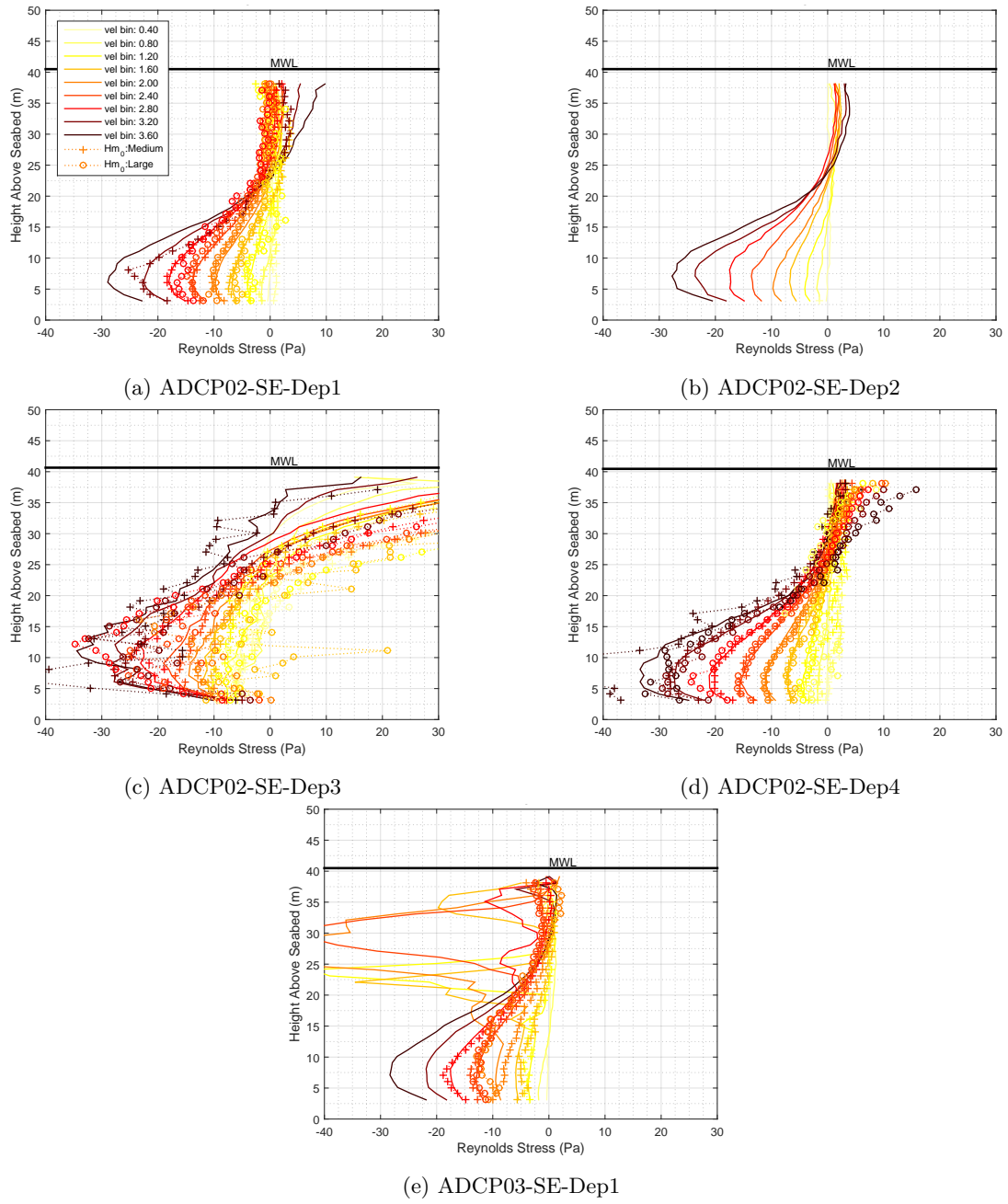
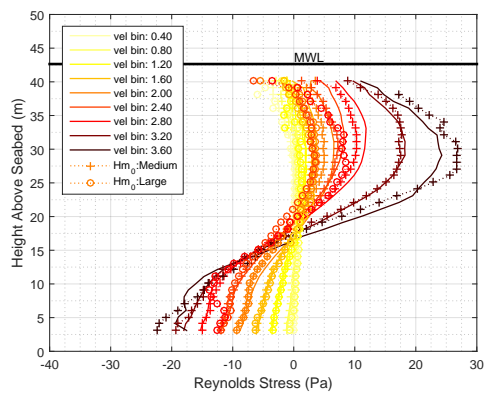
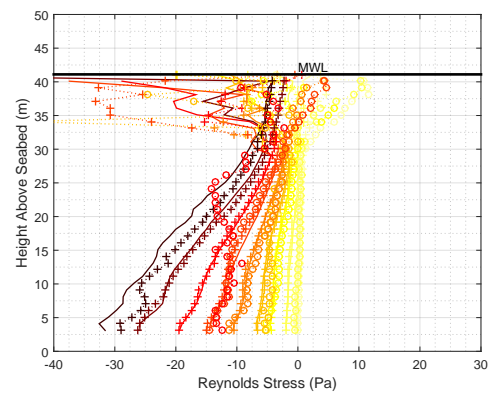


Figure 3.43: Depth profiles of Reynolds Stress (uw) for seabed ADCPs upstream of ebb tidal flow

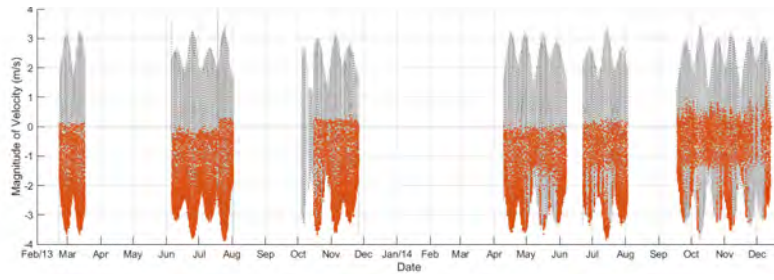


(a) ADCPTD7-01-Dep1

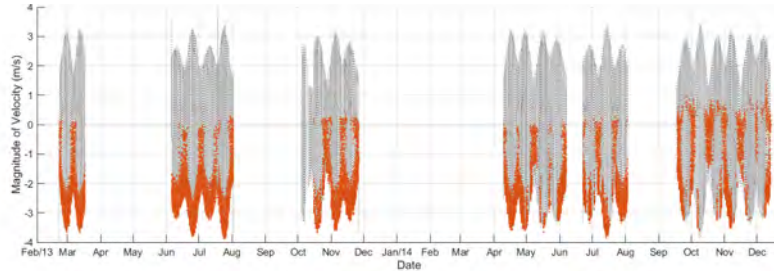


(b) ADCPTD7-02-Dep1

Figure 3.44: Depth profiles of Reynolds Stress (uw) for seabed ADCPs upstream of ebb tidal flow

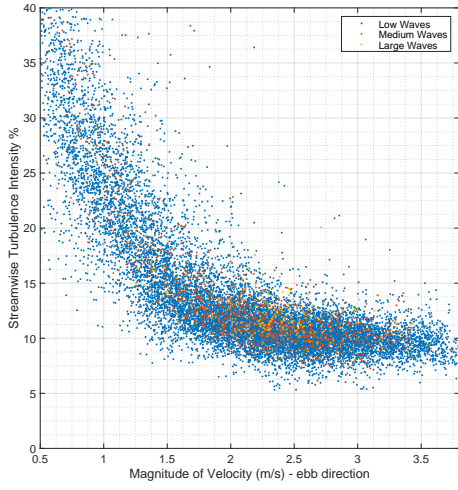


(a) No acceleration filter

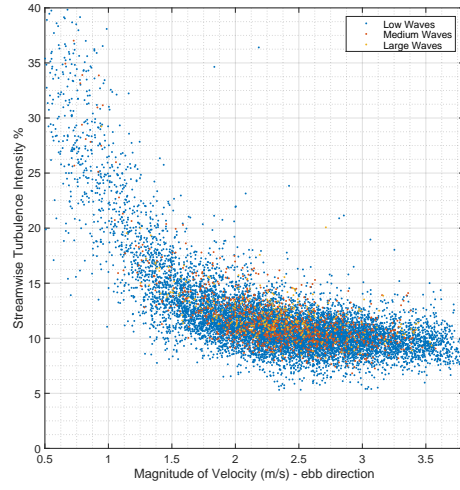


(b) Acceleration filter applied

Figure 3.45: Data Query:ebb flow; turbine generating power below 0.2MW

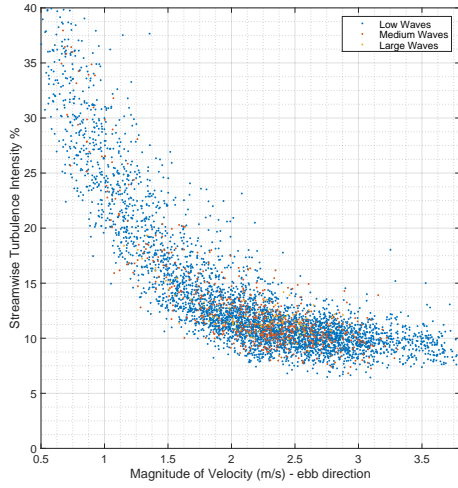


(a) No acceleration filter applied.

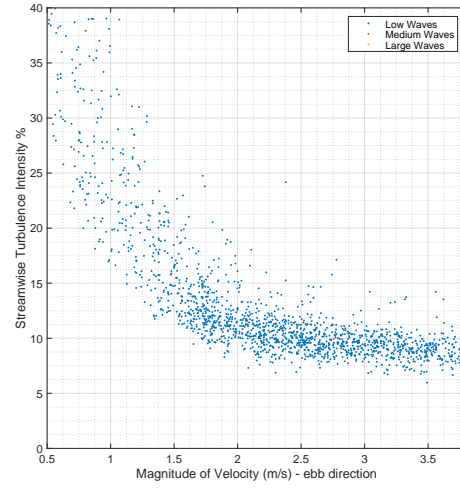


(b) Acceleration filter applied.

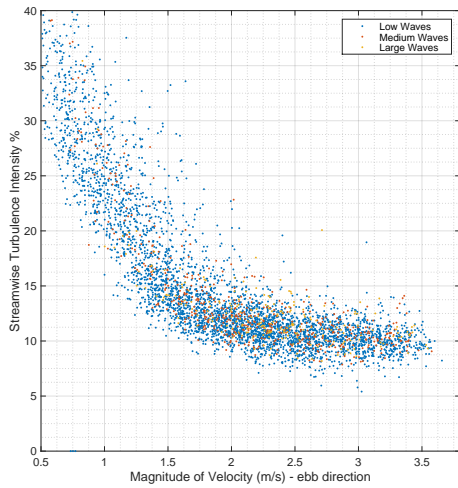
Figure 3.46: Aggregated Streamwise Turbulence Intensity at turbine hub-height for inline seabed ADCPs upstream of turbine on ebb tidal flow



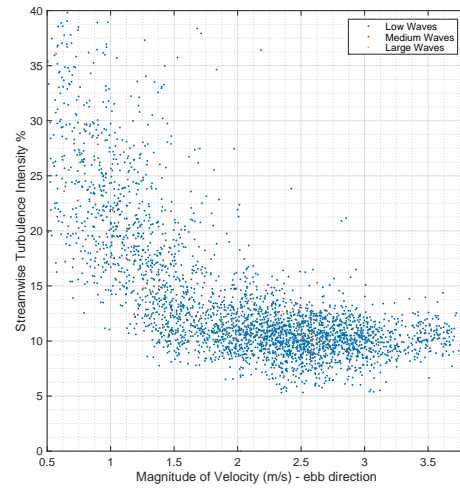
(a) ADCP02-SE-Dep1



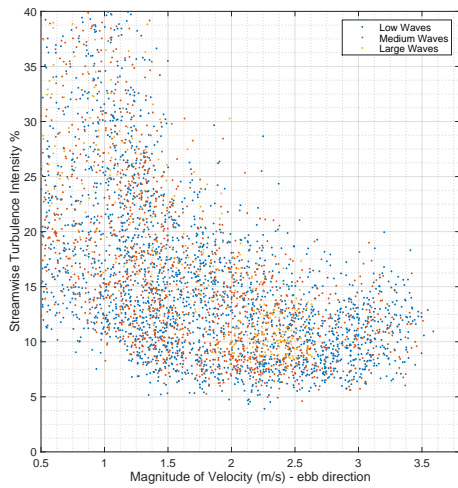
(b) ADCP02-SE-Dep2



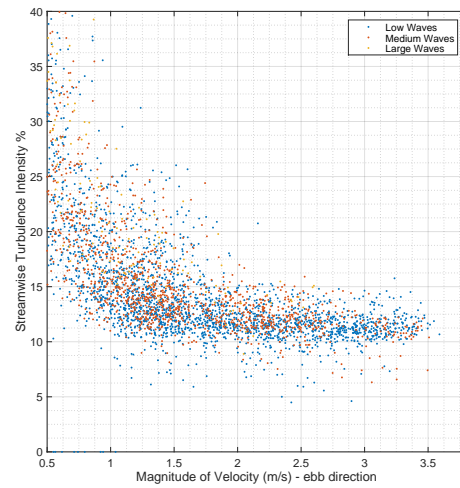
(c) ADCP02-SE-Dep4



(d) ADCP03-SE-Dep1

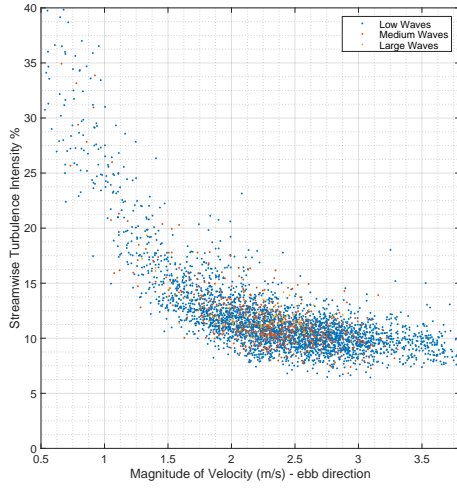


(e) ADCPTD7-01-Dep1

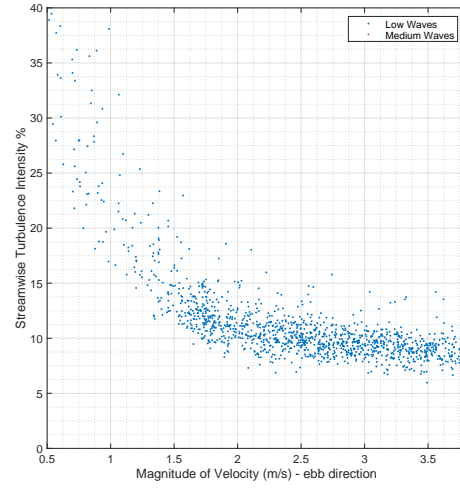


(f) ADCPTD7-02-Dep1

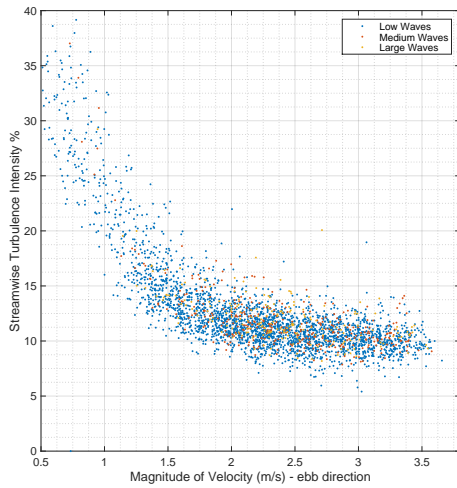
Figure 3.47: Streamwise Turbulence Intensity at turbine hub-height for seabed ADCPs upstream of turbine on ebb tidal flow. No acceleration filter applied.



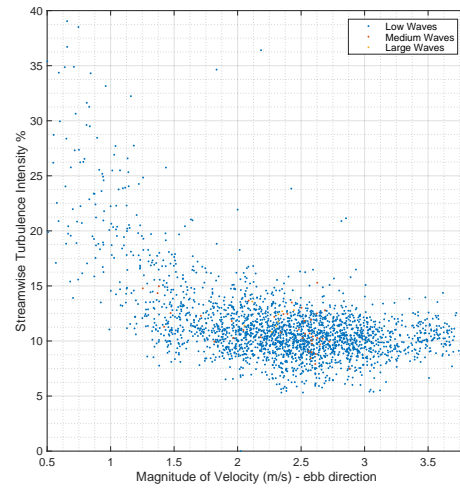
(a) ADCP02-SE-Dep1



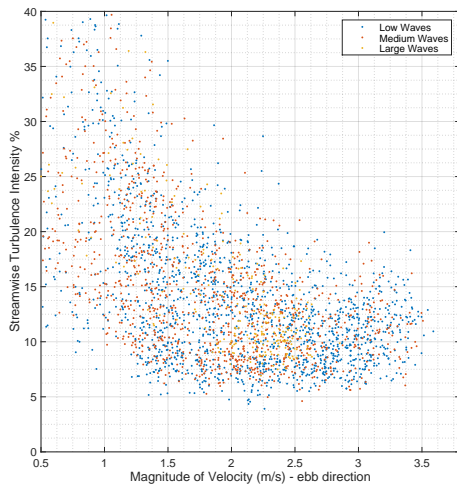
(b) ADCP02-SE-Dep2



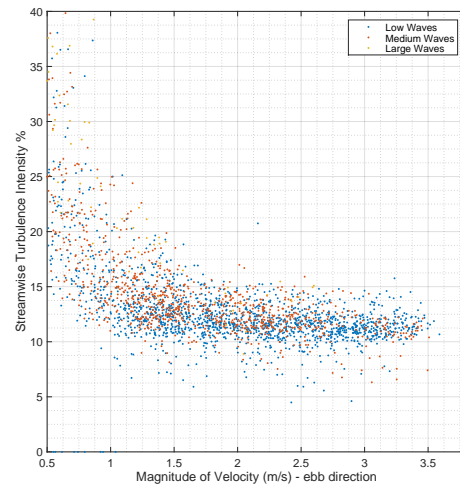
(c) ADCP02-SE-Dep4



(d) ADCP03-SE-Dep1

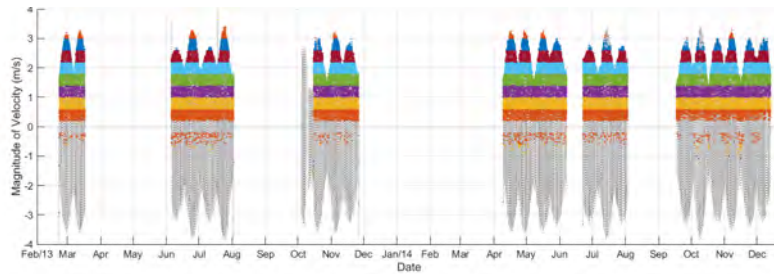


(e) ADCPTD7-01-Dep1

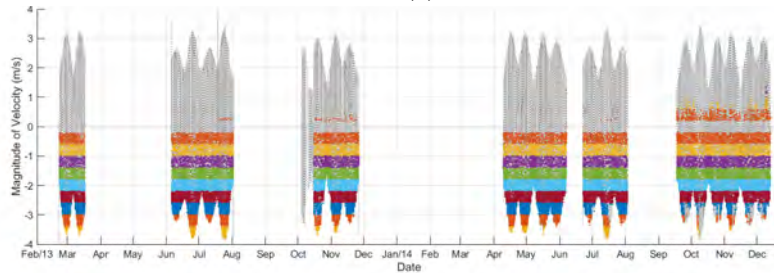


(f) ADCPTD7-02-Dep1

Figure 3.48: Streamwise Turbulence Intensity at turbine hub-height for seabed ADCPs upstream of turbine on ebb tidal flow. Acceleration filter applied.



(a) Flood Tide



(b) Ebb Tide

Figure 3.49: Data Query:flood and ebb flows; all waves; no acceleration filter applied

3.9 Analysis: Seabed Mounted Instrumentation

3.10 Advanced Measurement Techniques (2D Array vs SB)

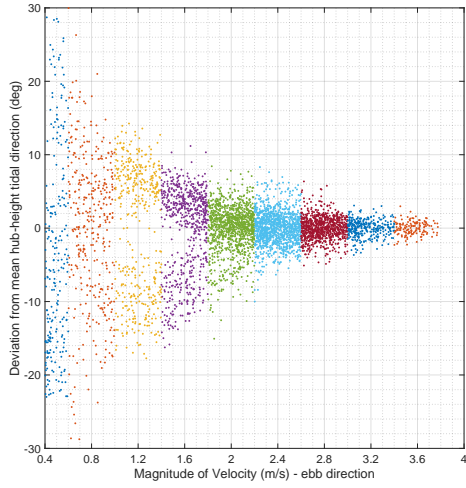
Duncan PhD noise-reduction using parallel sensors (broadside tests)

3.11 Advanced Measurement Techniques (C-ADP vs D-ADP)

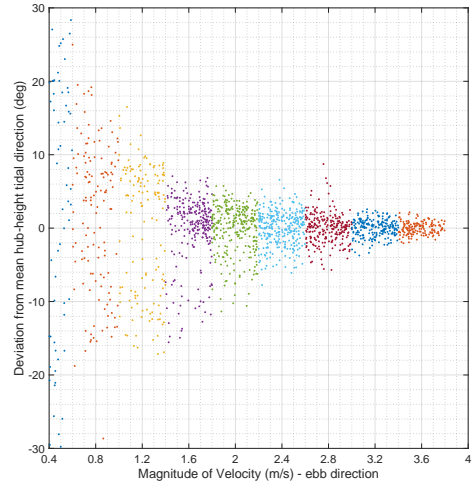
Summary of MST Journal Paper: High-resolution velocimetry in energetic tidal currents using a convergent-beam acoustic Doppler profiler” Sellar, Harding, Richmond

3.12 Sensitivity Analysis

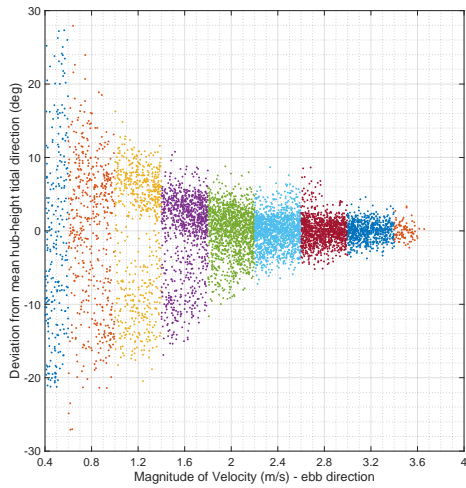
3.13 Conclusions on Convergence/Sensitivity/Uncertainty



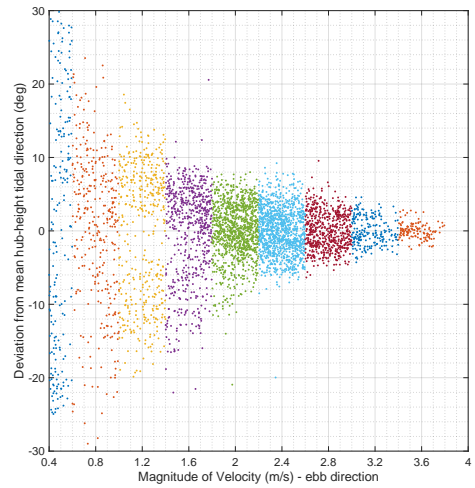
(a) ADCP02-SE-Dep1



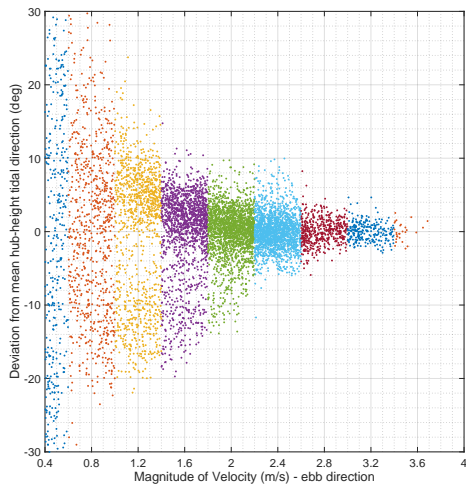
(b) ADCP02-SE-Dep2



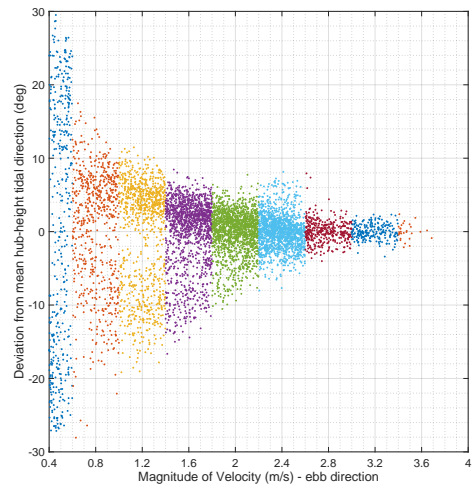
(c) ADCP02-SE-Dep4



(d) ADCP03-SE-Dep1

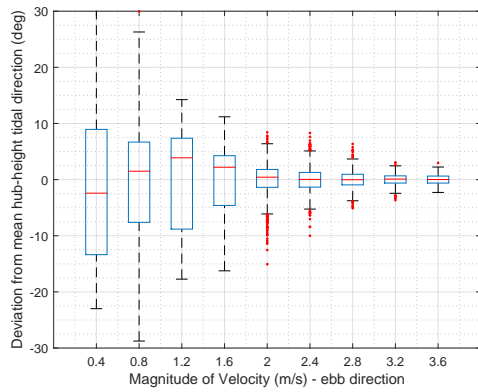


(e) ADCPTD7-01-Dep1

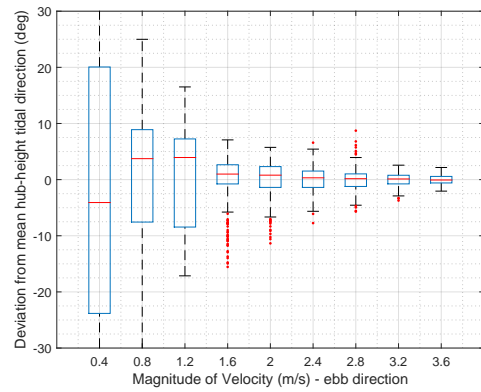


(f) ADCPTD7-02-Dep1

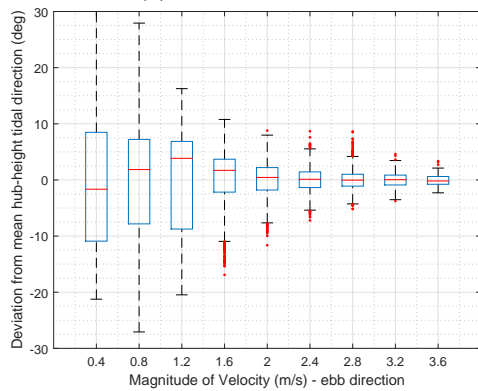
Figure 3.50: Deviation from mean hub-height tidal direction (degrees) for seabed ADCPs upstream of turbine on ebb tidal flow



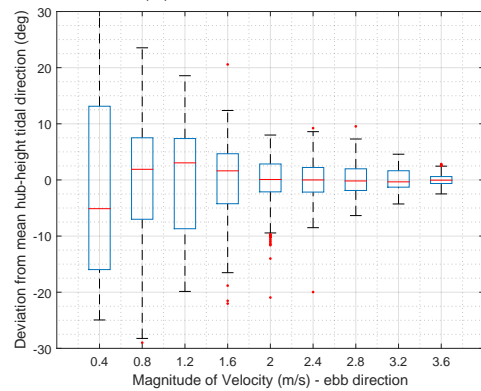
(a) ADCP02-SE-Dep1



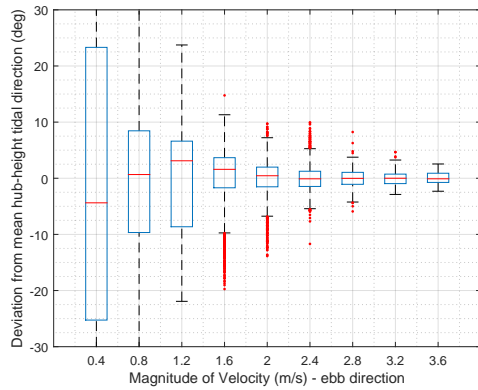
(b) ADCP02-SE-Dep2



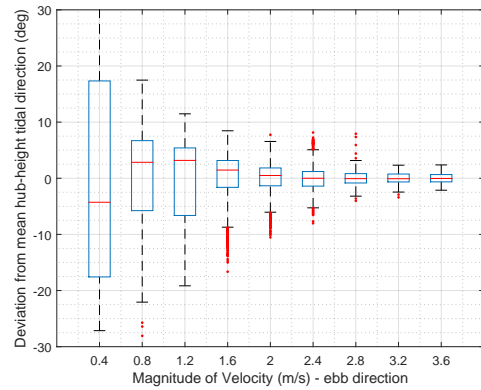
(c) ADCP02-SE-Dep4



(d) ADCP03-SE-Dep1



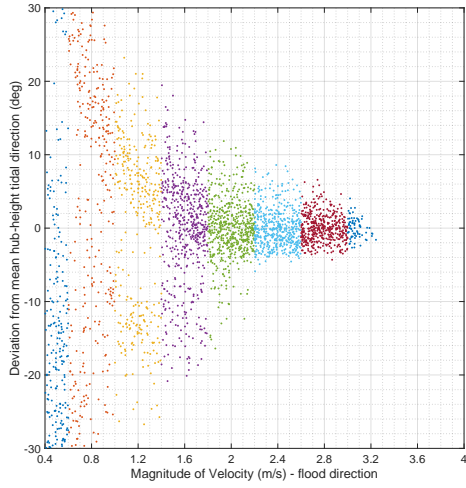
(e) ADCPTD7-01-Dep1



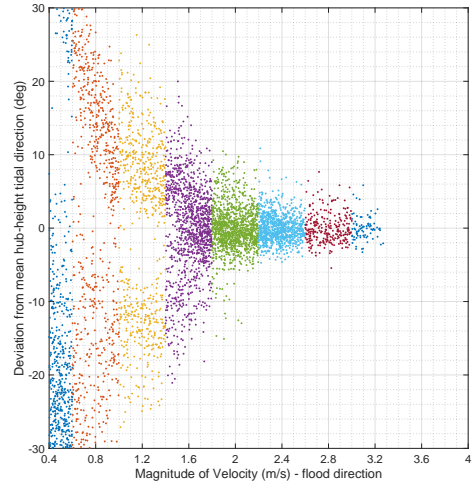
(f) ADCPTD7-02-Dep1

Figure 3.51: Deviation from mean hub-height tidal direction (degrees) for seabed ADCPs upstream of turbine on ebb tidal flow

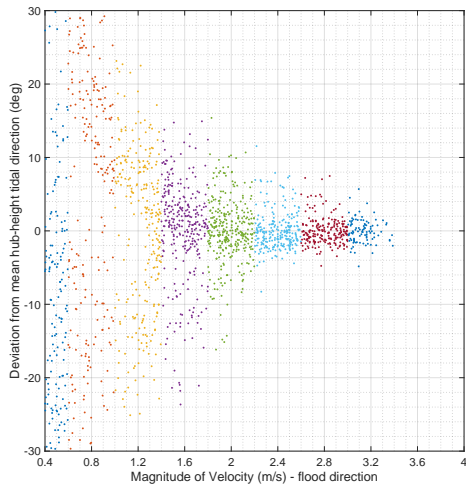




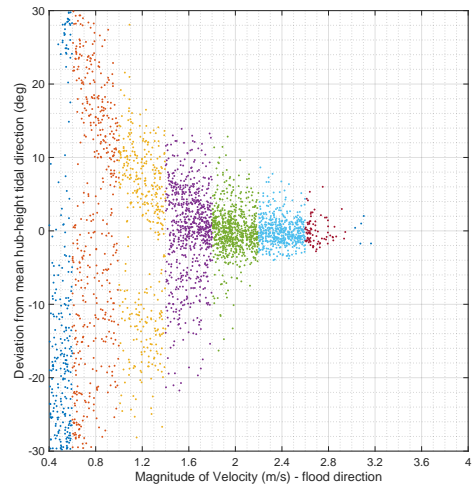
(a) ADCP01-NW-Dep0



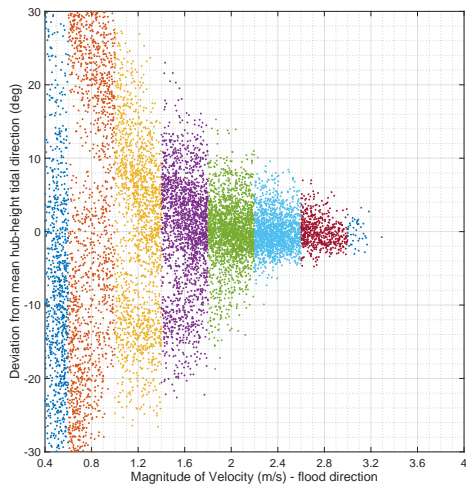
(b) ADCP01-NW-Dep1



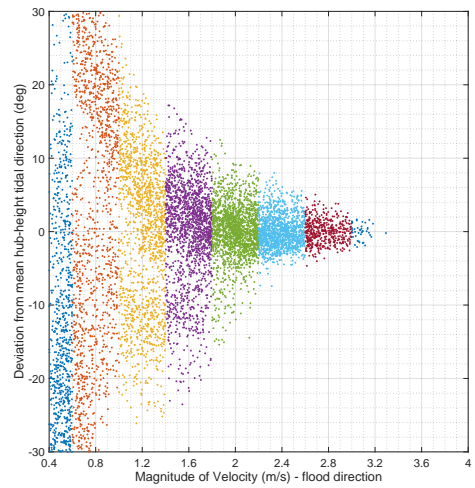
(c) ADCP01-NW-Dep2



(d) ADCP02-NW-Dep5

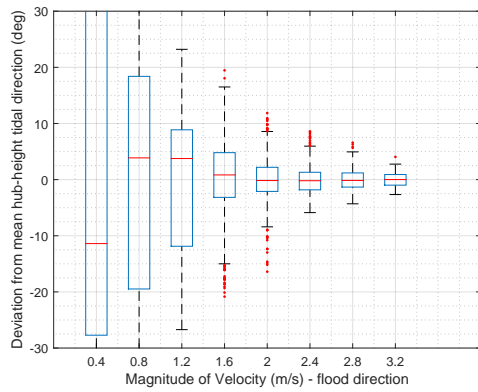


(e) ADCPTD7-01-Dep1

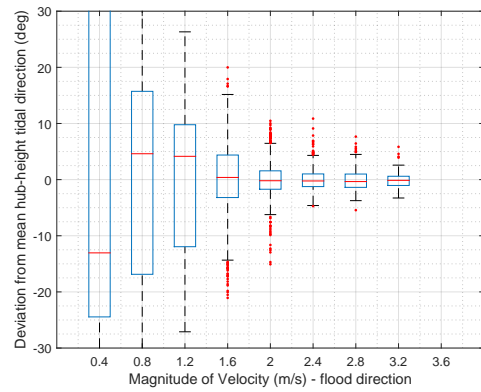


(f) ADCPTD7-02-Dep1

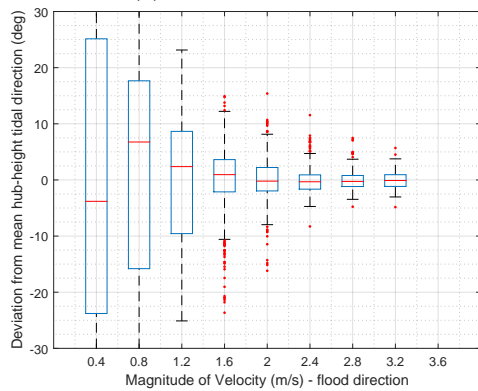
Figure 3.52: Deviation from mean hub-height tidal direction (degrees) for seabed ADCPs upstream of turbine on flood tidal flow



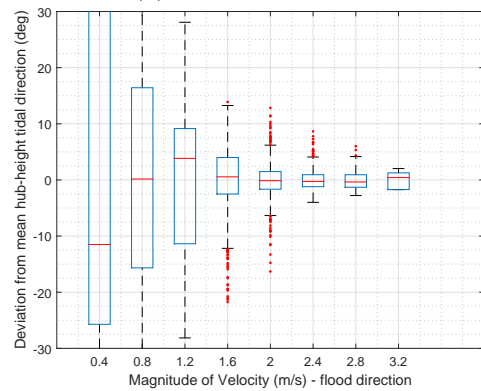
(a) ADCP01-NW-Dep0



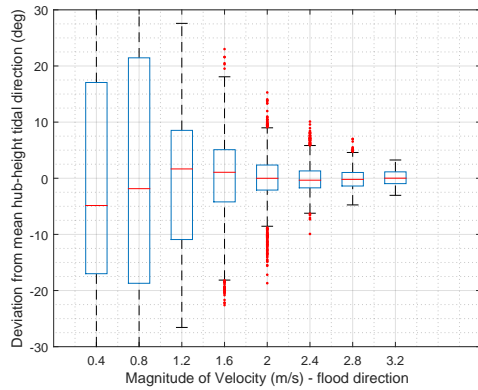
(b) ADCP01-NW-Dep1



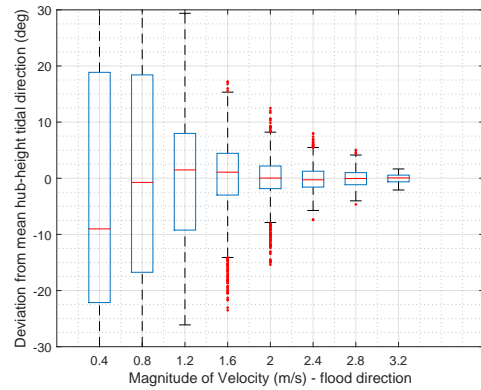
(c) ADCP01-NW-Dep2



(d) ADCPTD7-01-Dep1

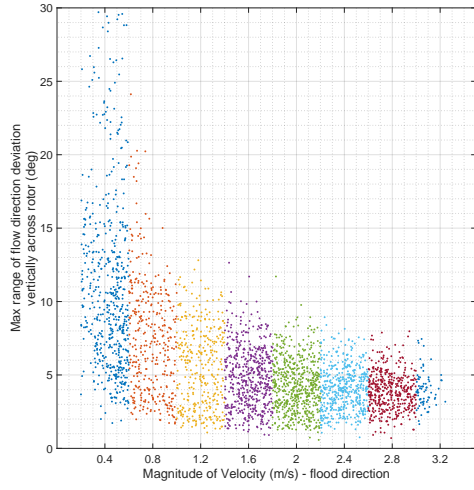


(e) ADCPTD7-02-Dep1

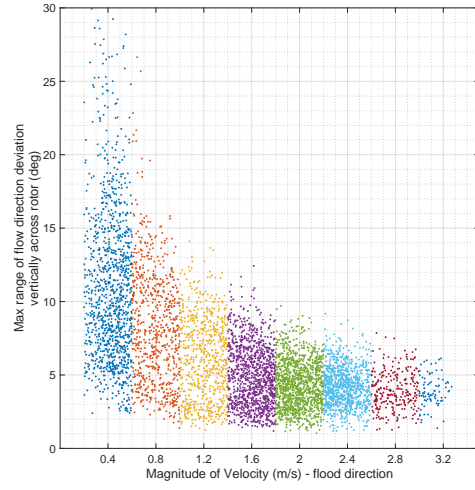


(f) CCombination (inline ADCPs)

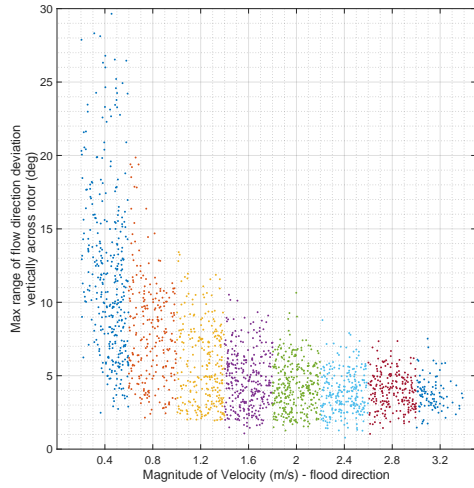
Figure 3.53: Deviation from mean hub-height tidal direction (degrees) for seabed ADCPs upstream of turbine on flood tidal flow



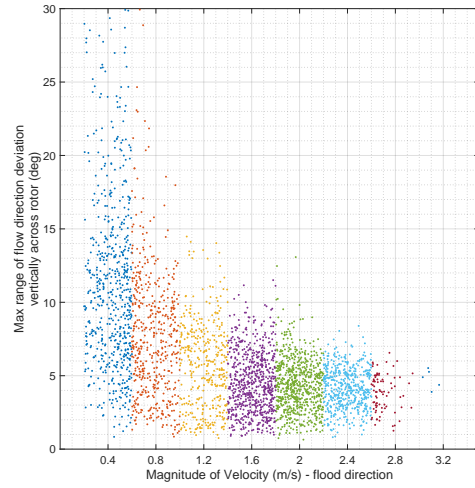
(a) ADCP01-NW-Dep0



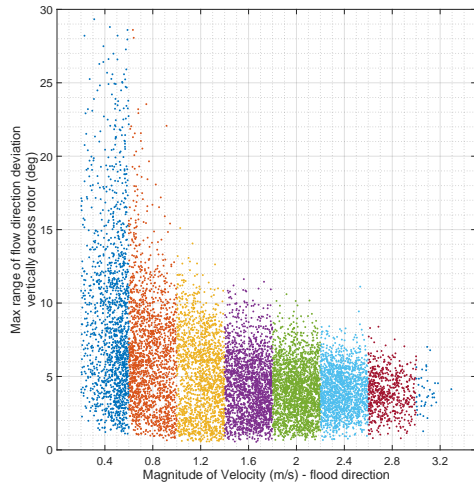
(b) ADCP01-NW-Dep1



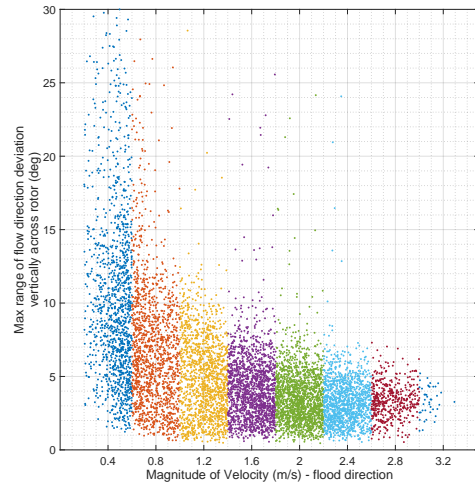
(c) ADCP01-NW-Dep2



(d) ADCP02-NW-Dep5

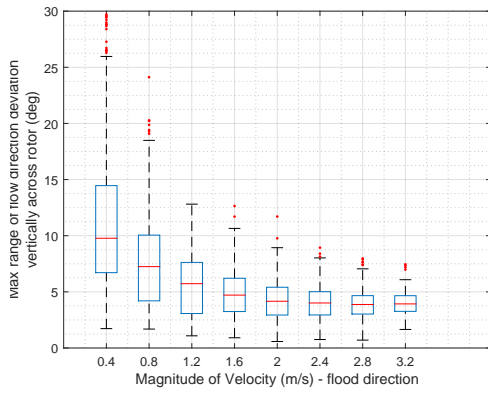


(e) ADCPTD7-01-Dep1

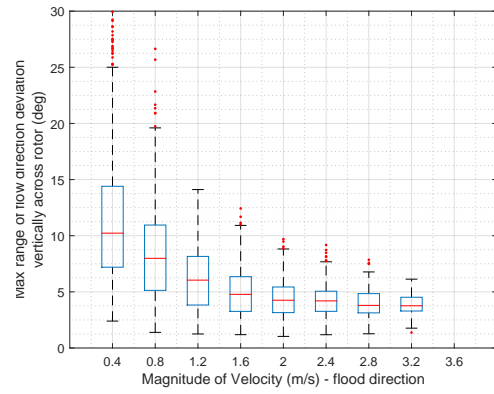


(f) ADCPTD7-02-Dep1

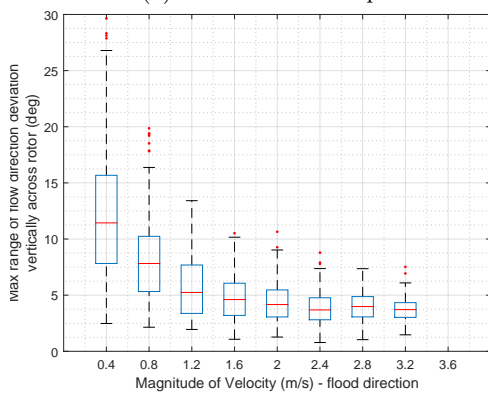
Figure 3.54: Max range of flow direction deviation vertically across rotor (deg)



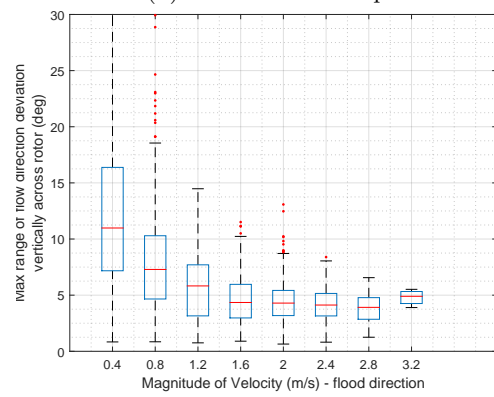
(a) ADCP01-NW-Dep0



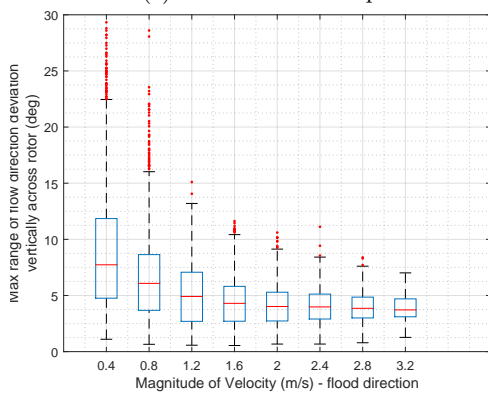
(b) ADCP01-NW-Dep1



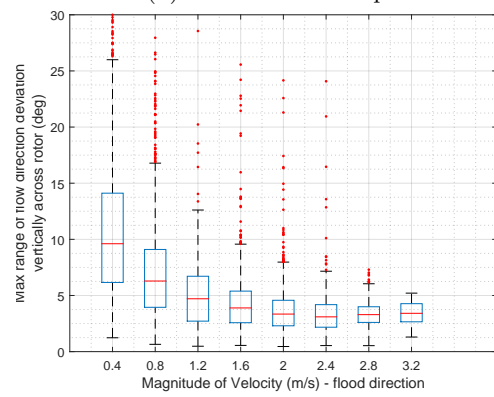
(c) ADCP01-NW-Dep2



(d) ADCP02-NW-Dep5

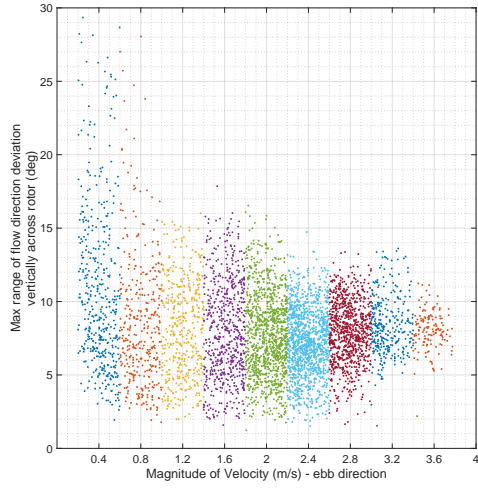


(e) ADCPTD7-01-Dep1

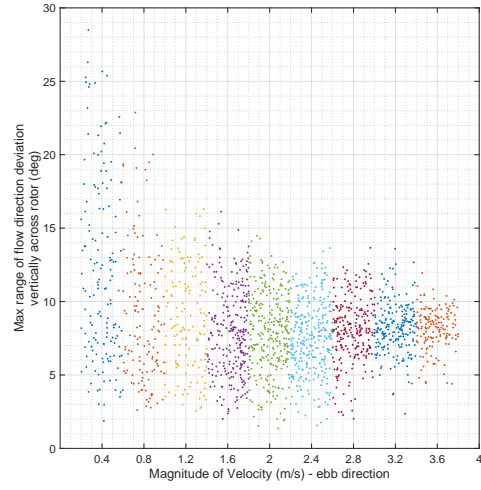


(f) ADCPTD7-02-Dep1

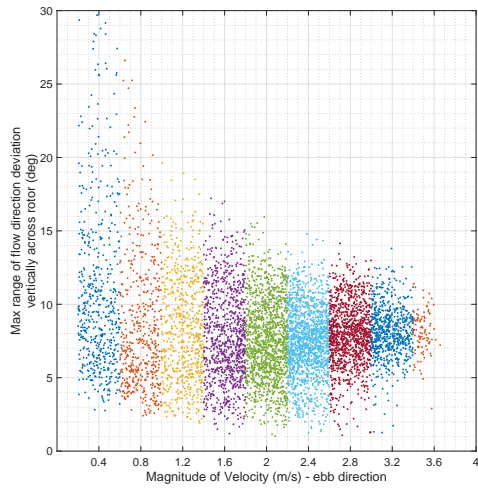
Figure 3.55: Max range of flow direction deviation vertically across rotor (deg)



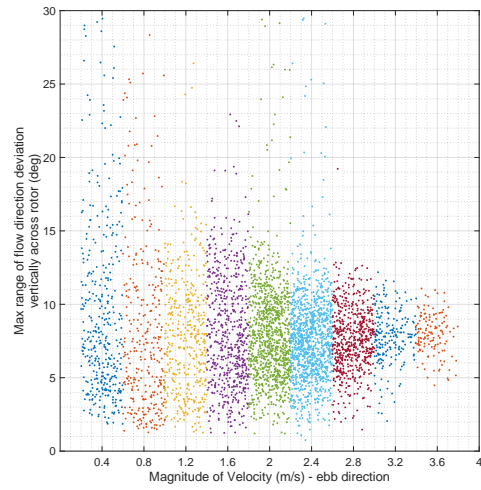
(a) ADCP02-SE-Dep1



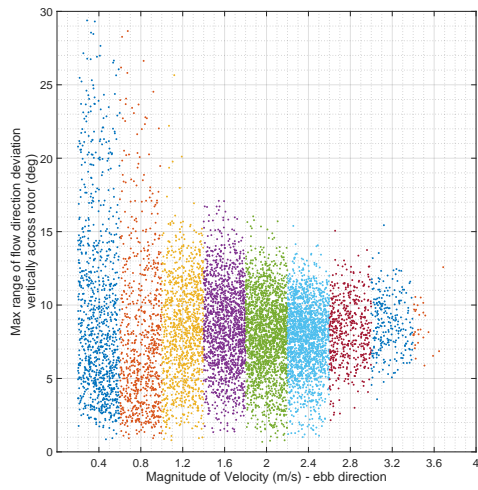
(b) ADCP02-SE-Dep2



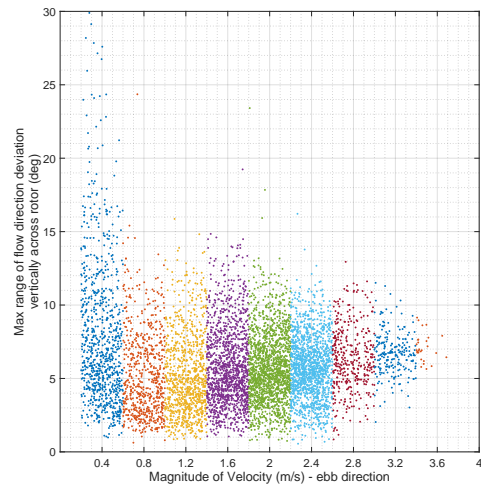
(c) ADCP02-SE-Dep4



(d) ADCP03-SE-Dep1

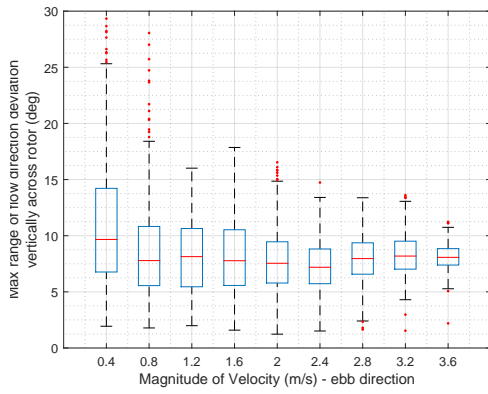


(e) ADCPTD7-01-Dep1

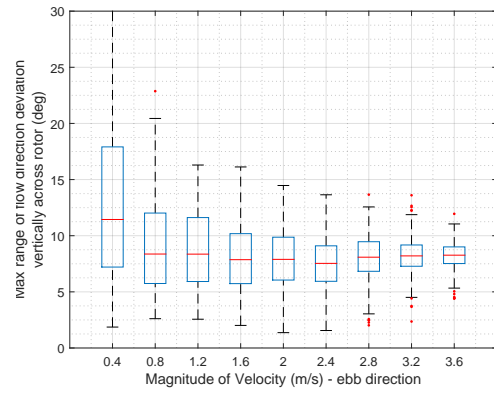


(f) ADCPTD7-02-Dep1

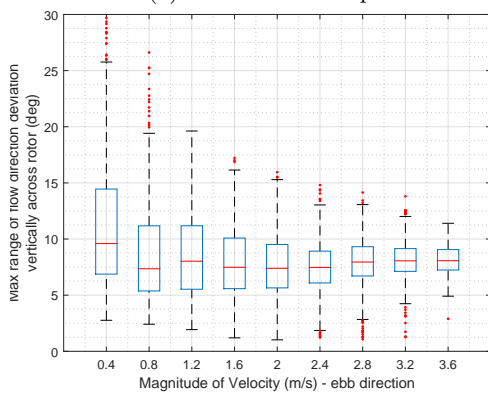
Figure 3.56: Max range of flow direction deviation vertically across rotor (deg)



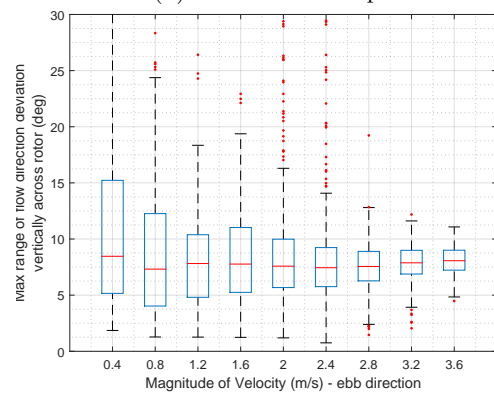
(a) ADCP02-SE-Dep1



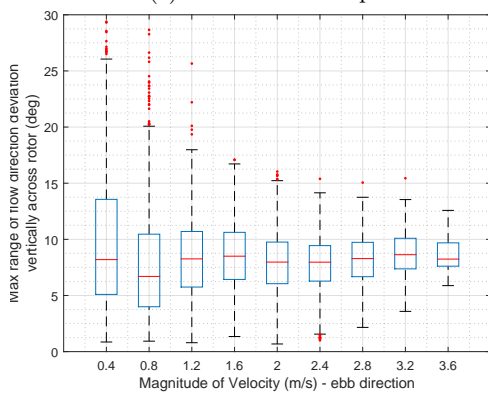
(b) ADCP02-SE-Dep2



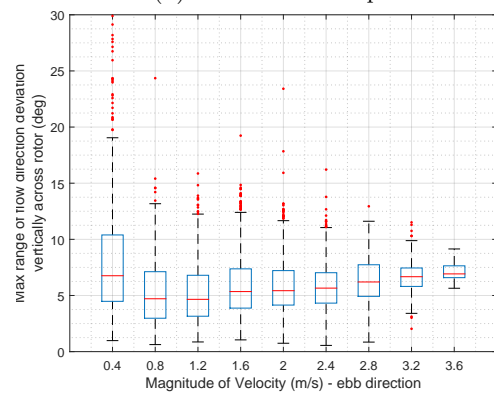
(c) ADCP02-SE-Dep4



(d) ADCP03-SE-Dep1



(e) ADCPTD7-01-Dep1



(f) ADCPTD7-02-Dep1

Figure 3.57: Max range of flow direction deviation vertically across rotor (deg)

Chapter 4

Lessons Learned and Industry Guidance



4.1 Introduction and Overview

The University of Edinburgh measurement campaigns of the ReDAPT project are summarised in section 4.2 and cover sensor system integration with the Alstom 500KW and 1MW tidal turbines as well as seabed-located sensor deployments. Lessons learned during these specific deployments are included. Section 4.4 outlines more broadly the data acquisition and data handling processes and makes recommendations for future campaigns where appropriate.

4.1.1 The Alstom DEEPGEN Turbines

Main features common to both designs:

- Horizontal axis, 3-bladed
- Buoyant nacelle
- Rated to (500KW) 1MW exported electrical power
- Deployed at berth six, EMEC Tidal Test Site
- Pitching blades
- Power conditioning on-board nacelle
- Optical-Fibre Ethernet connection to shore and Internet
- Capable of yawing to any requested heading position through use of integrated rear/tail thruster

The 500KW Alstom DEEPGEN III

((PARAPHRASE MAT HAWTHORN'S H2020 REPORT)) **IPSOR**

In February 2008 the Technology Strategy Board launched the DEEP-Gen III (Deepwater Economic Energy Prototype Generator) programme to manufacture and test a 500kW Tidal Turbine. This was intended to be a concept demonstrator in order to de-risk the design prior to development of a commercial scale device. The DEEPGen III 500kW turbine was installed on 19th September 2010 at the European Marine Energy Centre (EMEC) in Orkney, Scotland. The project was a collaboration between Tidal Generation Ltd (TGL), a wholly owned subsidiary of Rolls-Royce PLC (RR), Garrad Hassan and Partners (GH), Edmund Nuttall Limited (trading as Ritchies) and SLP Engineering Limited (SLP), each bringing different expertise to the project.



(a) The 500KW DEEPGEN III being lifted.



(b) The 1MW DEEPGEN IV on stand.

Figure 4.1: The Alstom DEEPGEN turbines at Hatston Quay, Orkney

The DEEP-Gen III concept includes a tripod which is pinned to the seabed and a buoyant nacelle which can be towed to the site, locked onto the tripod and connected to the grid. The installation of the tripod support structure was completed in early 2010 using an offshore dynamically positioned vessel. Dunk tests, the practicing of the turbine deployment and retrieval operations, were carried out during summer 2010 with a 30m deployment vessel to develop the turbine installation process. The first deployment of the turbine onto the tripod, was achieved in mid- September. Power generation soon followed and the power rating of the turbine was increased progressively, achieving full rating in mid-November.

The 1MW Alstom DEEPGEN IV

((PARAPHRASE REDAPT SLIDES)) **IPSOR**

4.2 Case Study: ReDAPT Instrumentation Systems

4.2.1 Introduction and Overview

Measurement campaigns were conducted by the University of Edinburgh from (xx) to October 2014. Measurement campaigns were carried out under a “Test Request” system (TRN) operated by the Project Lead, Alstom. Following completion of the UoE TRNs data collection continued in an ad-hoc manner up to January 2015 with a priority of collecting previously unattained winter storm measurements. Table 4.1 and figure 4.4 provide an overview and time-line of deployments. The target deployment strategy was based upon stand-alone ADCP deployments upstream and downstream of the tidal turbine with simultaneous acquisition of turbine-mounted instrumentation in real-time. TRNs were produced to: a) provide data at appropriate timings to project partners for their parallel works, namely numerical modelling validation and turbine operation monitoring and turbine performance assessment and b) provide sufficient data for Fall of Warness site characterisation work (see chapter 3). Turbine performance assessment and machine control required acquisition during periods of turbine generation. Site characterisation tests involved the scheduled (or opportunistic) acquisition of data during periods of turbine non-generation.

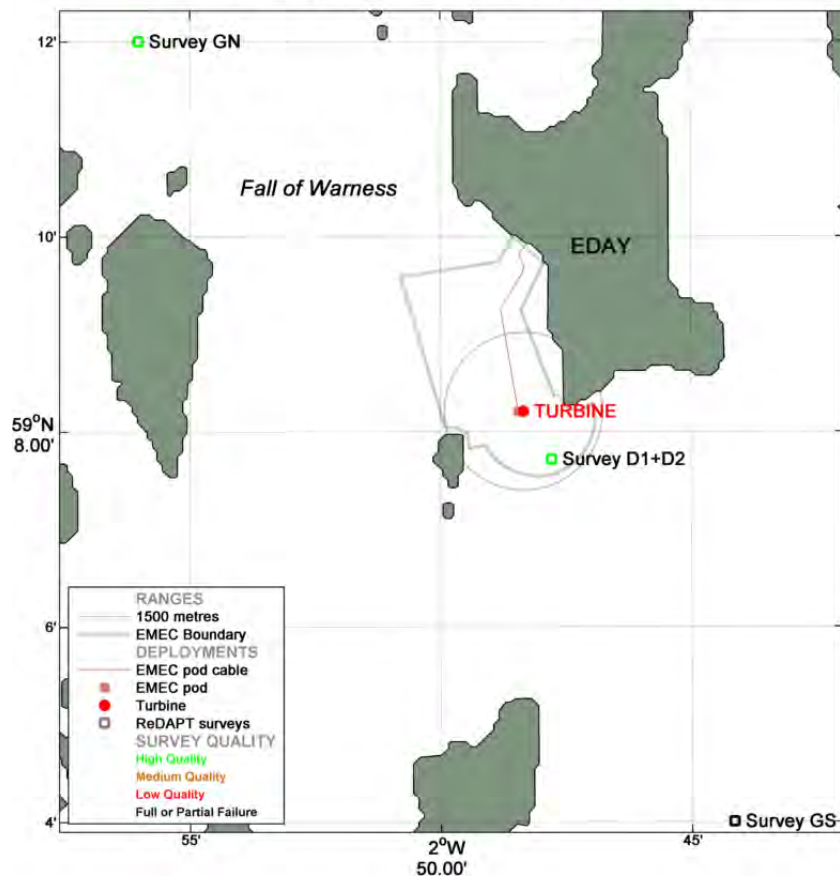


Figure 4.2: Far Field Deployments



Figure 4.3: Near Field Deployments

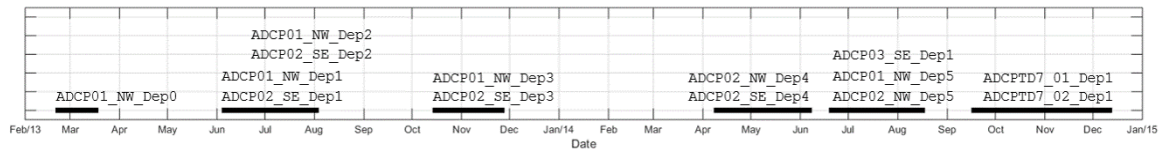


Figure 4.4: ADCP deployment time-line

4.2.2 Seabed Mounted Instrumentation

Turbine Deployment	ADCP Code	Date Deployed	Date Recovered	Duration (Days)
500KW	ADCP01_NW_Dep0	2013-02-21	2013-03-17	24
2	ADCP01_NW_Dep1	2013-06-05	2013-07-17	42
2	ADCP02_SE_Dep1	2013-06-05	2013-07-17	42
3	ADCP01_NW_Dep2	2013-07-18	2013-08-02	15
3	ADCP02_SE_Dep2	2013-07-18	2013-08-02	15
4	ADCP01_NW_Dep3	2013-10-15	2013-11-26	42
4	ADCP02_SE_Dep3	2013-10-15	2013-11-24	40
5	ADCP02_NW_Dep4	FAILED	FAILED	N/A
5	ADCP02_SE_Dep4	2014-04-09	2014-06-06	58
6	ADCP03_SE_Dep1	2014-06-20	2014-08-05	46
6	ADCP01_NW_Dep5	2014-06-22	2014-08-02	41
6	ADCP02_NW_Dep5	2014-07-07	2014-08-16	40
7	ADCPTD7_01_Dep1	2014-09-17	2014-12-11	85
7	ADCPTD7_02_Dep1	2014-09-17	2014-11-27	71

Table 4.1: ADCP Deployments - Missing D1,D2,EMECPODS

ADCP Gravity Foundations

For deployments outwith immediate proximity to the turbine stand i.e., ranges >100m, ADCP foundations of the type commonly deployed by EMEC - designated Type A - were used. For deployments in close proximity to the turbine an existing Alstom foundation (Type B) was used and was later augmented with a UoE design (Type C). All three designs can be seen in figure 4.5. Outline descriptions can be found in table 4.2.

Frame Type	Description	Dimensions (m)	Main Materials	Approx. Mass (Dry) (kg)	Approx. Mass (Wet) (kg)
Type A	S/S welded frame with S/S sheet panelling Lead weights attached to bottom frame section. Single lifting point.	(())W x L x B	Stainless Steel Lead	300	260
Type B	Concrete-filled S/S sheeted shell Single lifting point Patented ROV docking feature 3 reinforced feet	(())W x L x B	Concrete Stainless Steel	2200	1400
Type C	Concrete (from UoE mould) S/S reinforcing elements Single lifting point 3 feet	(())W x L x B	Concrete Stainless Steel	3000	2000

Table 4.2: ADCP frame Types A to C. Dimensions and construction type.

Type-B and Type-C foundations were selected to increase the level of force required to move or overturn the foundations post deployment and moreover to be deployed and recovered with the assistance



(a) Type A ADP frame.



(b) Type B ADP frame



(c) Type C ADP frame.



(d) Type B & C ADP frames.

Figure 4.5: Multiple instrumentation frames used during ReDAPT

of a remotely operated underwater vehicle (ROV). UoE designed Type-C featured deliberately enlarged equipment bays to allow modification after initial use. This feature proved useful following the requirement to install enhanced-duration battery packs.

Deployment Methods

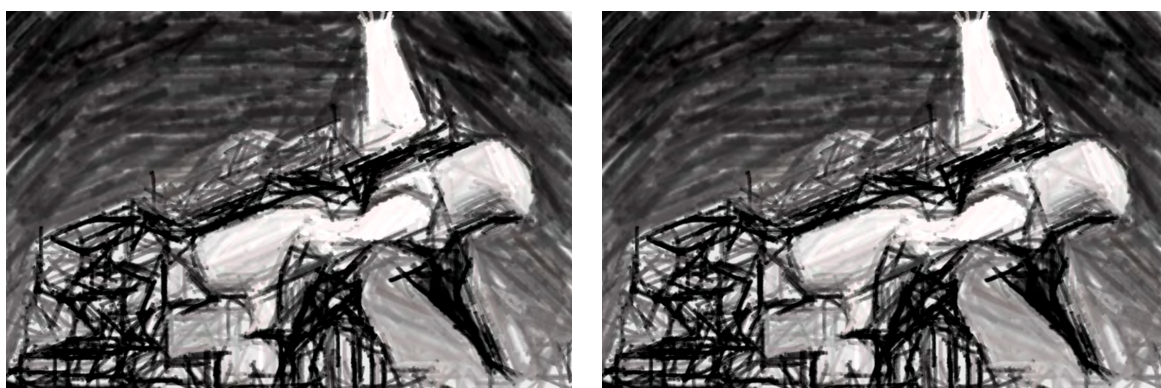
IPSOR

Type A frames and on-board instrumentation were deployed at positions D1,D2,GN and GS (see figure ??). Due to being relatively low in weight these frames were deployed with small vessels (see figure 4.3). Due to being sufficiently remote from other seabed assets within EMEC's site polymer side-lines were laid out either side of the gravity frame to approximately 100 m which were terminated and held down with clump weights. Attached to one end of these side-lines was a buoy marker which would breach the surface around slack-tide and enable retrieval. The presence of the side-lines both removes the buoy marker from the acoustic path of the profiling instrument and provides a contingency method for retrieval whereby the frame's side-lines can be grappled with the vessel conducting a series of transects perpendicular to the path of the laid out lines. On each occasion the frames were retrieved with no requirement for the contingency method. An additional

benefit of this method is in the simplicity of lowering equipment required i.e., there is no need for a hydraulically or acoustically operated release: the deployment is conducted on a single loop of rope that is pulled through and back up upon deployment.

Type B and C frames, due to their larger weight, required more powerful vessel-mounted hydraulically powered lifting equipment (often referred to as HIABs) in order to manoeuvre the frames into position on the vessels and for lifting over the side. Figure ?? shows a typical deployment including ROV assisted location on the SEABED. The presence of an ROV provides confirmation of the seabed positioning of the deployed frame, allowing the frames to be repositioned in the frequently occurring event of having been deployed on boulders or loose slabs of rock. Additionally, ROV assisted deployments have access to the ROV on-board sensor systems which feature acoustic positioning (relative to the vessel which is base-lined via GPS), depth gauges and heading sensors.

An alternative method of deployment was also successfully carried out whereby a sub-sea remotely operated camera was simultaneously lowered with the frame and used to enable fine-tuning of the deployment location and obstacle avoidance. In this case and in the absence of an ROV a hydraulically operated latch was used.



(a) Type C ADCP frame being lowered.

(b) TypeC ADCP frame being positioned by ROV

Multiple vessels were used to deploy and recover ADCPs over the course of the ReDAPT project as shown in table 4.3.

Vessel Operator	Vessel Name	Vessel Description	ADCP Frame-Type Deployed/Recovered
Leask Marine Ltd.	MV Uskmoor	16m Workboat Class 2	Type A
Leask Marine Ltd.	MV Challenge	14.4m Workboat Class 3	Type A
Leask Marine Ltd.	MV C-Odyssey	26m Workboat Class 1	Type B / C
Keynvor MorLift Ltd.	Severn Sea	30m Workboat Class 1	Type B / C

Table 4.3: Vessels used in ADCP deployments and recoveries

Instrumentation Configuration

The Teledyne RDI Workhorse Sentinel 600kHz Acoustic Doppler Current Profiler (ADCP) was selected to provide seabed acquired velocity profiles. This aptly named instrument has been used

worldwide and at the EMEC site over many years. The next generation Sentinel V model was not yet released during project procurement phase.

Whilst the electronics and software of the instrument are tried-and-tested and robust (for exceptions see failures) this leads to a disadvantage: restrictive memory due to the file allocation table (FAT) system in use leads to a limited data storage capacity of 4GB through the use of two 2GB PCMCIA SATA memory cards. This in turn limits the sampling frequency of the instrument in order to provide a sufficiently long deployment duration which is required to a) coordinate with other deployed assets b) measure sufficient data for long term flow prediction via harmonic analysis. In terms of coordinating with other deployments given that opportunities to deploy occur generally every 14 days (in summer) and during this period slack water typically lasts between 30 minutes and 1 hour (at the Fall of Warness) a failed deployment of either another ADCP unit or, more importantly, a tidal turbine could lead to an instrument deployment producing data that doesn't meet the test requirements. Activating a write-over-data-once-full feature brings similar problems since the retrieval schedule is inherently uncertain due to tides, performance of auxiliary equipment, boat availability and of course site weather conditions.

A trade-off between sampling frequency, power consumption and deployment duration was required. This had to be optimised depending on each turbine deployment taking into account multiple factors e.g., the stage of turbine commissioning, critical test schedules, season and weather windows.


Three main modes were utilised:

- 2.0Hz Sample Rate, 1m bin size, Current Only
- 1.0Hz Sample Rate, 1m bin size, Current Only
- 0.5Hz Sample Rate, 1m bin size, Current Only

Wave/Current Mixed Duty Cycle

A specific goal of the ReDAPT project involved the validation of state-of-the-art CFD ((LES, Rotating Domain etc.)) which was conducted by EDF and the University of Manchester. Ambient flow conditions were measured and provided to the CFD modellers. The loads from the modelled turbine subjected to these characterised flows were compared to the actual loads as measured by the 1MW machine. As anticipated it proved challenging to build up a large volume of measurement points where the 1MW tidal turbine was operating within an environmental system state sufficiently similar to that modelled. For this reason it was decided at preliminary stages of the project to not operate the ADCPs in a split Wave/Current mode whereby the instruments would measure waves for 17-20 minutes then switch back to current mode (reducing raw high frequency flow data duty cycle to as low as 0.66). With hindsight this decision should have been reviewed at each deployment (see recommendations). Whilst it was appropriate in summer months lack of direct and in-situ wave measurements makes more difficult the advanced analysis of highly wave affected flows.

Custom Peripherals

Following recovery of a preliminary ADCP and analysis of the data very high rates of instrument pitching and rolling were observed. At low velocity data was usable but at speeds relevant to power production (e.g., $U_{ref} > 1\text{ms}^{-1}$ the data was dominated by noise. It is believed (ROV/camera confirmation of the resting location was not carried out at this time) that a combination of too light ballasting of the ADCP unit and overly compliant gimbal set was the cause. 



(a) The 500KW turbine on site at Hatston Quay, Orkney, (b) Instrumentation and instrumentation control-box installed on the 500KW machine

Figure 4.7: A figure

Custom components were designed, tested and integrated into existing and new ADCP gravity frames following these early deployments:

- High stability polymer gimbals (with variable damping levels)
- Large working volume concrete 3000kg gravity foundation
- Cost effective pressure vessels for increased provision of battery power
- Axillary computer controller to circumvent 4GB memory limit (not completed during ReDAPT)



4.2.3 Turbine System Integration

Mechanical Interfacing on the 500KW turbine

Due to UoE velocimetry instrumentation being available prior to the completion of commissioning of the 1MW machine a preliminary deployment was conducted on the 500KW machine (see figure 4.7a) . Instrumentation was attached to the 500KW to de-risk later deployments by: providing earlier access to data for analysis; trial UoE-Alstom testing coordination; test the electrical and comms interfaces and assess instrument performance. Carbon steel plates were pre-drilled then welded to the turbine external rail mounts (see figure 4.7b).

Instrumentation layout is shown in figure 4.8). Orientation of the welded plates was set by a hand-held digital inclinometer held against the mounting positions. This is estimated to set orientation to within 5° of the specified angle. SBDs were mounted in the following orientations: vertically (two units) separated by ((x))m, transversely (two units) separated by ((x))m and streamwise (single unit). Additionally a single-beam long range Nortek Continental (198kHz) was mounted orientated streamwise within ((x))m of the streamwise-orientated SBD at the rear of the turbine. A three-beam Nortek AWAC (1MHz) was orientated vertically (estimated to be <5° pitch, roll and yaw) with the x-indicated beam aligned with the streamwise, rear-ward direction.

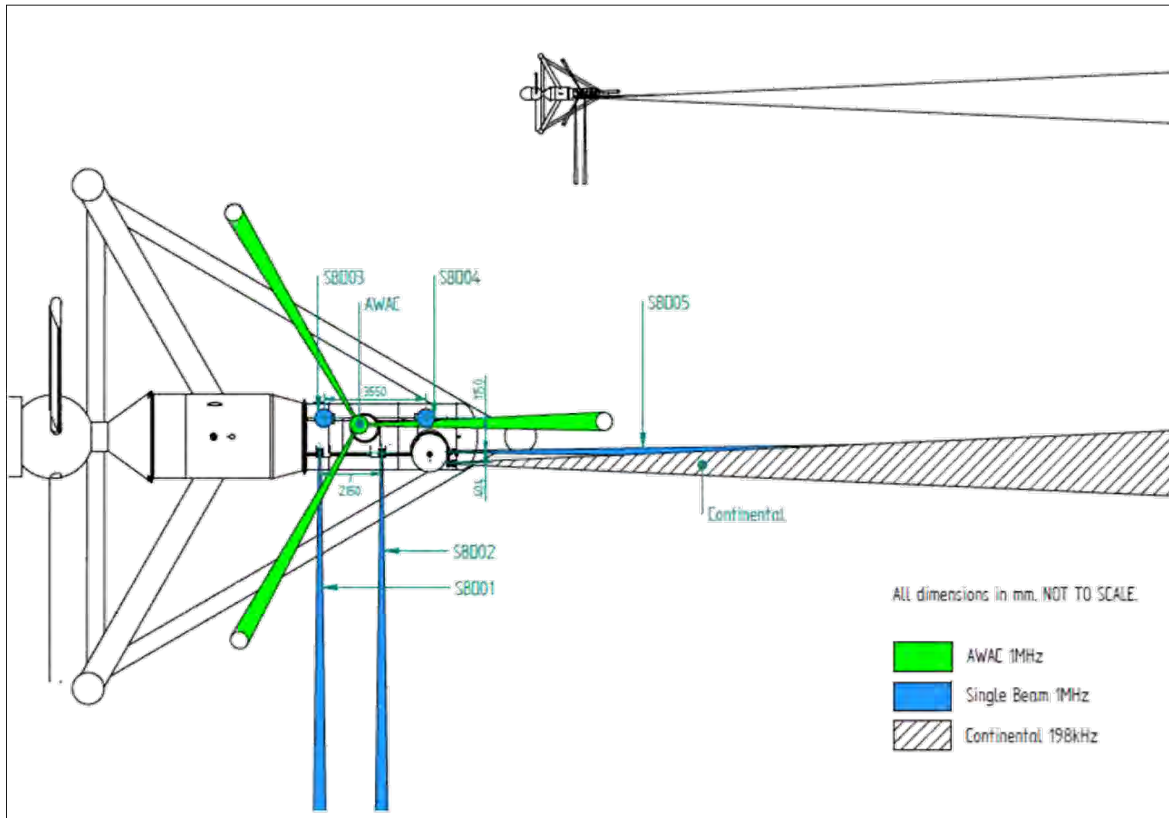


Figure 4.8: Instrumentation layout on the 500KW machine

Electrical and Communication Interfacing on the 500KW turbine

Three DC power supplies were provided to the 500KW instrumentation through an existing SEACON bulkhead penetrator. An 18.5 VDC supply powered the Continental device, a 24VDC supply powered the SBD array and a 12VDC supply powered the AWAC (see table 4.4). AWAC and SBD power and comms were pre-routed through the Instrument Control Box 1 (ICB1) as shown (blue cylinder) in figure 4.7b. ICB1 is a customised anodized and painted aluminium pressure vessel (tested to 80m) and provided by SEAPRO UK. Zinc anodes were fitted to the all-welded body and were changed during maintenance periods. The condition of this enclosure remained excellent throughout seven deployments (across the 500KW and 1MW) and totalling approximately ((x)) months of submersion. DIN rail (35mm top hat EN 50022) inside the enclosure and matching terminal fittings were used to allow adaptable and modular connectivity.

Instrument	Voltage (VDC)	Communications Protocol	Provided Via
SBD	24	TCP/IP Ethernet	Turbine Ethernet Switch
AWAC	12	Serial RS422	Vlinx Ethernet Serial Server
Continental	18.5	Serial RS422	Vlinx Ethernet Serial Server

Table 4.4: Instrument power and communications overview.

Mechanical Interfacing on the 1MW turbine

Integration of UoE instrumentation systems with the 1MW turbine was managed through a single document which in turn was produced by a three stage design review process featuring: Preliminary Design Review (PDR), Critical Design Review (CDR) and Installation Readiness Review (IRR). The integration process, “Interface Agreement and Outline Installation and Removal Plan for UoE ADP Instrumentation and ReDAPT 1MW Tidal Turbine” took approximately 6 months to finalise. Outline selections highlighting the level of detail required are shown in figures (to).

Given that the 1MW machine features a buoyant nacelle both the mass and displacement of instrumentation systems needs to be considered. Various design options for frames were proposed.

Top Frame

The following outline design specification for the Top Frame was developed:

- Tubular frame (originally S/S316 and later revised to painted Carbon Steel)
- Dry Mass 600kg
- 6 mounting point system (M16 S/S A4 bolts)
- Instrumentation plates (pre-drilled holes)
- Ability to remain electrically isolated from turbine if required
- Lifting eyes at four corners for easy removal for on-ground maintenance

The instrumentation system (frame, instruments, peripherals and fasteners) was designed holistically in CAD using Solid Edge and Solid Works software packages with material properties assigned to each sub-component. This allowed accurate total weight to be estimated and optimised.

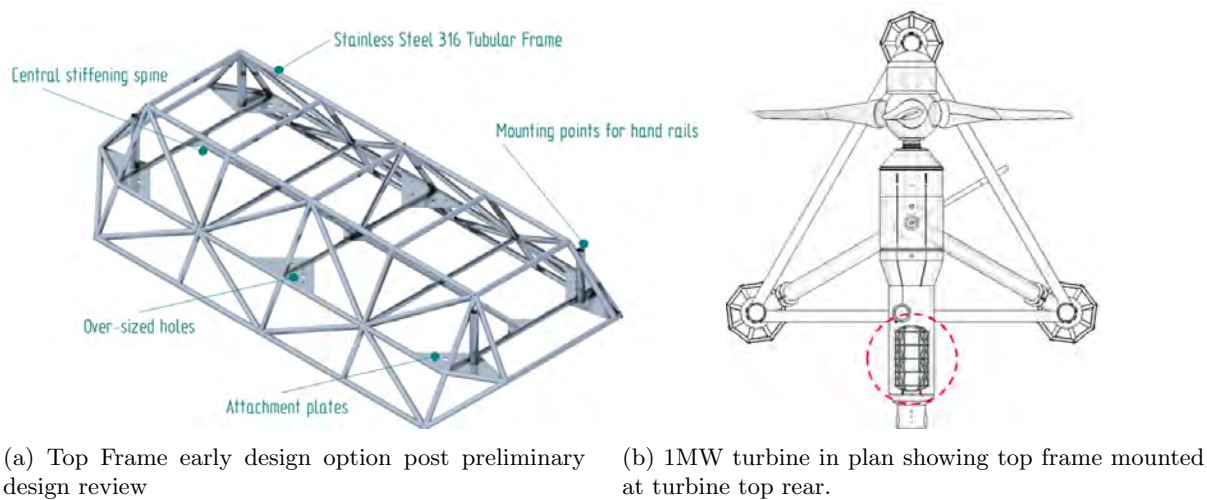


Figure 4.9: Top Frame early design option and positioning on 1MW turbine

For buoyant systems (the turbine in this case) centre of mass and centre of buoyancy are important. These were calculated using CAD tools and supplied to the turbine designers for inclusion in their buoyancy calculations.

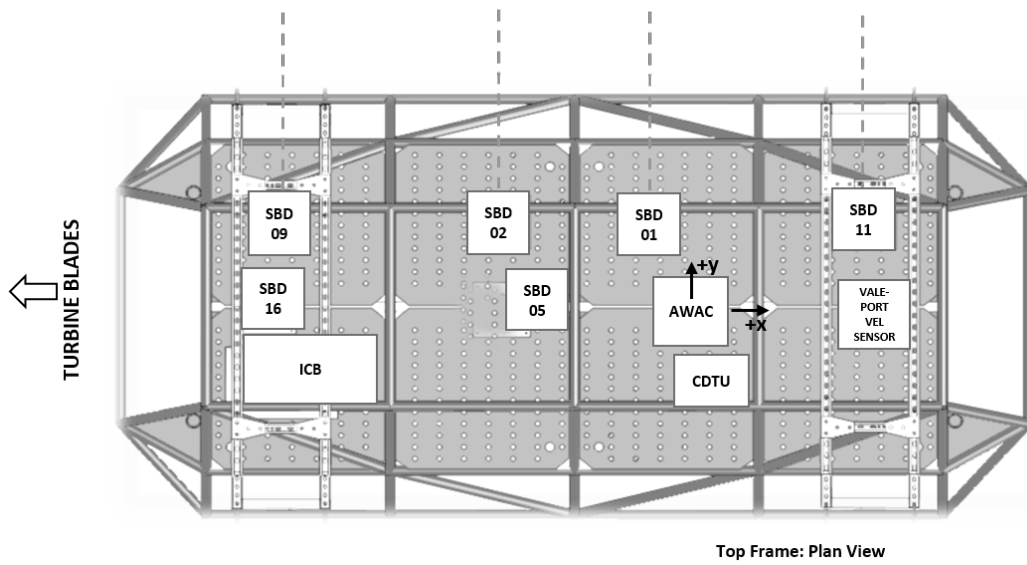
Instrument Layout

Instrument layout varied between turbine deployments as instruments were replaced for maintenance or moved in order to complete specific tests. Hole patterns on the Top Frame allowed instruments to be moved in 100mm increments in the x or y directions. A representative instrument layout schematic is shown in figure 4.10a. A standard setup involved multiple SBDs (up to 4 on each axis) orientated in the transverse and vertical directions.

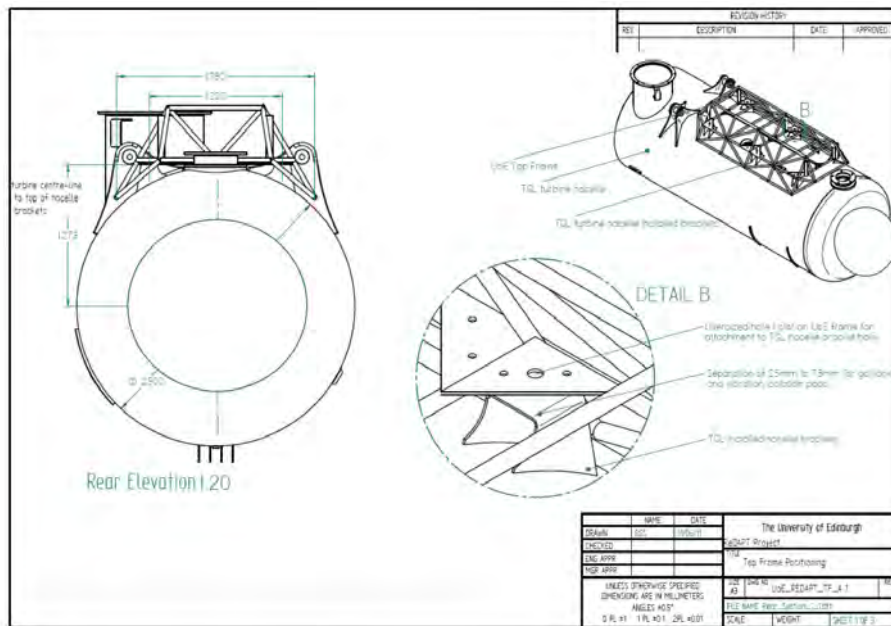
Rear Frame

The following outline design specification for the Rear Frame was developed:

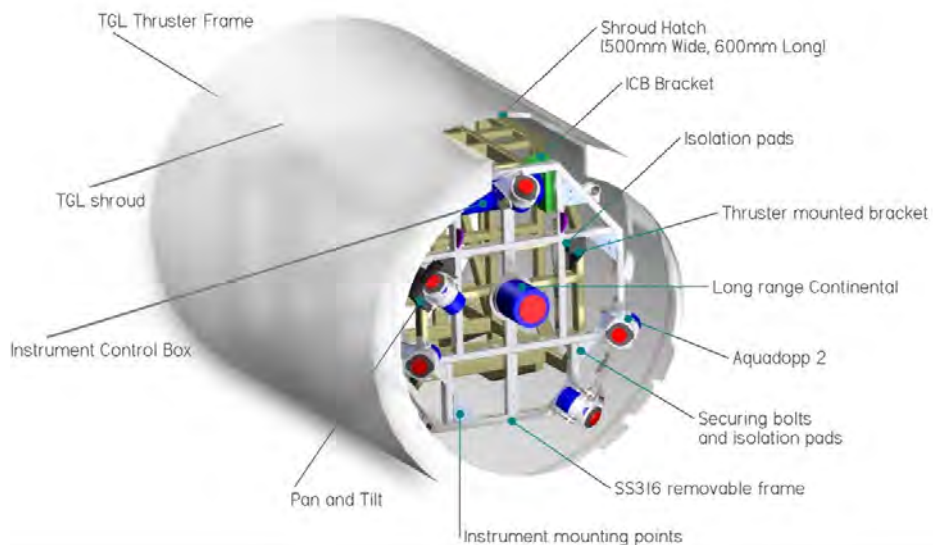
- Rectangular-section box frame (originally S/S316 and later revised to painted Carbon Steel)
- Dry Mass 215kg
- 4 mounting point system (M16 S/S A4 bolts)
- Instrumentation plates (pre-drilled holes)
- Ability to remain electrically isolated from turbine if required
- Lifting eyes at top 2 points for easy removal for on-ground maintenance



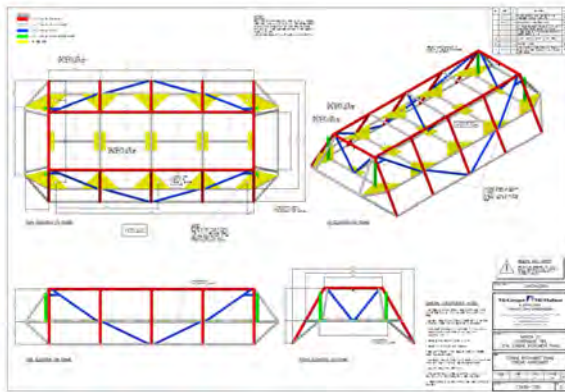
(a) representative instrument layout on the Top Frame.



(a) Top Frame positioning and attachment method on 1MW turbine (some turbine features have been masked)



(a) Rear Frame positioning, outline instrumentation positioning and attachment method on 1MW turbine rear thruster unit.



(a) Critical Design Review stage top frame development. Drawings provided by structural engineers.



(b) Top Frame fabrication

Figure 4.13: A figure



(a) Top Frame mounted on turbine at Hatston Quay, Orkney.



(b) Top Frame fabrication

Figure 4.14: A figure



(a) T



(b) T

Figure 4.15: A figure

Turbine Nose Mounted Instrumentation

Electrical and Communication Interfacing on the 1MW turbine

Top Frame

Two DC power supplies were provided to the 1MW Top Frame through a SEACON Split Pie ((series)) bulkhead penetrator. A 12 VDC supply powered the AWAC device and a 24VDC supply powered the SBD array (see table 4.4). AWAC and SBD power and comms were pre-routed through the Instrument Control Box 1 (ICB1) as shown (blue cylinder) in figure 4.16a. An OnTime Networks ethernet switch located inside ICB1 routed ethernet communications from the turbine to the ICB's internal CPU and sub-systems and the SBDs externally distributed hub (see figure ((x))). The ICB contained multiple fuses to prevent individual instrument failure (e.g., flooding of units) from disabling the entire array.

Power Supply Solution: Mark I

For turbine deployments 1-5 grounding was provided through each (12VDC and 24VDC) turbine-installed DC-DC transformers.

Power Supply Solution: Mark II

For turbine deployments 6-7 grounding was implemented in a user-selectable way to assess the impact of different grounding schemes on sensor performance.

Redundancy was increased by supplying the two Nortek ethernet switch boxes, EB1 and EB2, with separate power and ethernet connection via the ICB. This parallel set-up enabled ongoing operation of up to 7 SBDs in the event of a failure of one ethernet box.

4.2.4 Convergent Beam Doppler Velocimetry

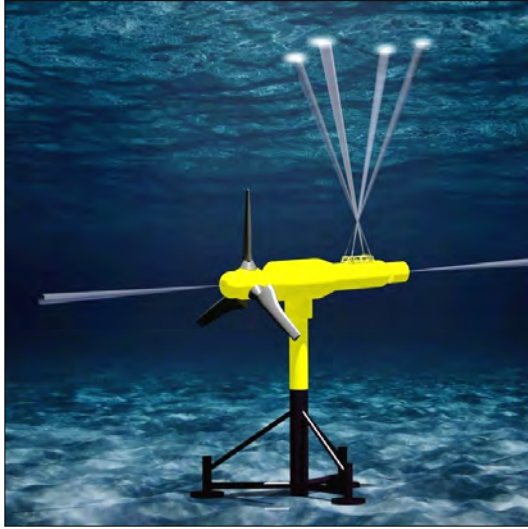
4.2.5 Power Curve Production: IEC Inspired Test

4.2.6 Case Study Recommendations

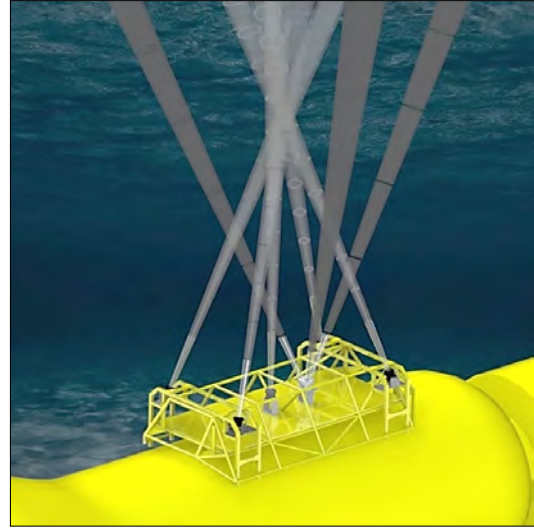
The following recommendations are based on our experience with multiple and changing prototype systems in a dynamic test environment. Suggestions should be assessed in respect of this situation. Bespoke solutions “designed-in”, bench-tested or trialled in more controllable conditions and importantly under consultation with engaged equipment suppliers will always provide more optimal results.

Connection Method

For prolonged deployments in these highly energetic and shallow waters where grounding has not been previously trialled connectors with larger diameters compared to those of the MCIL-8 range (for example Impulse and SEACON) are recommended. Larger pins seemed



(a) Convergent Acoustic Doppler Profiler (C-ADP)



(b) Convergent Acoustic Doppler Profiler (C-ADP)

Figure 4.16: Convergent Acoustic Doppler Profiler (C-ADP)

Mounting Solutions

Maintenance

Operation

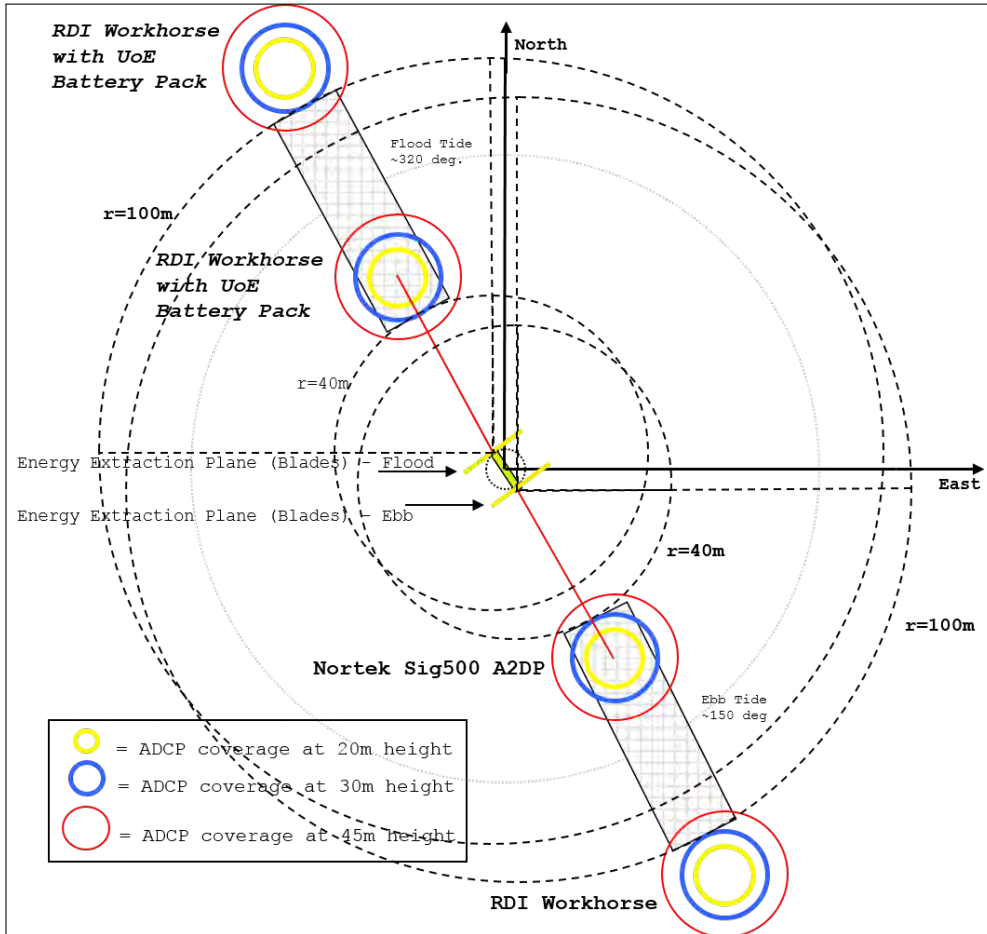


Figure 4.17: Power Curve Production: IEC Inspired Test

Component	Description	Supplier
Acoustic Doppler Profiler	Nortek, Single Beam Doppler (AD2CP)	Nortek UK
Acoustic Doppler Profiler	Nortek, AWAC	Nortek UK
Acoustic Doppler Profiler	Nortek, Continental	Nortek UK
Pressure Vessel	ICB1. 80m rated pressure vessel. Aluminium. Anodised and painted.	Greenaway Marine UK
Electrical Connectors	SEACON Bulkhead Connectors. MC((xx)). 8-way (male and female)	SEACON UK
Ethernet Hub (External)	Nortek, (Featuring OnTime Networks Ethernet Switch)	Nortek / OnTime Networks
Fasteners	Cable Ties (black nylon (66) , high tensile strength, non-resealable)	Hellerman / Tyton
Plates / Screws / Bolts	Stainless Steel 316	Various
xx		
xx		
xx		
xx		
xx		

4.2.7 Instrument Configuration - non-SBD

4.2.8 Instrument Configuration - SBD

4.3 The ReDAPT Database

Glossary

Bibliography

- [1] I. Afgan, U. Ahmed, D. Apsley¹, T. Stallard, and P. Stansby, “Cfd simulations of a full-scale tidal stream turbine: Comparison between large-eddy simulations and field measurements: ETI REDAPT MA1001 MD1.4,” School of MACE, University of Manchester, Tech. Rep., 2014.
- [2] I. Afgan, U. Ahmed, D. Apsley¹, T. Stallard, and P. Stansby, “Cfd simulations of a full-scale tidal stream turbine: Comparison between large-eddy simulations and field measurements: ETI REDAPT MA1001 MD1.5,” School of MACE, University of Manchester, Tech. Rep., 2014.
- [3] K. Gunn and C. Stock-Williams, “Fall of Warness 3D model validation report: ETI REDAPT MA1001 PM14 MD5.2,” E.ON New Build & Technology, Tech. Rep., 2012.
- [4] K. Gunn and C. Stock-Williams, “On validating numerical hydrodynamic models of complex tidal flow,” *International Journal of Marine Energy*, vol. 34, pp. 82 – 97, 2013. [Online]. Available: <http://www.sciencedirect.com/science/article/pii/S2214166913000398>
- [5] S. Way and M. Thomson, “Site characterisation and design basis report ETI REDAPT MA1001 MD6.1,” GL Garrad Hassan, Tech. Rep., 2011.
- [6] S. Way and M. Thomson, “Site characterisation and design basis report ETI REDAPT MA1001 MD6.2,” GL Garrad Hassan, Tech. Rep., 2011.
- [7] S. Way and M. Thomson, “Site characterisation and design basis report ETI REDAPT MA1001 MD6.3,” GL Garrad Hassan, Tech. Rep., 2011.
- [8] Andritz Hydro Hammerfest, “08.02.2012: Tidal Turbine getting ready to feed the grid,” 2012. [Online]. Available: <http://www.hammerfeststrom.com/news/08-02-2012-tidal-turbine-getting-ready-to-feed-the-grid/>
- [9] MCT, “Project Background — SeaGeneration.” [Online]. Available: <http://www.seageneration.co.uk/background.php>
- [10] P. Evans, S. Armstrong, C. Wilson, I. Fairley, C. Wooldridge, and I. Masters, “Characterisation of a Highly Energetic Tidal Energy Site with Specific Reference to Hydrodynamics and Bathymetry,” 2013.
- [11] J. G. Leishman, “Challenges in modelling the unsteady aerodynamics of wind turbines,” *Wind Energy*, vol. 5, no. 2-3, pp. 85–132, Apr. 2002. [Online]. Available: <http://doi.wiley.com/10.1002/we.62>
- [12] T. Burton, N. Jenkins, D. Sharpe, and E. Bossanyi, *Wind Energy Handbook*. JOHN WILEY & SONS, LTD, 2011.
- [13] H. Homann, J. Bec, and R. Grauer, “Effect of turbulent fluctuations on the drag and lift forces on a towed sphere and its boundary layer,” *Journal of Fluid Mechanics*, vol. 721, pp. 155–179, 2013. [Online]. Available: http://journals.cambridge.org/abstract_S0022112013000669
- [14] H. Diels, *Doxographi graeci*. De Gruyter, 1879.

- [15] J. A. Knauss, *Introduction to Physical Oceanography*. Prentice-Hall, 1978.
- [16] B. L. Polagye, “Hydrodynamic effects of kinetic power extraction by in-stream tidal turbines,” Ph.D. dissertation, 2009. [Online]. Available: [http://ezproxy.library.ubc.ca/login?url=http://search.proquest.com/docview/305016150?accountid=14656\\$\\delimiter"026E30F\\$nhhttp://gw2jh3xr2c.search.serialssolutions.com/?ctx_ver=Z39.88-2004&ctx_enc=info:ofi/enc:UTF-8&rft_id=info:sid/ProQ&rft_val_fmt=info:ofi/fmt:kev:mtx:disse](http://ezproxy.library.ubc.ca/login?url=http://search.proquest.com/docview/305016150?accountid=14656$\\delimiter)
- [17] S. Pope, *Tubulent Flows*, 1st ed. Cambridge University Press,, 2000.
- [18] Y. Çengel and R. Turner, *Fundamentals of thermal-fluid sciences*, 2nd ed. McGraw-Hill, 2005.
- [19] A. Kolmogorov, “A refinement of previous hypotheses concerning the local structure of turbulence in a viscous incompressible fluid at high Reynolds number,” *J. Fluid Mech*, vol. 13, no. 01, pp. 82–85, 1962. [Online]. Available: <http://journals.cambridge.org/production/action/cjoGetFulltext?fulltextid=368739>
- [20] T. Blackmore, W. Batten, M. Harrison, and A. Bahaj, “The Sensitivity of Actuator-Disc RANS Simulations to Turbulence Length Scale Assumptions,” *European Wave and Tidal Energy Conference*, pp. 390–399, 2011. [Online]. Available: <http://scholar.google.com/scholar?hl=en&btnG=Search&q=intitle:The+Sensitivity+of+Actuator-Disc+RANS+Simulations+to+Turbulence+Length+Scale+Assumptions#5>
- [21] L. Kilcher, J. Thomson, and J. Colby, “Determining the spatial coherence of turbulence at MHK sites,” in *2nd Marine Energy Technology Symposium*, Seattle, WA, 2014.
- [22] G. Taylor, “Spectrum of turbulence,” *Proceedings of the Royal Society of London. Series A, Mathematical and Physical Sciences*, vol. 164, no. 919, pp. 476–490, February 1938.
- [23] W. Rodi, *Turbulence Models and Their Applications in Hydraulics A state-of-the-art review*, 3rd ed. A.A. Balkema, 1993.
- [24] F. Archambeau, N. M chitoua, and M. Sakiz, “Code_saturne A finite volume code for the computation of turbulent incompressible flows industrial applications.” *Int. J. Finite*, pp. 1 – 62, 2003.
- [25] N. J. (a), b. S. Benhamadouche, a. D. Laurence, and a. R. Prosser, “A synthetic-eddy-method for generating inflow conditions for large-eddy simulations.” *International Journal of Heat and Fluid Flow*, vol. 27, no. Special Issue of The Fourth International Symposium on Turbulence and Shear Flow Phenomena - 2005, pp. 585 – 593, 2006.
- [26] G. McCann, G. Rawlinson-Smith, and K. Argyriadis, “2006 load simulation for tidal turbines using wind turbine experience,” in *ICOE*, 2006.
- [27] H. Tennekes and J. L. Lumley, *A First Course in Turbulence*. the MIT press, 1972.
- [28] A. Lohrmann, B. Hackett, and L. P. Rø ed, “High Resolution Measurements of Turbulence, Velocity and Stress Using a Pulse-to-Pulse Coherent Sonar,” *Journal of Atmospheric and Oceanic Technology*, vol. 7, no. 1, pp. 19–37, 1990.
- [29] Y. Lu and R. G. Lueck, “Using a Broadband ADCP in a Tidal Channel. Part I: Mean Flow and Shear,” *Journal of Atmospheric and Oceanic Technology*, vol. 16, pp. 1556–1567, 1999.
- [30] Y. Lu and R. Lueck, “Using a broadband ADCP in a tidal channel. Part II: Turbulence.” *Journal of Atmospheric & Oceanic ...*, pp. 1568–1579, 1999. [Online]. Available: <http://search.ebscohost.com/login.aspx?direct=true&profile=ehost&scope=site&authtype=crawler&jrnl=07390572&AN=5650969&h=y59I%>

2FNDujcK7QjofYnhFy8skJQb0KQgd7D1IJD6j0qInuHu0Q8gQeay8cSHrN6KmvTrFVMmT2SWaxR1fR%
2F9T0g%3D%3D&erl=c

- [31] J. Thomson, B. Polagye, M. Richmond, and V. Durgesh, “Quantifying turbulence for tidal power applications,” in *MTS/IEEE Seattle, OCEANS 2010*, no. 4, 2010. [Online]. Available: http://ieeexplore.ieee.org/xpls/abs_all.jsp?arnumber=5664600
- [32] E. Osalusi, J. Side, and R. Harris, “Structure of turbulent flow in EMEC’s tidal energy test site,” *International Communications in Heat and Mass Transfer*, vol. 36, no. 5, pp. 422–431, May 2009. [Online]. Available: <http://linkinghub.elsevier.com/retrieve/pii/S0735193309000530>
- [33] I. A. Milne, R. N. Sharma, R. G. J. Flay, and S. Bickerton, “Characteristics of the turbulence in the flow at a tidal stream power site Characteristics of the turbulence in the flow at a tidal stream power site,” *The Royal Society A*, 2013.
- [34] M. Togneri and I. Masters, “Comparison of marine turbulence characteristics for some potential turbine installation sites,” in *4th International Conference on Ocean Energy*, 2012, pp. 6–11.
- [35] C. Legrand, Black and Veatch, and Emec, *Assessment of Tidal Energy Resource*, 2009.
- [36] J. Thomson, B. Polagye, V. Durgesh, and M. C. Richmond, “Measurements of Turbulence at Two Tidal Energy Sites in Puget Sound, WA,” *IEEE Journal of Oceanic Engineering*, vol. 37, no. 3, pp. 363–374, 2012.
- [37] O. Reynolds, “On the Dynamical Theory of Incompressible Viscous Fluids and the Determination of the Criterion,” pp. 123–164, 1895.
- [38] H. Grant, “The Large Eddies of Turbulent Motion,” *J. Fluid Mech*, vol. 4, no. 02, pp. 149–190, 1958. [Online]. Available: <http://journals.cambridge.org/production/action/cjoGetFulltext?fulltextid=367456>
- [39] M. T. Stacey, G. Monismith, and J. R. Burau, “of Reynolds stress profiles in unstratified,” *JOURNAL OF GEOPHYSICAL RESEARCH*, vol. 104, pp. 933–949, 1999.
- [40] P. O’Neill, D. Nicolaides, D. Honnery, and J. Soria, “Autocorrelation Functions and the Determination of Integral Length with Reference to Experimental and Numerical Data,” in *15th Australasian Fluid Mechanics Conference*, vol. 1, no. December, 2004, pp. 1–4.
- [41] P. J. Wiles, T. P. Rippeth, J. H. Simpson, and P. J. Hendricks, “A novel technique for measuring the rate of turbulent dissipation in the marine environment,” *Geophysical Research Letters*, vol. 33, no. 21, p. L21608, Nov. 2006. [Online]. Available: <http://www.agu.org/pubs/crossref/2006/2006GL027050.shtml>
- [42] “Conductivity, Salinity & Total Dissolved Solids - Environmental Measurement Systems,” 2015. [Online]. Available: <http://www.fondriest.com/environmental-measurements/parameters/water-quality/conductivity-salinity-tds/>
- [43] Valeport, *Model 803 Operating Manual*, 2001.
- [44] Rockland Scientific, “rocklandscientific.com,” 2015. [Online]. Available: <http://rocklandscientific.com/>
- [45] S. Thorpe, *The Turbulent Ocean*. Cambridge University Press, 2007. [Online]. Available: http://www.tos.org/oceanography/archive/19-3_smyth.pdfhttp://books.google.com/books?hl=en&lr=&id=Ax2d94PODgIC&oi=fnd&pg=PR11&dq=The+Turbulent+Ocean.&ots=Mc0hNULvMG&sig=IzBIPp680JtMi5ySkKeR2ZfXskw

- [46] L. Goddijn-Murphy, D. K. Woolf, and M. C. Easton, “Current Patterns in the Inner Sound (Pentland Firth) from Underway ADCP Data,” *Journal of Atmospheric and Oceanic Technology*, vol. 30, no. 1, pp. 96–111, Jan. 2013.
- [47] T. Rippeth, E. Williams, and J. Simpson, “Reynolds Stress and Turbulent Energy Production in a Tidal Channel,” *Journal of Physical Oceanography*, vol. 32, pp. 1242–1251, 2002.
- [48] E. A. Nystrom, C. R. Rehmann, and K. A. Oberg, “Evaluation of Mean Velocity and Turbulence Measurements with ADCPs,” *Journal of Hydraulic Engineering*, vol. 133, no. 12, pp. 1310–1318, 2007.
- [49] I. Fairley, P. Evans, C. Wooldridge, M. Willis, and I. Masters, “Evaluation of tidal stream resource in a potential array area via direct measurements,” *Renewable Energy*, vol. 57, pp. 70–78, Sep. 2013.
- [50] B. Gunawan and V. S. Neary, “ORNL ADCP Post-Processing Guide and MATLAB Algorithms for MHK Site Flow and Turbulence Analysis,” Oak Ridge National Laboratory, Tech. Rep. September, 2011.
- [51] RD Instruments, *Acoustic doppler current profilers principles of operation: A practical primer*, 1989. [Online]. Available: <http://scholar.google.com/scholar?hl=en&btnG=Search&q=intitle:Acoustic+Doppler+Current+Profiler+Principles+of+Operation+A+Practical+Primer#0http://scholar.google.com/scholar?hl=en&btnG=Search&q=intitle:Acoustic+Doppler+Current+Profiler+Principles+of+Oper>
- [52] Nortek-AS, “Aquadopp HR-Profiler,” 2015. [Online]. Available: <http://www.nortek-as.com/en/products/current-profilers/aquadopp-hr-profiler>
- [53] Nortek-AS, “Continental 3D Current Profiler Datasheet,” 2015.
- [54] Nortek-AS, “Vectrino Data Sheet,” 2015.
- [55] . . RD Instruments, “ADCP Coordinate Transformation: Formulas and Calculations,” RDI Instruments, Tech. Rep. July, 1998.
- [56] J. A. Boldt, “Use of numerical simulations to investigate the performance of a virtual acoustic Doppler current profiler in characterizing flow,” Masters, University of Illinois, 2013.
- [57] J.-B. Richard, J. Thomson, B. Polagye, and J. Bard, “Method for identification of Doppler noise levels in turbulent flow measurements dedicated to tidal energy,” *International Journal of Marine Energy*, vol. 3-4, pp. 52–64, Dec. 2013.
- [58] V. Durgesh, J. Thomson, M. C. Richmond, and B. L. Polagye, “Noise correction of turbulent spectra obtained from acoustic doppler velocimeters,” *Flow Measurement and Instrumentation*, vol. 37, pp. 29–41, Jun. 2014.
- [59] A. Lohrmann, R. Cabrera, and N. C. Kraus, “Acoustic-Doppler Velocimeter (ADV) for Laboratory Use,” in *Fundamentals and Advancements in Hydraulic Measurements and Experimentation*, Buffalo, New York, 1994, pp. 351–365.
- [60] G. Voulgaris and J. H. Trowbridge, “Evaluation of the Acoustic Doppler Velocimeter (ADV) for Turbulence Measurements,” *Journal of Atmospheric and Oceanic Technology*, vol. 15, pp. 272–289, 1998.
- [61] D. Hurther and U. Lemmin, “A Correction Method for Turbulence Measurements with a 3D Acoustic Doppler Velocity Profiler,” *Journal of Atmospheric and Oceanic Technology*, vol. 18, pp. 446–458, 2001.

- [62] C. M. García, M. I. Cantero, Y. Niño, and M. H. García, “Turbulence Measurements with Acoustic Doppler Velocimeters,” *Journal of Hydraulic Engineering*, vol. 131, no. 12, pp. 1062–1073, 2005.
- [63] H. Chanson, M. Threveltham, and C. Koch, “Discussion of ”Turbulence Measurements with Acoustic Doppler Velocimeters” by Carlos M. García, Mariano I. Cantero, Yarko Niño, and Marcelo H. García,” *Journal of Hydraulic Engineering*, vol. 133, no. 11, pp. 1283–1286, 2007.
- [64] R. Cooke, “Design and Implementation of a 3-Axis Coherent Doppler Velocity Profiler,” in *2nd International Conference & Exhibition on Underwater Acoustic Measurements: Technologies & Results*, 2007, pp. 1019–1026.
- [65] H. D. T. P. D. B. M. L. U. and B. J. M., “A multi-frequency acoustic concentration and velocity profiler (ACVP) for boundary layer measurements of fine-scale flow and sediment transport processes.” *Coastal Engineering*, vol. 58, pp. 594–605, 2011.
- [66] J. Thomson, L. Kilcher, M. Richmond, J. Talbert, A. DeKlerk, B. Polagye, M. Guerra, and R. Cienfuegos, “Tidal turbulence spectra from a compliant mooring,” in *1st Marine Energy Technology Symposium (METS)*, Washington, D.C., 2013.
- [67] R. Craig, C. Loadman, B. Clement, P. Rusello, and E. Siegel, “Characterization and testing of a new bistatic profiling acoustic doppler velocimeter: The vectrino-ii,” in *Current, Waves and Turbulence Measurements (CWTM), 2011 IEEE/OES 10th*, March 2011, pp. 246–252.
- [68] M. Longuet-Higgins, D. Cartwright, and N. Smith, “Observations of the directional spectrum of sea waves using the motions of a floating buoy.” in *Ocean Wave Spectra*. Prentice-Hall, Englewood Cliffs, NJ, USA, 1963, p. 111136.
- [69] C.-C. Teng, T. Mettlach, J. Chaffin, R. Bass, C. Bond, C. Carpenter, R. Dinoso, M. Hellschmidt, and L. Bernard, “National data buoy center 1.8-meter discus buoy, directional wave system,” 29 2007-oct. 4 2007, pp. 1 –9.
- [70] K. E. Steele, D. W. Wang, M. D. Earle, E. D. Michelena, and R. J. Dagnall, “Buoy pitch and roll computed using three angular rate sensors,” *Coastal Engineering*, vol. 35, no. 1-2, pp. 123 – 139, 1998. [Online]. Available: <http://www.sciencedirect.com/science/article/pii/S0378383998000258>
- [71] J. Cruz, E. Mackay, and T. Martins, “Advances in wave resource estimation measurements and data processing.” in *Proc. 7th European Wave and Tidal Energy Conference (Oporto)*., 2007.
- [72] D. Ingram, “EQUIMAR, Equitable Testing and Evaluation of Marine Energy Extraction Devices in terms of Performance, Cost and Environmental Impact: D2.7 Protocols for wave and tidal resource assessment,” The Equimar Consortium, Tech. Rep., 2011.
- [73] J. Eshbaugh and S. Frasier, “Measurement of sea surface displacement with interferometric radar,” *J. Atmos. Ocean. Technol. (USA)*, vol. 19, no. 7, pp. 1087 – 95, July 2002.
- [74] K. Hessner, K. Reichert, J. Dittmer, and J. C. N. Borge, “Ocean wave measurements by x-band radar - from spectral wave parameters to single wave detection,” OceanWaveS GmbH, Tech. Rep., 2003.
- [75] Ocean Waves GMBH, “Wamos II data comparison and error statistics,” 2007. [Online]. Available: http://www.oceanwaves.org/download/PDF/E_STAT2007.pdf
- [76] K. Reichert, K. Hessner, I. Trankmann, and B. Lund, “X-band radar as a tool to determine spectral and single wave properties,” OceanWaveS GmbH, Luneburg, Germany, Tech. Rep., 2004.

- [77] “An overview of work by lews castle college (LCC),” 2015. [Online]. Available: <http://www.nortek-as.com/lib/user-seminars/donald-armstrong-uhi>
- [78] K. Rorbaek and H. Andersen, “Evaluation of wave measurements with an acoustic doppler current profiler,” *OCEANS 2000 MTS/IEEE Conference and Exhibition. Conference Proceedings*, vol. vol.2, pp. 1181 – 1187, 2000.
- [79] C. Boake, Nortek User Symposium, France, 2008.
- [80] T. RDI, ADCP Deployment Planning Software, 2011.
- [81] SonTek, “Sonwave-pro: Directional wave data collection,” SonTek, San Diego, CA, USA, Tech. Rep., 2001.
- [82] N. AS, “Datasheet: Awac / real time systems,” Oslo, Norway, 2011.
- [83] L. Wyatt, J. Green, and A. Middleditch, “Wave, current and wind monitoring using hf radar,” june 2005, pp. 53 – 57.
- [84] L. R. Wyatt, J. J. Green, A. Middleditch, M. D. Moorhead, J. Howarth, M. Holt, and S. Keogh, “Operational wave, current, and wind measurements with the pisces hf radar,” *Oceanic Engineering, IEEE Journal of*, vol. 31, no. 4, pp. 819 –834, oct. 2006.
- [85] M. Belmont, J. Horwood, R. Thurley, and J. Baker, “Shallow angle wave profiling lidar,” *J. Atmos. Oceanic Technol.*, vol. 24, pp. 1150 – 1156, 2007.
- [86] R. van Unen, A. van Beuzekom, G. Forristall, J. Mathisen, and J. Starke, “Wacsis-wave crest sensor intercomparison study at the meetpost noordwijk measurement platform,” in *OCEANS '98 Conference Proceedings*, vol. 3, sep-1 oct 1998, pp. 1757 –1761 vol.3.
- [87] S. F. Barstow, H. E. Krogstad, L. Lonseth, J. P. Mathisen, G. Mork, and P. Schjolberg, “Intercomparison of sea-state and zero-crossing parameters from the wacsis field experiment and interpretation using video evidence,” *Journal of Offshore Mechanics and Arctic Engineering*, vol. 126, no. 1, pp. 35–42, 2004. [Online]. Available: <http://link.aip.org/link/?JOM/126/35/1>
- [88] W. A. Birkemeier and E. B. Thornton, “The DUCK94 Nearshore Field Experiment,” in *Proceedings of the Conference on Coastal Dynamics '94*, 1994, pp. 815–821.
- [89] C.-H. Tsai, M.-C. Huang, F.-J. Young, Y.-C. Lin, and H.-W. Li, “On the recovery of surface wave by pressure transfer function,” *Ocean Engineering*, vol. 32, no. 10, pp. 1247 – 1259, 2005.
- [90] . . Nortek AS, “Comprehensive Manual,” Nortek, Tech. Rep., 2013.
- [91] *Nortek AS, (2005): AWAC Acoustic Wave And Current Meter User Guide. Document. No: n3000-126. First Edition.*
- [92] H. Lamb, “‘hydrodynamics’,” *Cambridge, England: Cambridge University Press, 6th ed.*, 1932.